Design and Applications of a Decade-Spanning Terahertz Frequency Comb Spectrometer: Doppler-limited Rotational Spectroscopy of Methanol and Methanol-OD

Thesis by

Jacob Thomas Good

In Partial Fulfillment of the Requirements

for the Degree of

Doctor of Philosophy

California Institute of Technology

Pasadena, California

2016

(Defended March 18, 2016)

To my past, present, and future teachers.

Acknowledgements

The pursuit of a PhD is in a broader sense the pursuit of new knowledge in one's chosen field. In today's interdisciplinary world knowledge does not exist in isolation, and one must draw upon the expertise of many different experts in a plethora of fields. My thesis would not exist if not for the contributions of a long list of people, of whom I will try to thank as many as possible here.

Of course, none of this work would have been possible without the support of Geoff Blake. First and foremost, Geoff has been an exemplary advisor. Despite possessing formidable knowledge in an impressively wide range of disciplines, he is one of the most approachable people I have met. From the moment I first requested to join his group, Geoff has been completely supportive and encouraging, both personally and academically. All of my experiences working with him have been rewarding, from TAing for him in CHEM 1B, to listening to his lectures in Cosmochemistry. Geoff has an amazing proclivity for creative thinking, and brainstorming sessions with him in the office are always productive and thought provoking. His enthusiasm for teaching and learning is contagious and I have become a better teacher and student as a result. Geoff, you consistently set a standard of excellence for both current and aspiring professors everywhere. I hope to emulate your talent as a scientist, your warmth as a mentor, and your passion as a teacher. Thank you so much for giving me the opportunity to learn from you!

With such an excellent leader at the helm, the Blake Group has attracted a truly spectacular group of people. Success comes naturally when you are surrounded by such an enthusiastic, intelligent, and motivated group of people. You have all enriched my life with as colleges and friends and although a cannot give an exhaustive list of your contributions here, I will thank you all in turn.

None of the work described in this thesis would be possible without he mastermind behind the spectrometer, Dan Holland. Thanks for entrusting your brainchild to me, and for your thoughtful advice on my results. I hope you enjoy reading about the advances we have made. I'm looking forward to reading more about your postdoctoral research in the application of THz spectroscopy to imaging of biological systems.

Ian Finneran has been my closest collaborator working with the ASOPS system. Without his expertise in frequency combs and programming, we never would have developed the high-resolution THz frequency comb spectrometer. Thanks for your many contributions to this project, especially the mouse clicker software. Long live the lazy comb! I have truly enjoyed all of our conversations about life, science, and everything in between. I hope to collaborate with you in the future, wherever our careers lead us.

Brandon Carroll, the DDS whisperer, has also made many important contributions to the ASOPS system. Your can-do attitude facilitated many key developments in this project, including the moment when we first tried to collect a multi-pulse record and generate the comb. Your C programming skills were instrumental for pushing the comb data collection to the limit. You are full of great ideas about what to do with the spectrometer and I'm looking forward reading about the execution of a few of them in your thesis.

Marco Allodi, despite having his hands plenty full with trying to keep the Legend system up and running, never hesitated to lend a hand or an ear throughout my time in the group. Thanks for putting up with my constant pestering and imparting your knowledge of alignment, ultrafast lasers, and THz-TDS. You are a great teacher, skilled researcher, and will be an excellent professor someday.

Most of my time with Brett McGuire was spent up in the office, but we still had many lively discussions, scientific and otherwise. Thanks for all of your thoughtful advice on presentations and figures and for showing us all around UIUC this year.

My overlap with Sergio Ioppolo's tenure in the Blake lab was brief, but I still benefited from his expertise in the astrochemistry of ices through interactions with him and the other ices guys.

Nate Crockett, was the only Blake Group astronomer who was willing to put up with sharing an office with the chemists. He was always willing to join in on our discussions and impart his data processing and astrochemistry expertise. Thanks for letting me pester you with astronomy questions and for encouraging my adventures in programming.

I'd also like to thank the members of my PhD committee for being supportive of my thesis project and providing many excellent suggestions on future improvements and collaborations.

I'd like to first thank Prof. Harry Gray for chairing my committee and for always being an advocate for me. Your long and distinguished career in Chemistry is a shining example that every Caltech Chemistry PhD student can aspire to. I look forward to the future collaborations between the Blake Group and the Gray Group in understanding the effects of large amplitude motion in proteins through Terahertz spectroscopy.

Prof. Jim Heath would probably have been my advisor if I had come to Caltech during the molecular memory project. Your track record of revolutionizing research in every field you have worked in is truly impressive and it has been an honor to have discussed my thesis research with you.

Finally, I'd like to thank Prof. Mitchio Okumura for assisting me in my transition between labs and for agreeing to be on my committee. You are a busy man with many responsibilities, but you still found time to make a positive impact on my thesis research. It has been a pleasure interacting with you and with your graduate students.

I'd like to thank the Planetary Science administrative staff — Irma, Ulrika, and Margaret — for their assistance and hospitality during my time with the Blake Group.

Also, thanks to Mike and Steve in the machine shop for building countless sample cells for me and for always being proactive in making sure that each design is built properly and in a timely fashion.

Thanks to Rich in the glass shop for the many fine pieces of glassware that he has made for me, and for graciously repairing the glassware that I have broken.

Of course, I must thank Agnes for her support and friendship during my time at Caltech. Thanks for always having an open door and for being willing to chat about anything and everything. I look forward to working with you after I defend to inspire the Caltech PhD students of the future.

My Caltech roommates were instrumental to maintaining my sanity throughout my PhD. From late night movie and Starcraft sessions, to summer softball games and Del Taco runs, you guys were always excellent company. Thanks for putting up with my guitar playing, and my sometimes questionable taste in music.

Adam N., you led us to back-to-back softball championships but always kept a fun and welcoming environment for everyone who wanted to play. Thanks for letting us heckle you while you played through Zelda.

Adam P., thanks for sharing your impeccable taste in music and gourmet soda. Your knowledge of Pokemon has come in handy for more than one trivia question. One day we will journey to the Karaoke promised land and it will be glorious.

Ben, I thoroughly enjoyed all of our discussions of the virtues of Mustangs, whiskey, and burgers. You are my go to consultant on fantasy football, quality movies, and top lane match ups.

I'd also like to thank my professors and mentors at UC Riverside who were instrumental to my development as a chemist and a spectroscopist.

Prof. Ludwig Bartels was my first mentor at UCR. Thanks for starting me off on a project that was both exciting and accessible for a first-year undergrad. I really learned how to think on a molecular level through my work in your lab.

Prof. Tom Morton was a mentor to me and to my entire honors sophomore organic chemistry section. Thanks for giving me an opportunity to take the lead on a group research project and guiding us along the way. You played an instrumental role in teaching me how to think about molecules like a spectroscopist.

Prof Chris Bardeen was my mentor for my senior year. Thank you for your dedicated support throughout my final year at UCR. I had a truly rewarding experience working for you, culminating in the publication of my research in a peer-reviewed journal. Working in your lab opened my eyes

to the many wonderful possibilities of ultrafast spectroscopy. You laid the foundation for my thesis research and taught me how to think analytically about my results.

I also must thank my first great chemistry teacher, Jeff MacLean. Thanks for going above and beyond the call of duty to set up after school chemistry labs, and to advise the Science Olympiad team. My experiences in your AP Chemistry class inspired me to major in Chemistry and eventually culminated in this thesis.

The two people who really laid the foundation for my entire education were my parents. Your love and support helped me to dream big enough to go for a PhD and to work hard to finish what I started.

Mom, you taught me the importance of education from the very beginning. I still have vivid memories of reading the Space Atlas and other educational books that you bought me. Thanks for taking us to the library on a weekly basis, letting me take my chess computer with me everywhere, and for encouraging me do science experiments at home. You taught me that the easiest path in life is seldom the most rewarding and that with hard work and integrity, anything is possible.

Dad, you taught me the importance of hands on learning and knowing how things work. Thanks for taking the time to explain to me how a car works, buying us model kits to put together, and letting me play with your multimeter and toolkit all the time. I have always been impressed by your natural ability to fix anything that is broken. You taught me that one of the most satisfying feelings is to really know how all the parts in a system work together.

Kyle and Brett, you were awesome brothers to grow up with. Thanks for going along with my sometimes overly complicated concepts of playtime. Through all of our adventures building things out of Lincoln Logs, Legos, pattern blocks, and whatever else we could get our hands on, I gained an appreciation for putting things together that has culminated in the construction of a world-class spectrometer.

I have also benefited from the love and support of my family-in-law. You guys have really taken me in and supported me as one of your own. Your flair for everything artistic and creative has helped me to stay balanced and to remember that there is a wonderful world outside of lab.

Anne-Marie, you have made sure that I have had a roof over my head, tasty food to eat, and fluffy dogs to cuddle throughout my time working on this thesis. Your steadfast support of everyone around you has enabled them to do great things, and I am no exception. Thanks for your encouragement in my endeavors at Caltech and in my marriage to your daughter. I am blessed to be counted as a part of your family.

Eloy, thanks for sharing your stories about the places you have seen and the people you have met. You always remind me that despite everything I have already learned about the world, there is so much more out there to experience. You are truly a student of the world, thanks for teaching me about it.

Ava and Elora, you are the sisters I never had. I always have so much fun with you guys whether we are playing Settlers of Catan or watching amazing musicals. Thanks for laughing and singing with me, it has helped keep me sane.

I have saved my most important acknowledgment for last: Marissa, my beautiful and beloved wife, you have taught me so much about life, love, and everything else that it is hard to believe that I have only known you for three years. You are the hardest working, most creative, and most dedicated person I know. You are my fiercest advocate and you have believed in me even when I have doubted myself. This thesis would not have been possible without your unwavering support and love. Since we were born less than a week apart in February, it is fitting that this thesis was defended within a week of our 1 year anniversary in March. We have accomplished so much together already, and I cannot wait to see what our future holds. I know that with your love and support I can achieve anything I put my mind to.

Abstract

This thesis details the design and applications of a terahertz (THz) frequency comb spectrometer. The spectrometer employs two offset locked Ti:Sapphire femtosecond oscillators with repetition rates of approximately 80 MHz, offset locked at 100 Hz to continuously sample a time delay of 12.5 ns at a maximum time delay resolution of 15.6 fs. These oscillators emit continuous pulse trains, allowing the generation of a THz pulse train by the master, or pump, oscillator and the sampling of this THz pulse train by the slave, or probe, oscillator via the electro-optic effect. Collecting a train of 16 consecutive THz pulses and taking the Fourier transform of this pulse train produces a decade-spanning frequency comb, from 0.25 to 2.5 THz, with a comb tooth width of 5 MHz and a comb tooth spacing of ∼80 MHz. This frequency comb is suitable for Doppler-limited rotational spectroscopy of small molecules. Here, the data from 68 individual scans at slightly different pump oscillator repetition rates were combined, producing an interleaved THz frequency comb spectrum, with a maximum interval between comb teeth of 1.4 MHz, enabling THz frequency comb spectroscopy.

The accuracy of the THz frequency comb spectrometer was tested, achieving a root mean square error of 92 kHz measuring selected absorption center frequencies of water vapor at 10 mTorr, and a root mean square error of 150 kHz in measurements of a K-stack of acetonitrile. This accuracy is sufficient for fitting of measured transitions to a model Hamiltonian to generate a predicted spectrum for molecules of interest in the fields of astronomy and physical chemistry. As such, the rotational spectra of methanol and methanol-OD were acquired by the spectrometer. Absorptions from 1.3 THz to 2.0 THz were compared to JPL catalog data for methanol and the spectrometer achieved an RMS error of 402 kHz, improving to 303 kHz when excluding low signal-to-noise absorptions. This level of accuracy compares favorably with the ∼100 kHz accuracy achieved by JPL frequency

multiplier submillimeter spectrometers. Additionally, the relative intensity performance of the THz frequency comb spectrometer is linear across the entire decade-spanning bandwidth, making it the preferred instrument for recovering lineshapes and taking absolute intensity measurements in the THz region. The data acquired by the Terahertz Frequency Comb Spectrometer for methanol-OD is of comparable accuracy to the methanol data and may be used to refine the fit parameters for the predicted spectrum of methanol-OD.

Published Content and Contributions

[1] "A decade-spanning high-resolution asynchronous optical sampling terahertz time-domain and frequency comb spectrometer," by J.T. Good*, D.B. Holland*, I.A. Finneran, P.B. Carroll, M.J. Kelley, and G.A. Blake, *Review of Scientific Instruments* **86**, 103107 (2015). DOI: 10.1063/1.4932567 [*Co-first author]

J.T. Good made modifications to the instrument used to acquire the data, acquired the data, analyzed the data, wrote the article, prepared figures and diagrams, and revised the article.

[2] "Decade-spanning high-precision terahertz frequency comb," by I.A. Finneran, J.T. Good, D.B. Holland, P.B. Carroll, M.A. Allodi, and G.A. Blake, *Physics Review Letters* **114**, 163902 (2015). DOI: 10.1103/PhysRevLett.114.163902

J.T. Good made modifications to the instrument used to acquire the data, acquired the data, assisted in analyzing the data, and revised the article.

Contents

List of Figures

List of Tables

Part I

Introduction

Chapter 1

Introduction to Terahertz Spectroscopy

Parts of this chapter are reproduced from "A decade-spanning high-resolution asynchronous optical sampling terahertz time-domain and frequency comb spectrometer," by J.T. Good, D.B. Holland*, I.A. Finneran, P.B. Carroll, M.J. Kelley, and G.A. Blake, Review of Scientific Instruments* ***86****, 103107 (2015). [*Co-first author]*

Throughout the history of the study of chemistry, our understanding of chemical phenomena has been closely linked with our ability to analyze light-matter interactions in a particular region of the electromagnetic spectrum. Many chemical insights have been gleaned from the careful study of the visible region of the spectrum, including a rigorous empirical description of the energy levels of the electronic transitions of the hydrogen atom that predated quantum theory. The need to describe the existence of discrete energy levels for the electronic transitions of the hydrogen atom, to explain the ultraviolet catastrophe in the study of black body spectra, and to understand the photoelectric effect led to the development of quantum theory. The scientists who developed quantum theory did not immediately realize its massive implications in the study of physics, chemistry, and all fields that involve light-matter interactions. They were simply trying to explain the confusing results of some experiments in the laboratory. It is therefore with a pioneering spirit that we embark on this exploration of spectroscopy in the Terahertz region with the hope that important insights, especially some unexpected ones, await us.

1.1 The Terahertz Region

Historically, the study of the electromagnetic spectrum has focused on the visible region of the spectrum. Lacking the insight provided by a theoretical understanding of electromagnetic radiation, scientists were initially surprised to discover the existence of infrared and ultraviolet radiation that behaved similarly to visible light, but was invisible to the naked eye. When Maxwell noticed the interaction between electric and magnetic fields, he was compelled to develop a theoretical understanding of this phenomena. The result of his efforts was a series of equations, Maxwell's equations, which predicted the existence of the entire electromagnetic spectrum. The predictions made by Maxwell's equations were verified when Hertz conducted an experiment in which electromagnetic radiation was induced by accelerating electrons within a plasma created by discharging capacitors across a spark gap. By strategically positioning a metal plate at a distance corresponding to an integral multiple of the wavelength of the resulting electromagnetic radiation, Hertz was able to generate a standing wave. He directly measured the associated electric and magnetic fields of both radio waves and microwaves and found the wavelength and frequency to be consistent with the speed of light as predicted by Maxwell's equations.

The application of the electromagnetic spectrum to spectroscopy had to wait for the development of technology for high intensity generation of photons, and sensitive detection of those photons in the region of interest. Strategies for the generation and detection of electromagnetic radiation generally fall into two categories: emission and absorption of radiation by the transitions of bound electrons between the energy levels of a solid state material or oscillation of free electrons in a metallic conductor or a plasma. For bound electrons there are limitations to the range of energies accessible based on the energies of the electronic transition or bandgap associated with the electrons. Most conventional materials support generation and detection of photons with energies ranging from the UV to the IR. Free electrons offer a method for the generation and detection of electromagnetic radiation across the range of frequencies accessible by conventional electronics. The oscillation of free electrons by electronic circuitry suffers a dramatic decrease in efficiency for frequencies exceeding those associated with the microwave region. The gap between these two methods for generation and

detection of electromagnetic radiation spans the terahertz (THz) region, defined here as frequencies between 0.1-10 THz or 3.33-333 cm^{-1}.

THz photons, with energies ranging from 0.41-41 meV, are lower in energy than infrared photons, which interact with pure vibrational and rotational-vibrational transitions of molecules, and higher in energy than microwave photons, which interact with pure rotational transitions of molecules, and as such they provide simultaneous access to these three classes of molecular transitions. Semiconductor phonon modes are efficient absorbers and emitters of THz radiation and as such many schemes for detecting and generating THz photons are based on semiconductor materials.[1] THz radiation provides an exciting method for probing the tertiary structure of proteins through collective large-amplitude motions.[2] The study of intermolecular vibrations of water, corresponding to ensembles of hydrogen bonds in aqueous systems, is an exciting frontier and active area of research that employs THz spectroscopy.[3] Along with numerous applications in the spectroscopy of condensed-phase matter, THz photons are additionally useful for gas-phase spectroscopy of small molecules, which have rotational transitions extending up to 10 THz.[4] This is by no means an exhaustive summary of interactions between THz photons and matter, and is provided as a small sampling of the many potential applications of THz spectroscopy across many disciplines.

The Blake group is primarily interested in the application of THz spectroscopy to the study of the condensed-phase and gas-phase matter populating the interstellar medium (ISM). Spectroscopy is an essential tool that enables the identification of molecular species anywhere in the universe, so long as they are accessible to photons with energies that match their rotational and vibrational transitions. Low energy THz photons are not scattered or absorbed strongly by planet forming nebulae, vast clouds of dust and gas at temperatures of $\sim$30 K. THz photons are low in energy, enabling emission spectroscopy of nebulae at temperatures cold enough to support the formation of stable, complex organic molecules. Nebulae at 30 K will primarily emit THz photons. These photons carry the spectral signatures of all of the molecular components of these nebulae, enabling the study of the chemistry of such nascent planetary systems. An understanding of the chemistry of these planetary nebulae provides the information needed to evaluate their potential to produce

the complex organic molecules required by life as we know it. Understanding the spectral signatures of gas-phase species[5] and solid-phase molecular ices[6; 7] is critical to researching the chemical pathways available for the formation of large organic molecules in the ISM. This thesis describes the development of a spectrometer capable of providing high-quality gas-phase reference spectra, supporting studies of the chemistry of gas phase-molecules found in the ISM. Of course, this is only one application of the spectrometer, which features many additional applications in chemistry, physics, and biology.

1.2 Terahertz Time-Domain Spectroscopy

Interest in THz spectroscopy and its potential applications has been building over the past three decades. Terahertz time-domain spectroscopy (THz-TDS) is especially promising, with the potential to provide high-resolution, broadband coverage of the entire THz region.[8] An experimental bandwidth that covers the entire THz region is important for nearly all applications of THz-TDS, but gas-phase THz-TDS is particularly demanding as it additionally requires high frequency resolution (ideally Doppler-limited) across the entire frequency range of interest. For THz-TDS to achieve such high resolution across intervals exceeding a decade in the frequency-domain, sampling of long time delays with high temporal fidelity is required. This in turn requires a mechanism for generating an accurate time delay between THz generation and detection subsystems.

In a typical THz-TDS setup, a pulse train from an ultrafast mode-locked laser is split into two.[9] The first pulse train is used as a pump to generate a THz pulse train, and the second pulse train is sent to a mechanical delay stage that adds an adjustable amount of path length corresponding to a variable time delay. This enables the second pulse train to act as a probe, sampling the entire THz waveform in the time domain, over the course of many THz pulses. A delay stage based THz-TDS system recently achieved an unprecedented bandwidth of $\sim$20 THz, but provided limited frequency resolution.[10] While simple and robust, delay stages suffer from several limitations: moving parts present a challenge in maintaining uniform alignment and focusing of the probe pulse train throughout the scan, the scan rate is limited by the speed of motors, and the length of time

delay scanned is limited by the length of the stage. These limitations make achieving both Doppler-limited resolution and decade spanning bandwidth extraordinarily challenging for conventional delay stages. Before turning to the main discussion of a dual oscillator THz-TDS system, the next section briefly outlines some prior approaches to overcoming the limitations imposed by delay stages.

1.3 High-Resolution THz Spectroscopy

The suite of THz-active processes outlined in Section 1.1 cover an extraordinary range of dynamical time scales and spectroscopic signatures. Interest in THz spectroscopy of both condensed-phase and gas-phase systems has driven the development of instrumentation and techniques for the generation and detection of THz radiation. This has led to a dichotomy of spectrometer development. Those optimized for rapid scanning of solid and liquid samples tend to specialize in bandwidth at the expense of resolution. Meanwhile, other systems have focused on the development of resolution, while neglecting bandwidth. This trade-off is characteristic of THz-TDS, since scan length must be increased to obtain improved resolution. Naturally, this leads to slower scan rates and fewer averages collected with an increased noise floor and decreased bandwidth. An attractive approach to avoiding the difficulty of high-resolution time-domain sampling is to use a narrow linewidth THz source and sample directly in the frequency domain with a cryogenically cooled bolometer. A few examples of the application of this approach to gas-phase spectroscopy in the THz region are provided below.

Frequency multiplier submillimeter spectrometers (FMSSs), for example, continue their significant history of improvement, with recent extensions into the far-infrared, providing a sensitive method for acquiring very high resolution THz gas-phase spectra.[11] Tunable continuous-wave (CW) quantum cascade lasers (QCLs) have also been used as a source of high brightness THz radiation, achieving sub-Doppler THz spectra of gas-phase samples.[12] Recently, a static frequency comb spanning an octave from 1.64-3.35 THz with a few kHz linewidth was generated by a QCL but interleaving of the comb to produce Doppler-limited spectra was not demonstrated.[13] The drawback of both QCL based THz spectrometers and FMSSs is their narrow bandwidth coverage due to the use of CW THz sources. Obtaining high precision measurements across multi-octave intervals

requires prohibitively long scan times as the narrow linewidth source must be tuned. Often, multiple sources are required to cover the entire THz region. This limitation has driven the development of methods for the high-resolution detection of decade-spanning THz pulses readily generated by high-bandwidth ultrafast oscillators.

1.4 Asynchronous Optical Sampling Based THz Time-Domain Spectroscopy

ASynchronous OPtical Sampling (ASOPS) is a technique that eliminates the need for a delay stage by employing two ultrafast mode-locked lasers in an offset locked configuration.[14] Importantly, ASOPS techniques are applicable to any region of the electromagnetic spectrum with processes driven by ultrafast laser pulses. The pump laser (historically referred to as the master laser) runs at a repetition rate f_{pump} and the probe laser (historically referred to as slave laser) is offset locked at a slightly slower repetition rate f_{probe}, such that the repetition rate offset Δf remains constant as described by Equation (1.1):

$$\Delta f = f_{pump} - f_{probe}. \tag{1.1}$$

In most systems, the time delay, τ_d, covered is the inverse of the pump laser repetition rate ($\tau_d = 1/f_{pump}$), since the ultrafast process of interest is initiated each time the pump laser fires. Periodically, a particular probe laser pulse will be delayed by exactly τ_d relative to a particular pump laser pulse, that is, the probe laser pulse will synchronize with the following pump laser pulse. The length of scanning time, t_d, needed to allow this pump-probe synchronization to occur is simply the inverse of the repetition rate offset, or $t_d = 1/\Delta f$. Scan rates from 100–1000 Hz are readily accessible via offset locking even for long time delays.

A theoretical maximum time-delay resolution, $\Delta\tau_d$, for an ASOPS system can be calculated by dividing the time delay, τ_d, by the number of probe pulses, N_{probe}, available for sampling the full time delay during each scan period, t_d, or $\Delta\tau_d = \tau_d/N_{probe}$. The number of probe pulses available is given by the equation $N_{probe} = f_{probe}\,\mathrm{x}\,t_d$. Equation (1.2) combines these expressions to define

the theoretical maximum time delay resolution of the instrument as defined by the minimum time delay step between consecutive probe pulses:

$$\Delta\tau_d = (\tau_d/t_d)\,\mathrm{x}\,(1/f_{probe}). \tag{1.2}$$

ASOPS is an attractive method for high-resolution time-domain spectroscopy thanks to the ability to access fine time-delay resolutions across long time delays. The particular point in time delay, $\tau(t)$, that is sampled is a function of scan time elapsed between a particular probe pulse at time, t, and the scan time corresponding to the most recent overlap of pump and probe pulses, denoted by t_0. When the elapsed scan time, $(t - t_0)$, is equal to t_d, a new scan begins with a new t_0. This repetitive progression of time delay is described by Equation (1.3):

$$\tau(t) = (\tau_d/t_d)\,\mathrm{x}\,(t - t_0). \tag{1.3}$$

Here the ratio τ_d/t_d is the *time scaling factor* introduced by ASOPS.[15] Effectively, this scaling factor converts the ultrafast time scales associated with the laser pulses into a scan (laboratory wall clock) time that is far more amenable to sampling by conventional electronics, and once characterized allows the generation of a time delay axis directly from the scan time axis of the acquired data.

ASOPS may be applied to THz-TDS by using two ultrafast oscillators, one to pump a broadband THz emitter and the other to probe the generated THz radiation in the time domain, typically via electro-optic sampling.[16] Frequency content is extracted from the time-domain data by a fast Fourier transform (FFT), allowing THz-TDS to overcome broadband detector noise through the multiplex principle. To highlight the potential of ASOPS based THz-TDS, the capabilities of two recent ASOPS-THz-TDS instruments are listed here: A high-speed 1 GHz oscillator ASOPS-THz-TDS system with 7 THz of bandwidth that has achieved a mean frequency deviation of 142 MHz when measuring the line centers of water vapor absorptions from 0.2 to 6.3 THz[17; 18], and a high-resolution ASOPS-THz-TDS system based on two Er-doped fiber lasers achieved a mean frequency deviation of 4 MHz when measuring line centers of acetonitrile absorptions from 642.0 GHz to

643.2 GHz.[19] We stress that a single system has yet to demonstrate the ideal combination of high frequency resolution applicable to Doppler-limited spectroscopy while maintaining multi-decade spanning THz bandwidth. It should also be emphasized that the application of a given ASOPS-THz-TDS system to Doppler-limited spectroscopy is best accomplished through the operation of the system as a THz frequency comb spectrometer (THz-FCS), discussed in Section 1.5.

1.5 THz Frequency Comb Spectroscopy

The stabilization of the repetition rates of the Ti:Sapphire oscillators by PLL electronics ensures precision time delay sampling of a THz pulse train across a continuous time delay axis. Since the conversion of optical photons to mobile charge carriers within the THz emitter is sensitive to the intensity but not to the phase of the electric field of the pump laser optical pulse train, the resulting THz output is effectively CEP stabilized, at a constant zero phase offset. This means that the instrument is always operating as a THz frequency comb spectrometer (THz-FCS), with the frequency resolution determined by the length of continuous time delay sampled.[20; 21]

In ASOPS-THz-TDS mode most instruments sample a time delay of $1/f_{pump}$, that corresponds to the spacing between THz pulses in the time-domain. With proper data acquisition hardware, the width of the sampling window acquired, N_{pump}/f_{pump}, may be expanded to include multiple pulses, where N_{pump} is the number of THz pulses included in the window. Taking the FFT of such a THz pulse train produces a series of comb teeth, with a tooth spacing of f_{pump} and a transform limited FWHM (tooth width) of f_{pump}/N_{pump}. The comb teeth generated by processing a single THz pulse, as in standard implementations of ASOPS-THz-TDS, have a tooth width equal to the comb tooth spacing. This relation between the length of time delay sampled and tooth width allows a ASOPS-THz-TDS system to increase its effective resolution at the expense of full spectral coverage at a static f_{pump}.

Because scanning longer time delay windows produces narrower comb teeth, THz-FCS with broadband THz spectral coverage is impossible at a static f_{pump}. Active control over the pump laser repetition rate is needed to interleave the comb teeth to perform broadband THz-FCS (since

Table 1.1: A summary of recently reported THz-TDS systems. Those THz-TDS systems that were additionally demonstrated as THz-FCS systems are listed along with their parent systems. Detected bandwidth is defined as the envelope of the power spectrum above the noise floor in the frequency domain. Frequency resolution is defined as the comb tooth width for THz-FCS systems or as the repetition rate for ASOPS-THz-TDS systems. For THz-FCS systems the step size employed to interleave comb teeth is given in parenthesis next to the frequency resolution.

Oscillator Type	Center Wavelength (nm)	Rep Rate (MHz)	Pulse Duration (fs)	Avg Power (mW)	Detected Bandwidth (THz)	Offset Lock (Hz)	Time Delay (ns)	Frequency Resolution (MHz)	Averaging Time (min)	Mean Dev (MHz)	Ref
Ti:Sapph	825	1000	45	800	7.0	2000	1.0	1000	1	142	17,18
Er:Fiber	1550	56	50	110	1.5	5	17.8	56	16.7	4.0	19
Freq Comb	1550	250	50	110	2.0	50	400	2.5(2.5)	50	0.5	22
Ti:Sapph	800	80	>100	420	3.5	100	12.5	80	70	11.6	24
Freq Comb	800	80	>100	420	2.5	400	200	5(1.4)	280	0.1	24, 25

the carrier envelop phase is fixed). To cover the entire spectral region of interest, it is necessary to vary f_{pump} stepwise, changing the spacing between the comb teeth, producing a series of combs with different comb tooth spacings. Combining this series of combs produces a broadband interleaved frequency comb, with full spectral coverage at a resolution of f_{pump}. The first demonstration of broadband THz-FCS employed an Er:Fiber oscillator system with a comb tooth spacing of 25 MHz and a tooth width of 2.5 MHz, interleaved at 2.5 MHz steps to partially resolve the rotational structure of a single K-stack of acetonitrile at 150 mTorr.[22] The use of an Er:Fiber oscillator limits the THz bandwidth of this system, but its general principles of operation are similar to those of the dual Ti:Sapphire oscillator system described in this thesis. Very narrow comb spacing and resolution via coherent multi-bunch THz emission from a synchrotron enabled comparable measurements on acetonitrile[23], but the broadband generation of THz radiation requiring a synchrotron source limits the potential for widespread spectroscopic applications.

1.6 Outline and Summary of the Thesis

This thesis presents the design and capabilities of a high-resolution, broadband ASOPS-THz-TDS and THz-FCS system using two mode-locked 80 MHz Ti:Sapphire femtosecond oscillators offset locked by a phase-locked loop (PLL) operating at the 60^{th} harmonic (4.8 GHz) of their repetition rate(s). Additionally, synchronization of the pump oscillator to a Rb frequency standard via a PLL operating at the 12^{th} harmonic (960 MHz) of the oscillator repetition rate is described. The capabilities of the new instrument are compared to selected ASOPS-THz-TDS and THz-FCS implementations in Table 1.1.

Chapter 2 discusses the design of the system. The optics and overall system design are described in Section 2.1. A full description of the PLL electronics employed by the instrument is given in Section 2.2. In Section 2.3 methods for characterization of the time delay sampling performance of the instrument are described, including time-domain measurement with an air-gap etalon and an optical cross correlator, and frequency domain measurement of the error signal produced by the PLL circuit. A full description of the operation of the instrument is given in Chapter 3. Procedures

relating to the operation of the Ti:Sapphire oscillators are covered in Section 3.1, use of the PLL electronics to offset lock oscillator repetition rates is described in Section 3.2, and in Section 3.3, the configuration of hardware and software for optimal spectrometer performance is discussed.

In Chapter 4, gas-phase spectroscopy applications of the ASOPS-THz-TDS mode of operation are demonstrated by ASOPS-THz-TDS of H_2O and acetontirile. A description of processing raw time-domain and frequency domain data is given in Section 4.1. ASOPS-THz-TDS of water vapor absorptions from 0.55-3.35 THz is discussed in Section 4.2 and of CH_3CN absorptions from 0.13-1.39 THz is discussed in Section 4.3. The ASOPS-THz-TDS system achieves a signal-to-noise ratio (SNR) of 50 dB after 70 minutes of acquisition time. Comparison of measured absorption center frequencies for water vapor to reference data yield a root-mean-square (RMS) frequency deviation of 14.7 MHz and a mean frequency deviation of 11.6 MHz. While this ASOPS-THz-TDS mode covers a decade of bandwidth and is applicable to high-resolution gas-phase spectroscopy from 0.13 to 3.35 THz, the Doppler-limited measurements demanded by remote sensing or in situ applications require even finer frequency resolution.

As such, Chapter 5 describes the generation and detection of a decade-spanning frequency comb using the existing ASOPS-THz-TDS hardware and software. The modifications of offset locking and sample rate needed to acquire longer records including multiple THz pulses are discussed in Section 5.1. The interleaving of generated comb teeth via active control of the repetition rate of the pump laser is covered in Section 5.2. Stabilization of the pump laser repetition rate and generation of comb teeth with a tooth width of 3.7 kHz is described in Section 5.3.

Chapter 6 elaborates on how the modifications discussed in Chapter 5 enable THz Frequency Comb Spectroscopy (THz-FCS) with Doppler-limited frequency resolution down to an RMS of $\sim$100 kHz across the decade from 0.25–2.5 THz.[24] In Section 6.2, we present a fully resolved K-stack of acetonitrile, which is not possible for the instrument in ASOPS-THz-TDS mode. Section 6.3 describes the collection of data over a 18 pulse window to obtain a decade-spanning comb whose tooth spacing and width were $\sim$80 MHz and $\sim$4.4 MHz, respectively. The precision of the comb

is tested by the measurement of Doppler limited linewidths for water rotational transitions at 10 mTorr.[25].

The THz-FCS capability of the instrument is used to collect spectra for MeOH and MeOD from 1.0 to 2.5 THz with a measurement accuracy of 400 kHz. These measurements are discussed in Chapter 7. Finally, Chapter 8 outlines near term upgrades to the system achievable via pulse compression and THz generation/detection optimization that would enable century-spanning bandwidth, that is, high-resolution gas-phase spectroscopy from 0.1 to 10 THz. Future spectroscopy applications of the spectrometer are covered in Chapter 9.

Part II

Static Terahertz Frequency Comb or Asynchronous Optical Sampling Based Time-Domain Spectroscopy

Chapter 2

System Design

Parts of this chapter are reproduced from "A decade-spanning high-resolution asynchronous optical sampling terahertz time-domain and frequency comb spectrometer," by J.T. Good, D.B. Holland*, I.A. Finneran, P.B. Carroll, M.J. Kelley, and G.A. Blake, Review of Scientific Instruments* ***86****, 103107 (2015). [* Co-first author]*

The successful implementation of an ASOPS-THz-TDS system requires a thorough understanding of the generation and detection of THz radiation, in addition to a knowledge of Time-Domain Spectroscopy. This chapter discusses the design principles of the spectrometer. Considerations relating to THz bandwidth, delay time sampling accuracy, and phase-locked loop (PLL) circuit design are covered. The proper choice of optics to minimize dispersion of pump and probe laser pulses is detailed. A full schematic of the PLL circuit design is provided, along with a description of the components and design elements of the circuit. Finally, the characterization of the delay time sampling accuracy of the system is described.

2.1 Optics and Overall System Design

We employ two Ti:Sapphire femtosecond oscillators (Micra-5, Coherent Inc.) factory equipped with cavity mirrors controlled by piezoelectric actuators to enable active control of their repetition rates. Both have repetition rates of ∼80 MHz, ∼420 mW of output power at a center wavelength of ∼800 nm, and a pulse duration of ∼50 fs, which can be shortened to a transform-limited duration of

15 fs with external pulse compression. The short pulse durations and high pulse bandwidths of these oscillators are ideal for pulsed THz generation, and also enable broadband electro-optic (EO) sampling of the generated THz pulses in the time-domain. The repetition rates of the pump and probe lasers are offset locked maintaining an offset of 100 Hz. With this offset, the system covers 12.5 ns of time delay in 10 ms of scan time, supporting a time-delay sampling resolution of 15.6 fs.

The entire spectrometer is contained on a single floated optical table to isolate the system from low frequency acoustic noise and both the pump and probe lasers are chilled by the same water chiller to ensure that any temperature fluctuations are common mode. Other than these two considerations no additional care is needed to operate the instrument as a frequency comb spectrometer. A schematic detailing the optical elements and the associated electronics employed by the system is shown in Figure 2.1. Due to the high bandwidth of the 800 nm pulses, it is advisable to use low group velocity dispersion (GVD) optics to minimize broadening of the pulses. As such, low GVD high-reflectivity mirrors (10B20UF.25, Newport) are employed throughout the system. Even so, external pulse compression is needed to mitigate the effects of GVD added by the chosen optics as demonstrated in Chapter 3.

2.1.1 THz Generation via Photoconductive Emitter

The pump laser is used to generate pulses of THz radiation. First, a periscope is used to rotate the polarization of the laser pulses from s- to p-polarized. A low GVD beam sampler (10B20-01NC.2, Newport) reflects 10% of the pump laser power, which is subsequently split by a series of two identical low GVD beam splitters (10RQ00UB.2, Newport) to provide power to the pump and clock photodiodes and the scan triggering subsystem, discussed in Section 2.1.3, and transmits 90% of the power. The transmitted power is focused through a low GVD plano-convex fused silica (FS) lens (SPX028, Newport) to a spot size of 300 μm to pump an interdigitated photoconductive GaAs THz emitter (Tera-SED 3, Laser Quantum).[26] The polarization and the spot size of the pump beam incident on the emitter must be optimized for ideal emitter performance as discussed in Section 3.3.1.

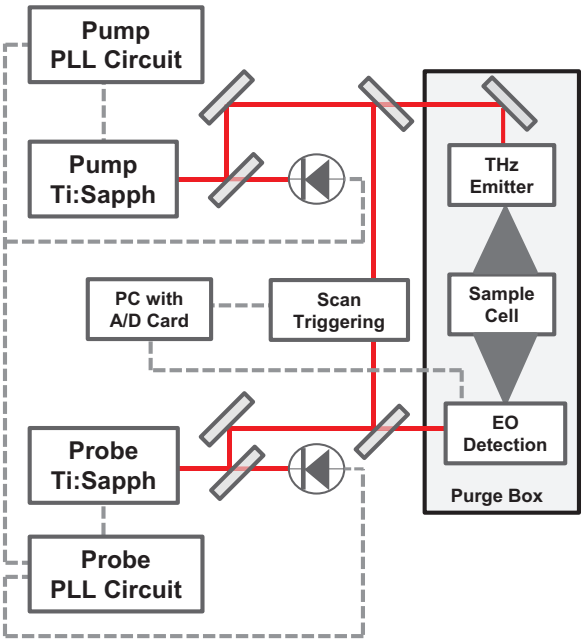

Figure 2.1: A schematic of the ASOPS-THz-TDS system design. Solid red lines represent optical paths, dashed grey lines electrical signals. THz beam paths are represented by triangles. Figure 2.2 provides a more detailed schematic of the overall system design and optics while Figure 2.3 provides a detailed circuit diagram for the PLL electronics.

Such large area emitters provide a substantial increase in average THz power, and have bandwidth extending well into the 3-6 THz region when properly optimized.[27] The emitter is DC biased at 15V. Each pump laser pulse incident on the emitter produces a pulse of THz radiation that is routed by off-axis parabolic mirrors (OAPMs) through a custom built sample cell with Topas (cyclic olefin copolymer) windows, an inner diameter of 5 cm, and a path length of 12.7 cm. Once THz pulses have interacted with the sample, they are focused onto a 1 mm thick, wedged ZnTe (110) crystal (INGCRYS Laser Systems Ltd.). A custom built purge box (Cleatech LLC) with an extra thick base and FS windows (210-1202E, Eksma Optics) encloses all of the THz routing optics and is flushed with dry nitrogen to remove water vapor from the THz beam path. THz pulses are subsequently detected via EO sampling by the THz detection subsystem.

2.1.2 THz EO Detection

The probe laser is used to detect the pulses of THz radiation generated by the pump laser. A low GVD beam splitter (10RQ00UB.2, Newport) reflects half of the power from the probe laser to the THz detection subsystem and transmits half of the power to the scan triggering subsystem, discussed in Section 2.1.3. A low GVD beam sampler (BSF10-B, Thor Labs) subsequently reflects 10% of this transmitted power to the probe photodiode. The detection system senses THz pulses via the electro-optic effect.[28] Probe laser pulses are sent through an indium-tin oxide (ITO) window, which is reflective at THz frequencies, allowing 800 nm probe pulses and THz pulses to be simultaneously focused onto a ZnTe crystal.

The THz pulses generate a transient birefringence in the ZnTe crystal, which rotates the polarization of the probe pulse by an amount directly proportional to the magnitude of the THz electric field (this is hereafter referred to as Electro-Optic detection). The probe laser pulses gate the Electro-Optic (EO) detection, and so their duration at the ZnTe crystal is critical to the detection bandwidth. Optimization of the probe laser pulse width through the use of low GVD optics along the probe beam path leading to the EO detection set up, and the choice of EO detection crystal is further discussed in Section 3.3.2. Once the THz and probe pulses have interacted, it is no longer important to avoid high dispersion optics. A doublet achromat (AC254-75-B, Thor Labs) is used to focus the probe pulses through the polarization detection optics. The change in polarization induced by the THz electric field is measured by sending the probe pulse through a quarter waveplate ($\lambda/4$, 10RP54-2, Newport), followed by a Wollaston prism (WP10-B, ThorLabs), which splits the probe pulse into its component polarizations. Finally, the THz-induced shift in polarization is detected by an AC-coupled balanced photodetector with 15 MHz detection bandwidth (PDB440A-AC, ThorLabs).

2.1.3 Optical Scan Triggering

An ASOPS based THz-TDS system requires a reliable scan triggering method to ensure accurate averaging of multiple scans. In our instrument, the scan triggering subsystem is essentially an optical

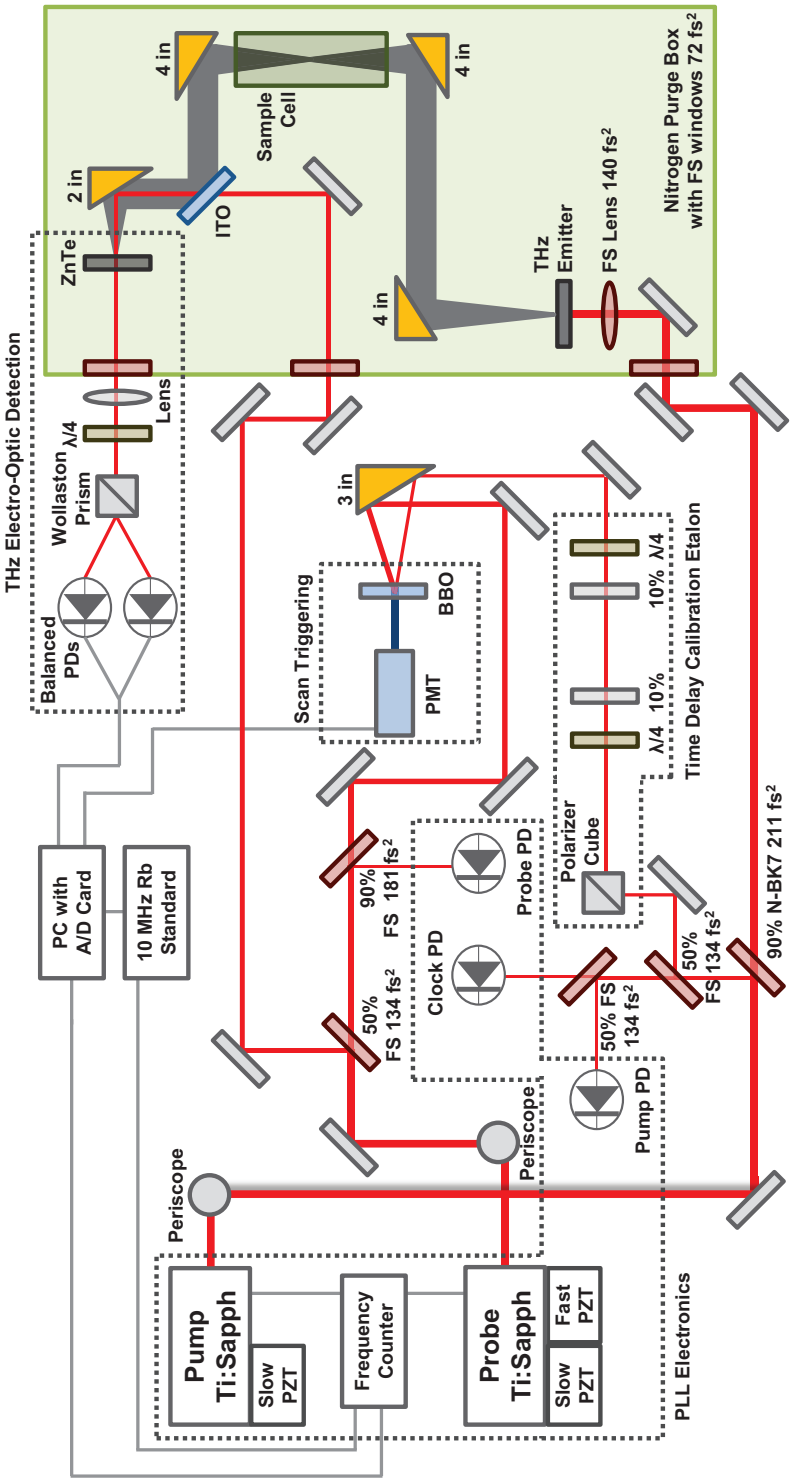

Figure 2.2: A schematic of the ASOPS optical table layout. Broadband high-reflecting mirrors are unlabeled. Beam splitters (90%), beam samplers (50%), and etalon mirrors (10%) are labeled with their transmission percentage. OAPMs are labeled with their reflected focal length. Transmissive optics are shown in red and are labeled with their material and total GDD contribution. The PLL electronics used for laser repetition rate control are omitted here and depicted in Figure 2.3 for clarity. Optical paths are shown in red with widths proportional to the beam power in each path. Electrical signals are shown in grey.

cross-correlator in which pump and probe pulses are focused off of the same OAPM onto a β-barium borate (BBO) frequency doubling crystal. This configuration emits a pulse of 400 nm light each time a synchronized pump-probe pulse pair arrives. An iris is used to block any 400 nm signal originating from single pulses and a band-pass filter (10BPF70-400, Newport) is used to block any residual 800 nm light from reaching a photomultiplier tube (PMT) (R928, Hamamatsu), which is part of an assembly that includes a built in high voltage power supply (H957-08, Hamamatsu). The PMT converts these 400 nm pulses into an electrical signal which is subsequently amplified using a current preamplifier (SR570, Stanford Research Systems). The amplified PMT signal is used as the trigger for the digitizer card (ATS9462, AlazarTech) that records the time-domain signal generated by the balanced photodetector. With the addition of optics described further in Section 2.3.1, this subsystem can alternately be used as a time delay calibration etalon to characterize the time-delay accuracy of the instrument.

2.1.4 Signal Digitization and THz Bandwidth

Over the course of a full scan, the electric field of the THz waveform is sampled across the entire time delay between successive THz pulses. The analog signal from the balanced photodiodes is digitized by the 16-bit digitizer card (within a 32-bit averaging environment) at a user determined sampling rate and stored on a personal computer. The digitizer card sampling rate is referenced to a 10 MHz Rb frequency standard (SIM 940, Stanford Research Systems) housed within a SIM 900 mainframe (Stanford Research Systems) to ensure an accurate time base, as any deviations in sampling rate will translate to errors in time delay, which will ultimately limit the frequency accuracy of the spectrometer. A frequency counter (5384A, HP) is also referenced to the Rb standard and monitors the pump laser repetition rate, which determines the precise amount of time delay covered during a single scan. This frequency counter simultaneously monitors the probe laser repetition rate, which allows the user to verify that the PLL electronics are maintaining a constant offset.

We are able to use a balanced photodetector with a 3 dB point of 15 MHz thanks to the time scaling effect of ASOPS. For a repetition rate of 80 MHz and an offset lock of 100 Hz the time

scaling factor is 1.25x10^{-6}, meaning that a maximum bandwidth of 12 THz can be sampled with these settings. When acquiring ASOPS-THz-TDS data, we set the sampling rate to 160 MSa/s which gives two data points per probe pulse (incoming at a rate of 80 MHz). This sampling rate may then be decimated to lower rates such as 40 MSa/s for the acquisition of THz-FCS data, where we operate at an offset lock of 400 Hz with a time scaling factor of 5x10^{-6}. This allows the acquisition of multiple THz pulses in a single record, while still sampling the full system bandwidth.

Provided there are no limitations imposed by the data sampling rate, we should be able to detect frequency content out to the roll-off bandwidth of the balanced photodetector at 12 THz as shown in Section 3.3.3. However, for the present system with a ZnTe EO detection crystal, we only observe frequency content out to 3.5 THz. In Section 3.3.2, we substitute GaP for ZnTe in the EO detection subsystem, but do not observe frequency content above 3.5 THz.

For a GaAs THz emitter such as the one employed by our setup, bandwidth is highly dependent on the duration of the 800 nm pump pluses used. Drude-Lorentz simulations of GaAs interdigitated THz emitter behavior predict that a pulse width of 50 fs will limit the emitter bandwidth to 12 THz and a pulse width of 100 fs will limit the emitter bandwidth to 6 THz.[10] Efforts at reducing the pump laser pulse width at the emitter covered in Section 3.3.1 were successful in increasing the system bandwidth. However, without employing a pulse compressor, the pump laser pulse width is broadened to >100 fs, limiting the emitter bandwidth to 3.5 THz. The covered bandwidth can therefore be improved in the future by compression of pulse width to below 50 fs to ensure emitter output up to 10 THz. This level of pulse compression is readily accomplished for the Coherent Micra lasers employed in our spectrometer, which support a transform limited pulse duration of 15 fs. We measure the timing jitter of the system in Section 2.3, which is another potential factor that can limit the observed bandwidth.

2.2 Phase-Locked Loop Circuit Design

Our ASOPS based THz-TDS system employs a microwave frequency PLL circuit operating at the 60^{th} harmonic of the respective laser repetition rates to maintain a constant frequency offset between

the pump and probe lasers. The probe laser is equipped with two piezoelectric actuators (PZTs), one fast and one slow, which enable offset locking of the probe laser via adjustments of its cavity length by displacement of two separate cavity mirrors. To enable the use of our system as a frequency comb spectrometer we additionally synchronize the pump laser repetition rate relative to a reference frequency via a second PLL operating at the 12^{th} harmonic of the pump laser repetition rate. The pump laser is equipped with a slow PZT allowing active control of the pump laser repetition rate via displacement of a cavity mirror.

Our system, shown in detail in Figure 2.2, achieves superior performance as a THz frequency comb spectrometer thanks to the high quality PLL employed to offset lock the pump and probe lasers. Since such a high quality lock circuit is not currently commercially available, we detail the construction of the lock circuit from commercially available components. A circuit diagram of the PLL is provided in Figure 2.3. Operating at high harmonics enables excellent phase discrimination and thus superior repetition rate control. For example, in previous synchronization of two 100 MHz Ti:Sapphire lasers across a long time delay, a precision of 4.3 fs was achieved with a PLL operating at the 80^{th} harmonic.[29] Here, the 60^{th} harmonic was chosen as a balance between the performance of high bandwidth photodiodes and microwave circuitry and cost. Verification of the pump stabilization PLL circuit performance is readily accomplished via monitoring of the pump laser repetition rate by the frequency counter. Characterization of the time delay fidelity of the pump-probe offset lock is more involved, requiring measurement of precisely delayed laser pulses directly in the time-domain. We perform this measurement using an air-spaced etalon, as described in the following section.

2.2.1 Monitoring the 60^{th} Harmonic of the Pump and Probe Repetition Rates

In order to operate the PLL at the 60^{th} harmonic of the pump and probe laser repetition rates, we combine high-quality band pass filtering with low-noise amplification to generate a monitoring signal for each laser. For the purposes of the following description, assume the lasers are offset locked at $\Delta f = 100$ Hz with the pump repetition rate synchronized to 80.0001 MHz and the probe repetition

rate following at 80.0000 MHz. A small amount of power from the pump and probe lasers is routed to a pair of 12.5 GHz GaAs PIN photodiodes with 30 ps rise/fall times (ET-4000, Electro Optics Technology). Their output is run through a pair of tunable band-pass filters (201925, Coleman Microwave) to select the 60^{th} harmonic of the photodiode signals. The filtered 4.800006 GHz signal from the pump photodiode is first amplified by a 25 dB low-noise amplifier (ZX60-542LN-S+, Mini Circuits) and then by a 15 dB secondary amplifier (ZX60-V62+, Mini Circuits), to levels near +7 dBm. This signal is monitored by a directional coupler (2617S, Krytar) and routed to the LO input of the pump double balanced mixer (M14, Watkins Johnson). The filtered signal of 4.800000 GHz from the probe photodiode is first amplified by a 25 dB low-noise amplifier (ZX60-542LN-S+, Mini Circuits) and then by a 15 dB secondary amplifier (ZX60-V62+, Mini Circuits), again to levels near +7 dBm. This signal is monitored by a directional coupler (26732, Narda) and routed to the LO input of the probe double balanced mixer (M14, Watkins Johnson). The combination of each monitoring signal with an appropriate offset signal by these mixers is described below.

2.2.2 Monitoring the 12^{th} Harmonic of the Pump Repetition Rate

To avoid cross-talk between the two PLL circuits and to provide the appropriate monitoring frequency for the pump control circuit, we use a similar circuit as that described above to generate a separate monitoring signal at the 12^{th} harmonic. Another fraction of power from the pump laser is routed to a separate clock 1.2 GHz Si PIN photodiode with a 300 ps rise/fall time (ET-2030, Electro Optics Technology). A tunable band-pass filter (937931, Integrated Microwave) is used to select the 12^{th} harmonic of the photodiode output. The filtered 960.0012 MHz signal from the clock photodiode is amplified to +8 dBm by a 30 dB low-noise amplifier (ZRL-1150LN, Mini Circuits) and monitored by a directional coupler (10014-10, Anaren). This amplified signal is split by a series of two identical power splitters (ZAPD-900-5W-S+, Mini Circuits). Half of the output of the first splitter, at a power level of +5 dBm, is used as a monitor signal of the pump laser repetition rate by the pump synchronization PLL circuit described later. The other half is routed to the second splitter, which outputs two signals, both at a power level of +2 dBm, used to clock two identical

direct digital synthesizer (DDS) boards (AD9912, Analog Devices). These DDS boards are then used to add the desired frequency offset to the monitoring signals.

2.2.3 Asynchronization via DDS Generated Frequency Offset

Since we desire an offset lock of 100 Hz and are monitoring the laser repetition rates at their 60^{th} harmonic, we use the DDS boards to add a 6 kHz relative offset between the pump and probe laser monitor signals. After adding this frequency offset, the monitoring signals may be compared directly by a phase detector to generate an error signal as in a standard synchronization PLL circuit. The pump DDS board is programmed to generate a +2 dBm signal at 70.0000 MHz, which is routed to the IF input of the pump mixer where it mixes with the 4.800006 GHz signal from the pump photodiode. A tunable band-pass filter (565-5246-004, Collins) is used to select the mixer addition signal at 4.8700006 GHz. This signal is attenuated by 3 dB (VAT-3+, Mini Circuits) and then amplified (ZX60-5916M-S+, Mini Circuits, 18 dB gain) to +7 dBm (ZX60-5916M-S+, Mini Circuits). This signal is monitored by a directional coupler (4203-10, Narda) and routed to the RF input of the final double balanced mixer (M14, Watkins Johnson).

The probe DDS board is programmed to generate a +2 dBm signal at 70.0060 MHz, which is routed to the IF input of the probe mixer where it mixes with the 4.800000 GHz signal from the probe photodiode. A tunable band-pass filter (565-5246-004, Collins) is used to select the mixer addition signal at 4.8700006 GHz. This signal is routed through a 3 dB attenuator (VAT-3+, Mini Circuits) and then amplified (ZX60-5916M-S+, Mini Circuits, 18 dB gain) to +7 dBm. This signal is monitored by a directional coupler (1211S, Krytar) and routed to the LO input of the final mixer, which operates as a phase detector such that any deviation from the offset lock at $\Delta f = 100$ Hz produces an error signal.

The error signal from the IF output of the final mixer is passed through a 1.9 MHz low-pass filter (BLP-1.9+, Mini Circuits) to block unwanted high frequency mixer addition products and the error signal is amplified by a low-noise voltage preamplifier (SR560, Stanford Research Systems) set to a gain of 100. This preamplifier is equipped with an onboard low-pass filter, which is set with its

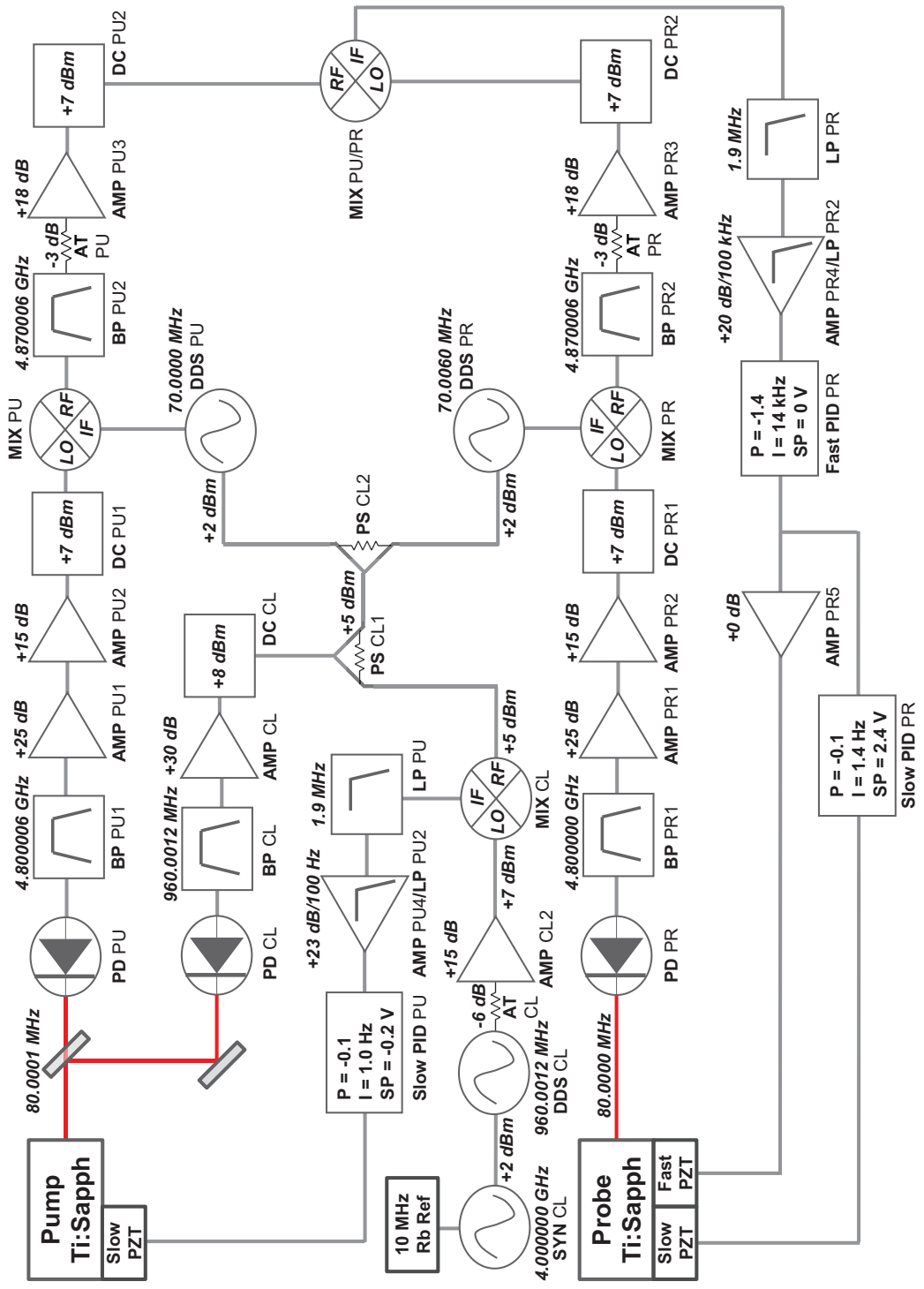

Figure 2.3: A schematic of the PLL electronics used to offset lock the repetition rates of the pump and probe lasers and to lock the pump repetition rate to a frequency standard. Optical paths are shown in red, and electronic signals are shown in grey. Abbreviations are as follows: PU = pump, PR = probe, CL = clock, PD = photodiode, BP = band-pass filter, AMP = amplifier, DC = directional coupler, AT = attenuator, PS = power splitter, DDS = direct digital synthesizer, MIX = mixer, LP = low-pass filter, PID = proportional-integral-derivative controller, PZT = piezoelectric actuator, SYN = frequency synthesizer.

Table 2.1: PID controller parameters used for offset locking of the pump and probe lasers and for stabilization of the pump laser to a frequency standard.

PID Loop	P	I (Hz)	SP (V)	Off (V)	Limits Lower/Upper (V)
probe fast	-1.4	14000	0	5	0/+10
probe slow	-0.1	1.4	2.4	0	-5/+5
pump slow	-0.1	1.0	-0.2	0	-5/+5

-3 dB point at 100 kHz with a 6 dB/octave roll-off, to further attenuate unwanted high frequency mixer products. The conditioned error signal is used to offset lock the laser repetition rates via PID control of the probe laser repetition rate.

2.2.4 Offset Locking Pump and Probe Repetition Rates via PID Control

We employ two PID controllers working in tandem to apply corrections based on the error signal, maintaining a high-fidelity offset lock. The slow and fast probe PID controllers (SIM 960, Stanford Research Systems) are both housed in the SIM 900 mainframe and operate according to Equation (2.1):

$$Output = P \,\mathrm{x}\, (\epsilon + \; I \,\mathrm{x} \int \epsilon \, dt) + Off. \tag{2.1}$$

Here Off is a static offset and ϵ is the error signal given by the equation $\epsilon = SP - Input$, where SP is a static set point. The chosen values of I effectively limit the bandwidth of the probe fast PID to 14 kHz and the bandwidth of the probe slow PID to 1.4 Hz, thus preventing interference between the two PID controllers. The chosen values for the variables in Equation (2.1) for the various PID controllers are given in Table 2.1.

The conditioned error signal is routed to the input of the of the probe fast PID, the output of which is amplified by a line driver evaluation board (THS6012 EVM, Texas Instruments) to ensure that there is enough current to drive the low capacitance, fast PZT without phase delay. The board is powered by a ±15 V supply and acts as a current buffer, producing unity gain. The amplified probe fast PID signal compensates for transient deviations in the probe laser repetition rate for offset deviations of ±22 Hz. The output from the probe fast PID is sent to the input of the probe slow PID

and the output of the probe slow PID is routed to the probe slow PZT. The probe slow PZT has a high capacitance and effectively acts as a low pass filter, correcting for gradual offset deviations of ±3.2 kHz. This dual PID configuration allows the probe slow PID to monitor the probe fast PID, keeping the probe fast PID within its voltage limits. With both probe PID controllers engaged, the probe laser and pump laser will remain offset locked at $\Delta f = \Delta f_{DDS}/60$, where Δf_{DDS} is the difference between the programmed frequency outputs of the probe DDS and pump DDS and 60 is the number harmonic of the monitoring circuit.

2.2.5 Stabilization of Pump Laser Repetition Rate

The stabilization of the pump laser repetition rate is accomplished by a standard synchronization PLL circuit that compares the actual repetition rate of the laser to a desired value generated by a frequency synthesizer that is referenced to the Rb frequency standard mentioned previously. The synthesizer (5008, Valon Technology LLC) generates a reference frequency of 4.000000 GHz at a power level of +2 dBm that serves as the clock signal for the clock DDS board (AD9914, Analog Devices), which divides this reference frequency down to the 12^{th} harmonic of the desired repetition rate of the pump laser – 960.0012 MHz for this description.

The clock DDS board is tunable in 1 Hz steps, enabling tuning of the pump laser repetition rate to mHz precision. The -2 dBm output of the clock DDS is first attenuated by 6 dB (VAT-6+, Mini Circuits) and then amplified to +7 dBm by a 15 dB low-noise amplifier (ZFL-1000LN+, Mini Circuits). This signal is routed to the LO input of a level 7 mixer (ZFM-12-S, Mini Circuits). The +5 dBm signal from the first power splitter is routed to the RF input of this mixer, which operates as a phase detector. The resulting error signal from the IF port is low pass filtered (BLP-1.9+, Mini Circuits) and amplified by a low-noise voltage preamplifier (SR560, Stanford Research Systems) set to a gain of 200. This preamplifier is equipped with an onboard low-pass filter, which is set with its -3 dB point at 100 Hz with a 6 dB/octave roll-off.

The conditioned error signal may then be used to stabilize the pump laser repetition rate. The amplified error signal is routed to the input of the pump slow PID controller (SIM 960, Stanford

Research Systems) housed in the SIM 900 mainframe, which is tuned according to the parameters listed in Table 2.1. The output of the pump slow PID is routed to the pump slow PZT which corrects for slow drifts in the pump laser repetition rate. It has a high capacitance and corrects for deviations of ±2.9 kHz. The tuning of the pump slow PID controller limits its bandwidth to 1.0 Hz to avoid disturbing the stability of the pump laser repetition rate on short timescales. All three PID controllers may be run simultaneously to stabilize both lasers to an accuracy dictated by the Rb frequency standard, 10^{-11}, which corresponds to ∼0.8 mHz precision relative to the ∼80 MHz pump laser repetition rate.

2.3 Characterization of Instrument Time-Delay Performance

The actual time-delay resolution of an ASOPS system is determined by the degree of accuracy to which the PLL electronics can maintain a constant repetition rate offset.[15] The time delay axis is reset every time a new scan is triggered, but time-delay jitter can accumulate during each scan period. An additional concern is variable time-delay performance from scan to scan. To characterize these effects we utilize a time delay calibration etalon.[30]

2.3.1 Time-Domain Analysis with an Air-Spaced Etalon

Here an air-spaced etalon formed by 90% reflective mirrors is inserted into the path of the pump laser before the cross-correlator.[31]. A pair of quarter wave plates (10RP54-2, Newport) and a polarizing beam splitter cube (05FC16PB.5, Newport) serve to prevent back reflections from propagating toward to the pump laser. This configuration transmits 1% of the pump laser power as a trigger pulse with no added time delay and 9% of the pump laser power as a series of pump laser pulses that have taken successively more round trips in the etalon cavity, with corresponding successive addition of time delay as described by Equation (2.2):

$$\tau_\eta = (2 \text{ x } N \text{ x } l_\eta)/c, \tag{2.2}$$

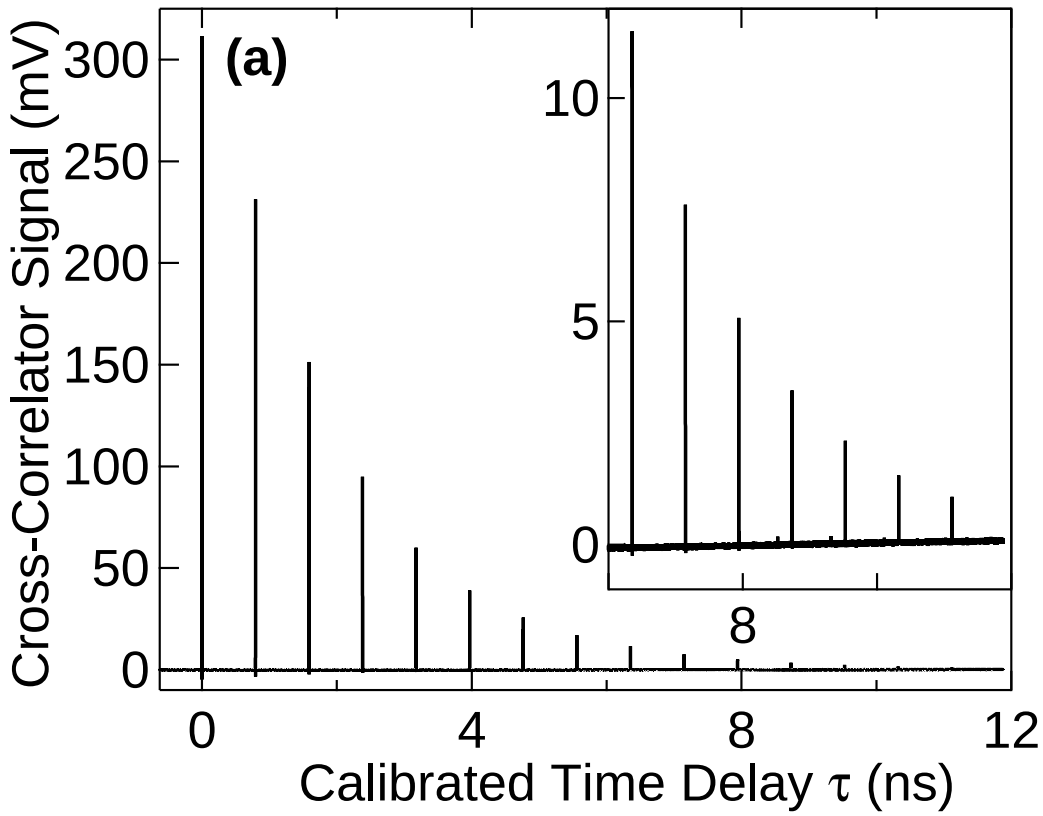

Figure 2.4: Raw time domain trace of successively delayed cross-correlator peaks. To obtain the calibrated time delay, the center of the first peak, which is used to trigger the scan, is set to zero. The inset details signal extending to 12 ns.

where τ_η is the time delay added to a particular pump laser pulse by the etalon cavity, N is the number of round trips taken by the pulse, l_η is the distance between the inner faces of the etalon cavity mirrors, and c is the speed of light. These pulses are detected by the triggering subsystem and digitized. The pump and probe lasers are offset locked at 100 Hz during the measurement and so the ultimate sensitivity of the following measurements is limited by the 2.2 ns rise time and 1.2 ns transit time jitter of the PMT, which are converted by the time scaling factor to 2.8 fs and 1.5 fs, respectively.

A time-domain trace of the trigger signal acquired by averaging 10000 scans over 3.5 minutes of wall clock time is shown in Figure 2.4, and the inset provides a zoomed in view to reveal signal out to 12 ns of delay. The peak centers and FWHM values for this averaged trace are fit using Gaussian

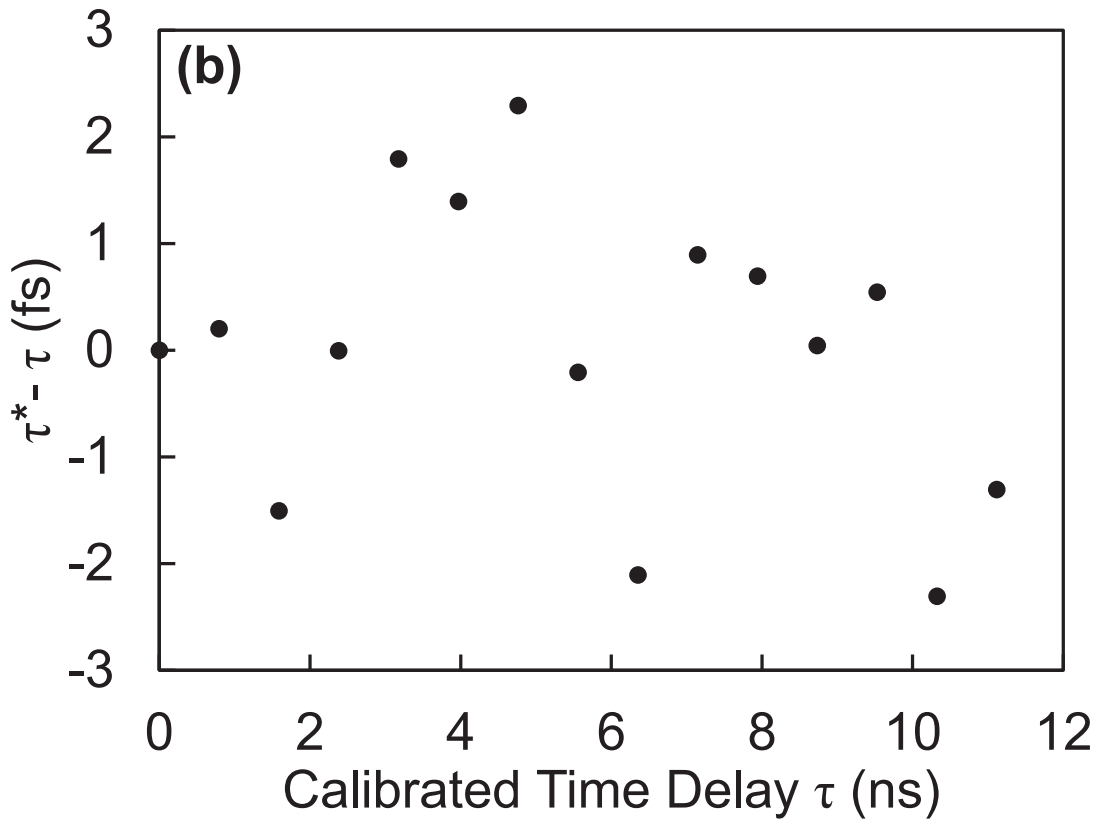

Figure 2.5: Deviation of the measured minus calibrated time delay ($\tau^* - \tau$) vs. calibrated time delay (τ). The RMS deviation is 1.4 fs with a maximum deviation of 2.3 fs.

line shapes. The average spacing between extracted peak center positions is calculated and used to determine that $\tau_\eta = 794.089$ ps, $l_\eta = 11.9031$ cm. This value of τ_η is used to generate a calibrated delay-time axis. The measured time delay, τ^*, is extracted from each peak center and compared to the calibrated time-delay, τ, yielding a RMS deviation of 1.4 fs and a maximum deviation of 2.3 fs. The deviation for each peak center in Figure 2.4 is plotted in Figure 2.5. Since this is a co-added measurement, any systematic timing jitter will accumulate and shift the mean deviation of the peaks away from zero, while random timing jitter will broaden the peaks, without shifting their mean deviations. Random timing jitter that changes from scan-to-scan can be observed by measuring deviations in the FWHM of the peaks obtained. The RMS deviation is 3.7 fs with a maximum deviation of 4.9 fs as shown in Figure 2.6.

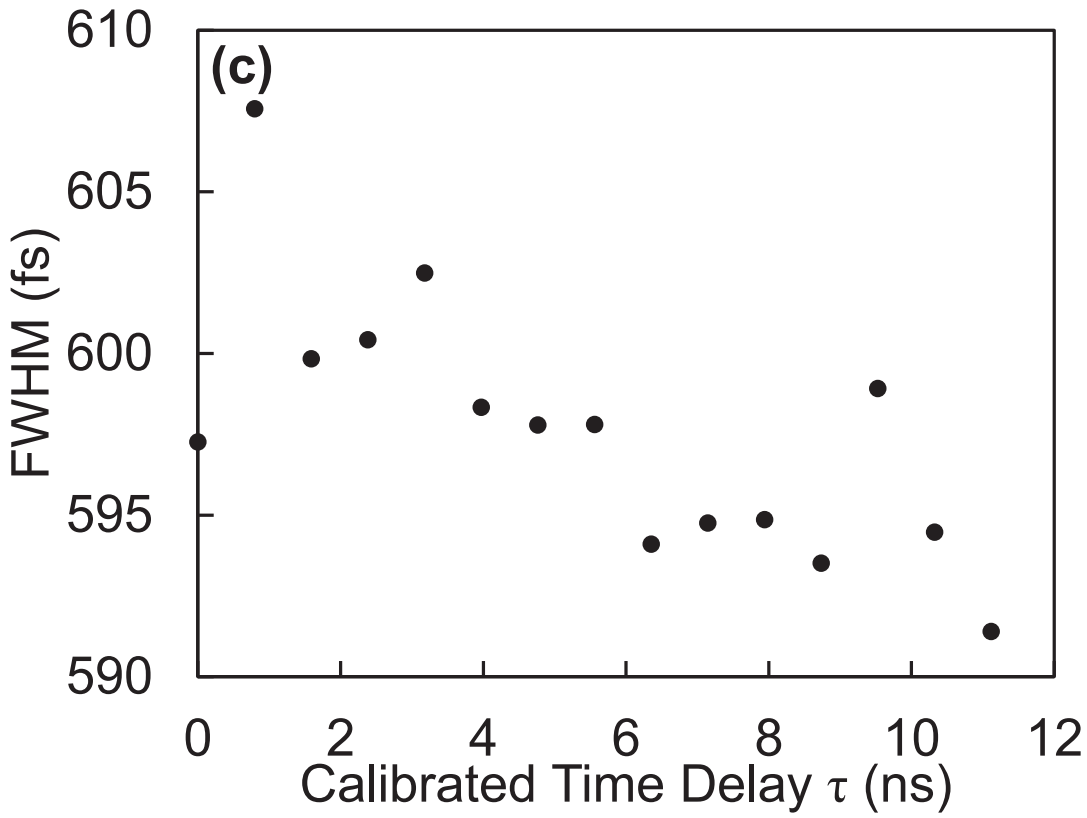

Figure 2.6: FWHM of etalon cross-correlation peaks vs. calibrated time delay. The RMS deviation is 3.7 fs with a maximum deviation of 4.9 fs.

Calibration of time delay using an air-spaced etalon is an attractive method for the precise characterization of timing jitter thanks to the simultaneous acquisition of all of the time delay peaks by a single measurement, and the accuracy of the fixed length of the etalon cavity.[32] However, the optics associated with the air-spaced etalon and cross-correlator, especially the polarizing beam splitter cube, add significant GDD (>1000 fs^2). Consequently, the measured FWHM values of 600 fs are not indicative of the actual laser pulse widths at the THz emitter and electro-optic detection crystal. The 1 MHz bandwidth of the current preamplifier additionally limits the time delay resolution of the measured pulse widths. The actual jitter of the PLL circuit is likely near the detection threshold of these measurements.

2.3.2 Frequency-Domain Analysis of the PLL Error Signal

To confirm this assumption, we conducted an additional measurement of the timing jitter of the system by determining the power level of the noise relative to the carrier signal of 4.87 GHz at +7 dBm in the frequency domain. We characterized the frequency content and power level of the error signal of the final mixer using a baseband network analyzer (SR770, Stanford Research Systems). Since the bandwidth of the probe fast PID controller is 14 kHz and scan triggering is at 100 Hz, we integrated the noise contributions from 100 Hz to 14 kHz corresponding to the values of the black trace shown in Figure2.7 according to Equation (2.3):

$$J_{RMS} = \frac{1}{2\pi f_c}\sqrt{2\int_{f_1}^{f_2} 10^{\frac{L(f)}{10}} df}, \tag{2.3}$$

where the RMS jitter, J_{RMS}, is integrated over the bandwidth of interest from f_1 to f_2, the carrier frequency is f_c, and the power relative to the carrier as a function of frequency is $L(f)$, in units of decibels relative to carrier (dBc). The error signal was measured with a power gain of 100, so we applied a correction of -20 dBc to the error power relative to the carrier frequency power account for this. This calculation estimates the random RMS jitter over the PLL bandwidth to be 15.4 fs. Since the theoretical maximum time delay sampling of this instrument is 15 fs, a timing jitter at or near this level implies that the bandwidth of the instrument is not currently limited by the PLL electronics. These measurements may be verified via detection of improved bandwidth in the future, once improvements to the THz generation and detection subsystems have been implemented.

Monitoring of the error signal in real time while tuning PID controller parameters is an excellent way to characterize the performance of the lock circuit. Some experimentation with different values of I shows that the chosen value of 1.4 x 10^4 is ideal in terms of reducing the error signal. Although the higher bandwidth tuning performs better at low frequencies, this improvement is offset by poorer performance at higher frequencies. The performance of different circuit components may also be characterized by monitoring the error signal. Optimization of the error signal should be verified by measuring the THz bandwidth and actual performance of the spectrometer, but measurement of the

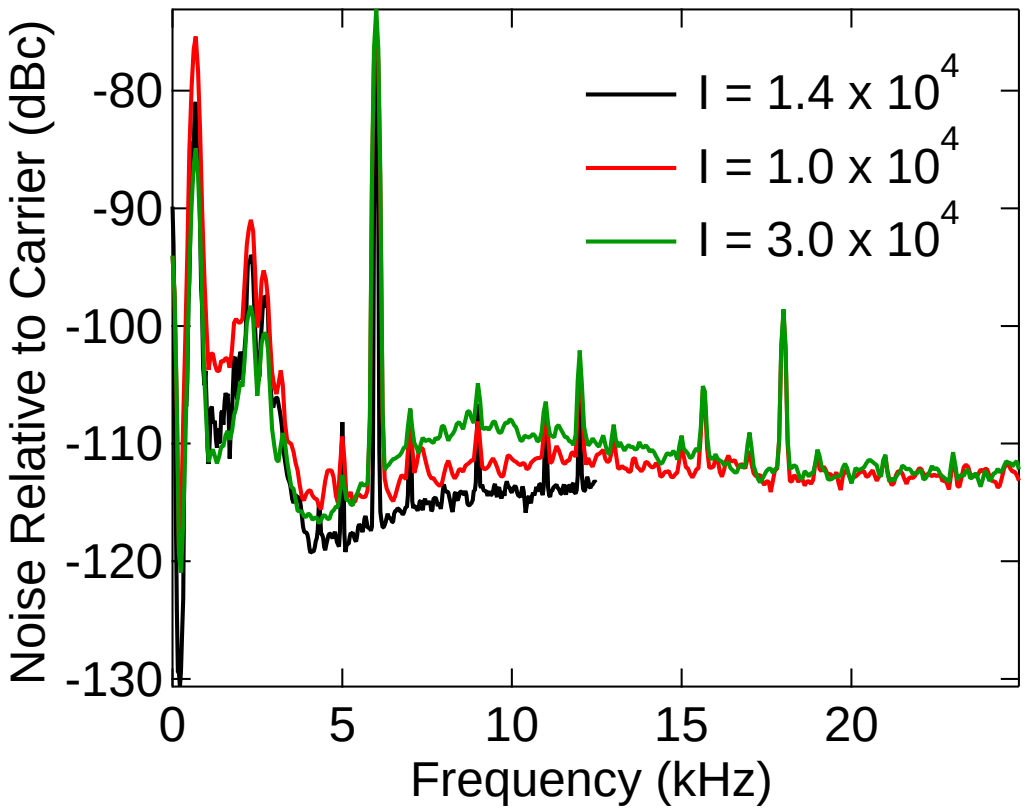

Figure 2.7: Magnitude relative to the carrier signal intensity of the frequency content of the offset lock PLL error signal, most of the error is within a bandwidth of 5 kHz relative to the carrier frequency. The bandwidth of the PLL circuit in units of Hz is equal to the value of the I parameter chosen for the probe fast PID controller.

error signal provides an excellent indicator of the expected spectrometer performance for a given set of PID controller tuning parameters.

Chapter 3

Acquisition of THz-TDS Spectra

This chapter is intended to serve as a user's manual for operation of the spectrometer and troubleshooting of common issues. A detailed overview of how to operate its numerous components is given, along with preferred power on and off procedures and specific hardware and software settings not covered previously. Also provided are descriptions of the monitoring software for the PLL circuitry and laser repetition rates, and software for automated control of the repetition rates of the pump and probe lasers.

3.1 Laser Startup Procedures, Maintenance, and Monitoring

Since the performance of the entire spectrometer depends upon the stability of both the power and the repetition rates of the Ti:Sapphire lasers, we shall begin with a discussion of optimal start up and maintenance procedures for the lasers. A major source of both power and repetition rate fluctuation for the lasers is temperature variation of the laboratory environment throughout the day. In order to minimize such fluctuations, both lasers are equipped with a metal baseplate in thermal equilibrium with cooling water that is temperature controlled and recirculated by a single chiller. The focusing of laser light onto the Ti:Sapphire crystal is the main source of heat within the laser cavity, and as such the laser cavities should be allowed to come to thermal equilibrium once the lasers have been powered on. This focusing of light onto the Ti:Sapphire crystal also tends to burn small pieces of dust onto the crystal, requiring periodic cleaning of the crystal, described later.

3.1.1 Chiller Startup Procedure

The optimal procedure for minimizing the required equilibration time is to first turn on the chiller and allow the laser cavities to cool down to near the set point temperature, generally 21 °C. This reduces the thermal load on the chiller and allows the laser baseplates to reach thermal equilibrium more quickly. The ideal scenario is to cool to near the equilibrium temperature of the laser cavities with the laser on. This requires the user to wait about 30 minutes after powering on the chiller to power on the lasers themselves. When this is done properly, it will take roughly 30-45 minutes for the lasers to come to thermal equilibrium.

If the lasers are turned on too quickly, the chiller will be under a larger thermal load while it attempts to bring the laser cavities into thermal equilibrium. Since the focusing of laser light adds heat to the laser cavities, the actual equilibrium temperature of the cavities tends to be in the range of 24-25 °C as given by the reading on the front control panels of the lasers. As such the ideal starting temperature for turning the lasers on is 23 °C. If the chiller is left on for too long before turning on the lasers, one must wait for the heat input of laser focusing to slowly heat the cavity back up to equilibrium. Both of these non-ideal scenarios can take 2-3 hours of equilibration time to allow for full equilibration of the laser repetition rate, so it is better to use the optimal startup procedure whenever possible. The progress of thermal equilibration may be monitored by using the frequency counter to monitor the repetition rates of the lasers as described in Subsection 3.1.4.

3.1.2 Laser Startup Procedure

Once the ideal baseplate startup temperature has been achieved, the lasers may be started by turning the ignition keys from standby to on. Before turning on the lasers be sure that all potential beam paths are contained to ensure that there are no stray beams that may harm the user or other occupants of the lab. Upon turning the key, the laser will slowly increase the current on its green pump laser until sufficient green laser power is focused on the Ti:Sapphire crystal to induce lasing, producing 800 nm light. At this point the laser will apply a voltage pulse to the galvo, or slow PZT, attached to a starter mirror, vibrating the mirror. These vibrations will rapidly vary the

amplitude of the laser light, and variations with a frequency corresponding to the path length of the cavity will constructively interfere. Such constructive interference leads to a pulsed output with a repetition rate that is precisely controlled by the length of the laser cavity in a process referred to as mode-locking.

Typically, the lasers will mode-lock within a few minutes of initial power on. Upon achieving mode-lock, the display on the laser control box will indicate MODELOCKED and display the power level as measured by an internal slow photodiode within the laser cavity. An additional fast photodiode within the laser cavity monitors the repetition rate of the laser. The signal from this fast photodiode is routed from the back of the laser and to the frequency counter, so that the repetition rate may be monitored. Occasionally, the starting mechanism of the pump laser will fail to initialize. The user can manually start the process by accessing Main Menu, Micra Settings, AutoModelock ON/OFF and cycling the AutoModelock setting from ON to OFF to ON. This menu also has an option for Power Track ON/OFF. Power Track is a feature that rasters the green laser beam across the Ti:Sapphire crystal face, until optimal power level and mode-locking is achieved. Cycling this feature from ON to OFF to ON can also help with mode-locking issues where the green laser beam is stuck in a dirty or non-ideal spot on the Ti:Sapphire crystal. If the lasers still fail to achieve mode-lock after these settings have been cycled, then the Ti:Sapphire crystal is likely too dirty and requires cleaning as described in the next section.

3.1.3 Ti:Sapphire Crystal Cleaning

Focusing of green pump light onto the Ti:Sapphire crystal enables lasing at 800 nm but has the unfortunate side-effect of burning tiny pieces of dust and other contaminants onto the surface of the crystal. As dirt accumulates on the crystal face, Power Track has a more difficult time finding clean spots on the crystal that support lasing. Eventually, light scattering off of dirty spots on the crystal will start to produce unwanted power noise. If allowed to get dirty enough, the crystal will no longer support mode-locking. Periodically, a rigorous cleaning is required to scrub dirt off of the crystal and restore high-quality laser performance.

Although sapphire is a very hard material, care must still be taken when cleaning to avoid damage or further contamination of the crystal surface. The Ti:Sapphire crystal may be safely cleaned according to the following procedure. Open the top panel of the laser to be cleaned, and unscrew the manual interlock override tab from the top of the laser. Screw the tab in to engage the interlock lever, and press the Menu Exit button on the laser control box to clear the error message. Turn on the laser to be cleaned, and press the appropriate Power Level button on the front panel to decrease the green pump laser power to a safe level. Once the green laser is on, inspect the front and back faces of the Ti:Sapphire crystal for specks of dirt, which very noticeably reflect green light.

If there are unacceptable levels of scattering, proceed to clean the crystal surface with a folded piece of lens tissue held with a hemostat and moistened with several drops of reagent-grade (99.9%) methanol (don't waste spectroscopic grade Methanol for cleaning!). Before cleaning the crystal, block the green beam with a matte black object such as a short post holder so you can see what you are doing and avoid dangerous reflections of the beam off of the hemostat. Since sapphire is hard and the dirt you are trying to clean is well adhered to the surface, use a firm scrubbing motion across the face of the crystal several times, followed by a single sweep of the lens tissue from one side to the other to clear any dirt that was dislodged by the scrubbing. Let the green laser beam pass through the crystal to see if your cleaning was effective, checking to see if the amount of scatter is significantly reduced. Repeat the scrubbing process with fresh pieces of lens tissue until you are satisfied with the reduction of scattered green laser light. Replace the top cover and then press the appropriate Power Level button to restore full power and check to see if mode-locking occurs. Note the power level and the fact that the laser was cleaned in the laser log file.

3.1.4 Laser Repetition Rate Monitoring Software

Once the lasers are on, they will come to thermal equilibrium with the chiller water being circulated through their baseplates. The thermal expansion or contraction of the laser cavities will manifest itself as a respective decrease (an expanding cavity will have an increasing path length) or increase in repetition rate. Automated software is used to monitor the changes in repetition rate to ensure

that the lasers are stable before engaging the offset lock and taking data. To use this software, first turn on the frequency counter. Then call the software located in the following directory using the command prompt:

```
C:\freq_counter_code\frequency_combs.py
```

This Python program will bring up a GUI with two buttons, click the Plot Stripchart button. The program will then communicate with the frequency counter via GPIB, displaying the repetition rates of the pump and probe lasers in the command prompt every second. A chart plotting the repetition rate of the pump laser will also be displayed, an example is shown in Figure 3.1.

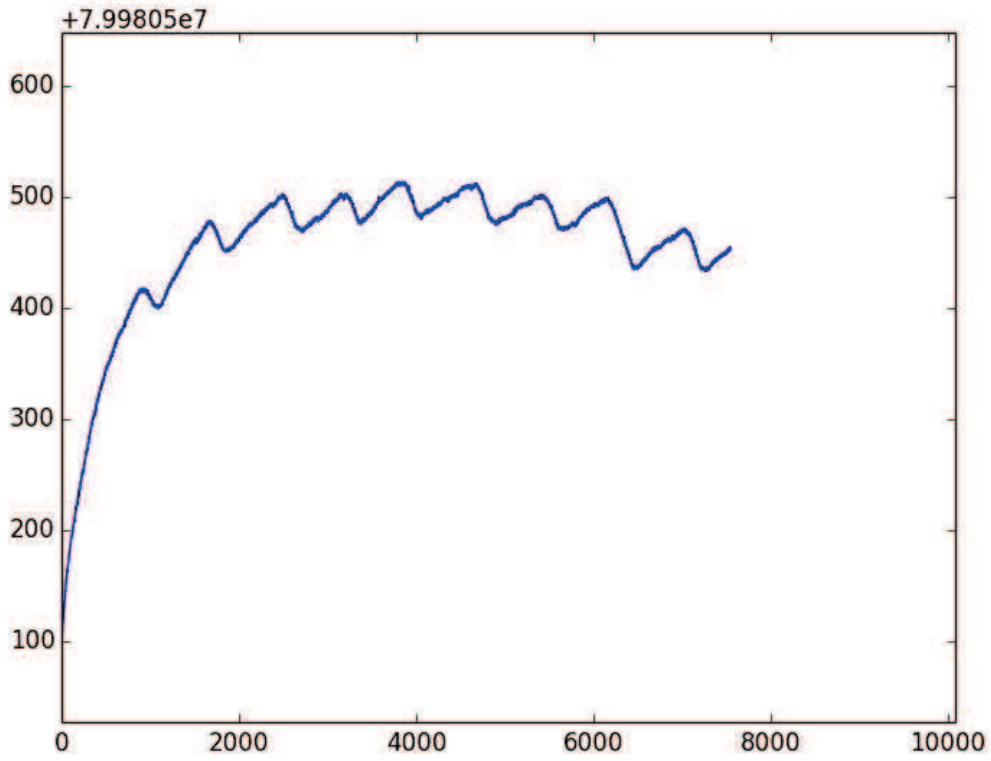

Figure 3.1: A plot of pump laser repetition rate in Hz versus time in seconds. The sinusoidal variation has a peak-to-peak amplitude of approximately 50 Hz and is due to the limited ability of the chiller to hold a precise temperature.

The large systematic variation of several hundred Hz in Figure 3.1 occurs while the lasers are approaching thermal equilibrium. Once thermal equilibration is complete, the repetition rate of the

lasers is mostly flat, but will still feature sinusoidal variations over short timescales. These variations are due to the limited ability of the chiller supplied by Coherent to hold a precise temperature. The system may benefit from an upgrade to a more stable chiller in the future. Once the system has come to thermal equilibrium as indicated by repetition rate monitoring, the PLL offset lock may be engaged, along with the pump laser control circuit.

3.2 PLL Monitoring and Operation

The part numbers, circuit design, and circuit diagram for the PLL circuits employed by the spectrometer were given in Chapter 2. Procedures for the daily operation of the PLL to offset lock the pump and probe lasers and to stabilize the pump laser are given here. Engaging both the offset lock PLL and pump laser stabilization PLL will eliminate the slow sinusoidal drift shown in Figure 3.1, stabilizing the repetition rates of both lasers to milliHertz (mHz) precision.

3.2.1 PLL Monitoring

The offset lock PLL is used to maintain a constant offset between the pump and probe lasers, enabling ASOPS. The pump laser stabilization PLL is used to stabilize and control the pump laser repetition rate, enabling THz-FCS. A circuit diagram of the both PLL circuits is given in Figure 2.3. The successful operation of these circuits depends on maintaining appropriate RF power levels at key points in the circuits, monitored by directional couplers. These directional couplers output a DC voltage proportional to the RF power passing through the coupler. The user may simultaneously monitor the coupler DC voltages using an external USB DAQ card (USB-6001, National Instruments) and monitoring software written in LabVIEW. To run the monitoring software, double click on the ASOPS_monitor.vi program located on the desktop. Once the program initializes, click the Run button to begin monitoring. This software displays the RF power levels in dBm that correspond to the DC monitor voltages measured by the directional couplers during operation of the PLL circuits. In addition, control of the repetition rates of the lasers may be verified using the repetition rate monitoring software described previously.

3.2.2 Offset Lock PLL Operation

Once the lasers are in thermal equilibrium, it is time to power up the offset lock PLL circuit. First, turn on both fast photodiodes to begin monitoring the repetition rates of the pump and probe lasers. The slow photodiode is always on. For daily operation, the amplifiers and DDS boards are left powered on, so there should now be RF power in the system. Check the power level readouts in the monitoring software to ensure the power levels before all three mixers are within 1 dB of +7 dBm. Additionally check that the power level before the power splitters is within 1 dB of +8 dBm to ensure that the DDS boards are receiving an adequate clock signal. If the power levels before the pump and probe mixers are not within 1 dB of their set points, carefully adjust the incoming laser power on the fast photodiodes until correct the power level is displayed. If the pre-splitter power level is wrong, correct it by adjusting the incoming laser power on the slow photodiode. Slight adjustments should be sufficient here and if the power levels continue to drop even after adjustment, then the batteries that power the photodiodes are likely near dead and need replacing (confirm this using a voltmeter). Once appropriate power levels are obtained at all monitoring points the DDS boards should be updated if necessary.

The design of the offset lock PLL circuit allows us to choose the value of Δf, the offset lock between the pump and probe lasers, by adjusting the difference between the output frequencies of the DDS boards. A value of 100 Hz is used for ASOPS-THz-TDS and a value of 400 Hz is used for THz-FCS. Ensure that the outputs of the DDS boards are set to the proper values according to the equation $\Delta f = \Delta f_{DDS}/60$. An unfortunate drawback of the AD9912 DDS boards is that support for their USB to serial drivers was discontinued in versions of Windows newer than Windows XP. As such, they are controlled by a separate older Dell laptop running Windows XP located on the laser table. To adjust the programmed output of one of the DDS boards, plug the appropriate USB cable into the Dell laptop and open the AD9912 control software located on the desktop. For the most precise measurements, additionally update the clock frequency to the 12^{th} harmonic of the exact value of the pump laser repetition rate. Since the output frequency is calculated based on the clock frequency, be sure to update the desired output frequency after adjusting the clock frequency.

Once programmed, the DDS boards will continue running at the desired frequency until they are powered down or issued a new command. If appropriate power levels are observed before the pump and probe mixers, but incorrect power levels are observed before the final mixer, this means that the DDS boards are not functioning properly, and need to be reset. Once the DDS boards have been programmed and the power levels before the final mixer are at +7 dBm (deviations of ±1 dBm are acceptable) the offset lock PLL may be engaged.

With the offset lock PLL circuit energized, the final probe mixer will output an error signal which is routed to the probe fast PID controller. To engage the probe fast PID, adjust the manual voltage to +5 V, moving the probe fast PZT to the middle of its range of motion. Never change the 0 V lower limit and +10 V upper limits since these are used to prevent overdriving the probe fast PZT past its allowed range of motion. Then use the manual voltage control on the probe slow PID controller to adjust the repetition rate of the probe laser until it is within 5 Hz of the desired offset. Once the repetition rate offset is within 5 Hz, switch the probe fast PID controller from manual to PID control. At this point the $P\mathrm{x}\epsilon$ and *Out* LED displays should be near the center of their ranges with only one LED illuminated. If two lights are illuminated near the limits of the display, the controller is outside of its range. Switch back over from PID control to manual and use the probe slow PID controller to move the repetition rates close to the desired offset and try switching into PID control mode again. Once the probe fast PID is engaged, increase the gain on the probe SRS voltage preamp from 1 to 100 and verify that the lock is holding using the repetition rate monitoring software. The output signal of the probe fast PID is monitored by the probe slow PID, which applies corrections to keep the probe fast PID from going outside of its limits. To engage the probe slow PID, make sure that the controller is set to an internal setpoint and then switch from manual to PID control. At this point the Out display on the probe fast PID should move to the center of its range, if it was not already there. The offset lock PLL is now engaged and the pump and probe repetition rates will remain offset at the chosen value of Δf. The pump lock PLL may now be engaged, if desired.

3.2.3 Pump Repetition Rate Stabilization PLL Operation

With the pump and probe offset locked, stabilization of the pump laser repetition rate by the pump lock PLL will stabilize the repetition rates of both lasers to mHz precision. Such stabilization is necessary for long scans or high-precision spectroscopy. With only the offset lock PLL engaged, the repetition rate of the pump laser will still wander over long time periods as shown in Figure 3.2.

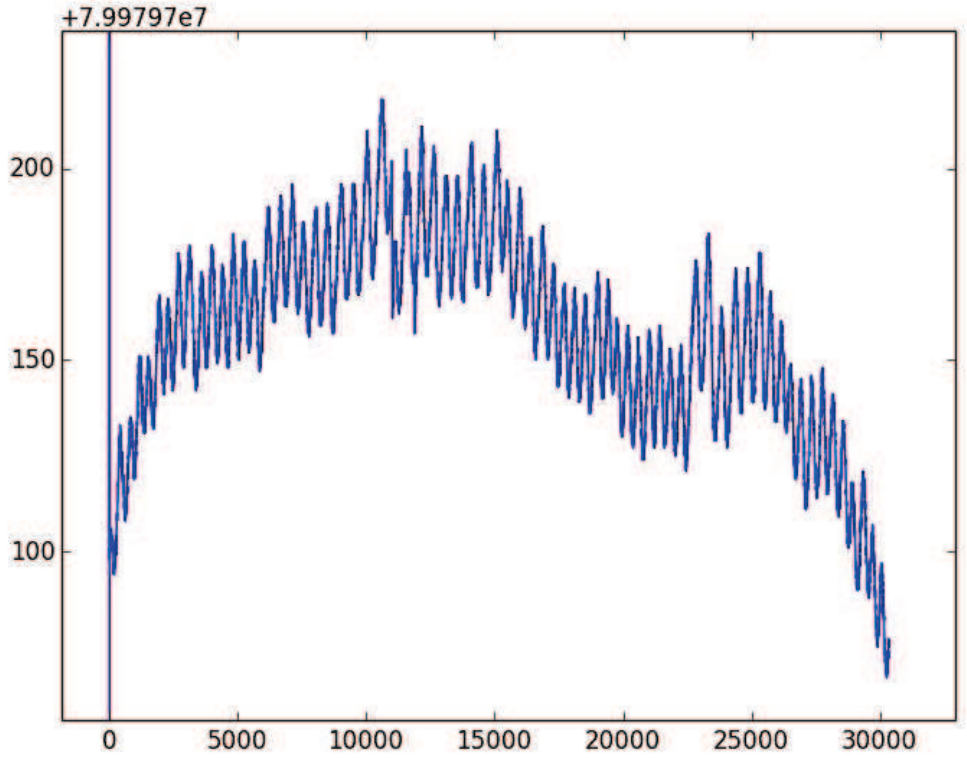

Figure 3.2: A plot of the pump laser repetition rate in Hz versus time in seconds. A consistent sinusoidal variation due to the chiller is superimposed on the long term wander of the repetition rate. This data set was taken over a time period of 8 hours.

The pump repetition rate stabilization (lock) PLL is employed to mitigate this unwanted repetition rate variation. To stabilize the pump repetition rate to an absolute frequency, a reference signal must be generated. We accomplish this in three stages. First we multiply the 10 MHz reference signal from our Rb clock up to 4 GHz using a Valon 5008 frequency synthesizer. Second we divide down from the referenced 4 GHz signal to the 12^{th} harmonic of the desired repetition rate with a

AD9914 DDS board. Finally, we compare the desired repetition rate with the actual repetition rate and generate an error signal, using PID control to stabilize the repetition rate.

To power up the pump lock PLL circuit, we must first program the frequency synthesizer. Open the Valon control software located on the desktop of the main control computer. Input the desired reference frequency of 4 GHz and click the RF output enable button so that it reads, RF output enabled. Be sure to set the reference frequency to 10 MHz and the reference select to external. Next, we will program the DDS board using the AD9914 control software, also located on the desktop. Open the control software and input the clock frequency of 4 GHz (important since the program will default to 3.5 GHz). Enable profile mode and input the 12^{th} harmonic of the desired pump laser repetition rate, and set the power scaling factor to 1.0. Then click the load button to upload the desired settings to the board, which will continually run using the specified settings until a new command is issued. For daily use, the amplifiers will already be powered up so the final pump mixer will generate an error signal that will be used by the pump slow PID controller to stabilize the pump repetition rate.

In order to engage the pump slow PID controller we will follow a similar procedure as for the probe fast PID controller. Here the error signal is too weak to engage the lock without gain, so first increase the gain on the pump SRS voltage preamp from 1 to 200. Then use the manual voltage control on the pump slow PID controller to bring the repetition rate of the pump laser within 1 Hz of the desired value and observe the value of the error signal. If necessary, adjust the internal setpoint to match the error signal while the pump laser repetition rate is at the desired value. Then switch the pump slow PID from manual to PID control. Check the repetition rate monitoring software to ensure that the lock is holding. If it is holding, the sinusoidal variations should be gone as shown in Figure 3.3. The gate time on the frequency counter may be increased to 10 seconds to show that the repetition rate is indeed stabilized to sub-Hz precision. Proper operation of the lock may also be verified by checking to see if the error signal readout on the pump slow PID controller is within 5 mV of the setpoint voltage. Once the desired repetition rate settings have been implemented, ASOPS-THz-TDS or THz-FCS spectra may be taken.

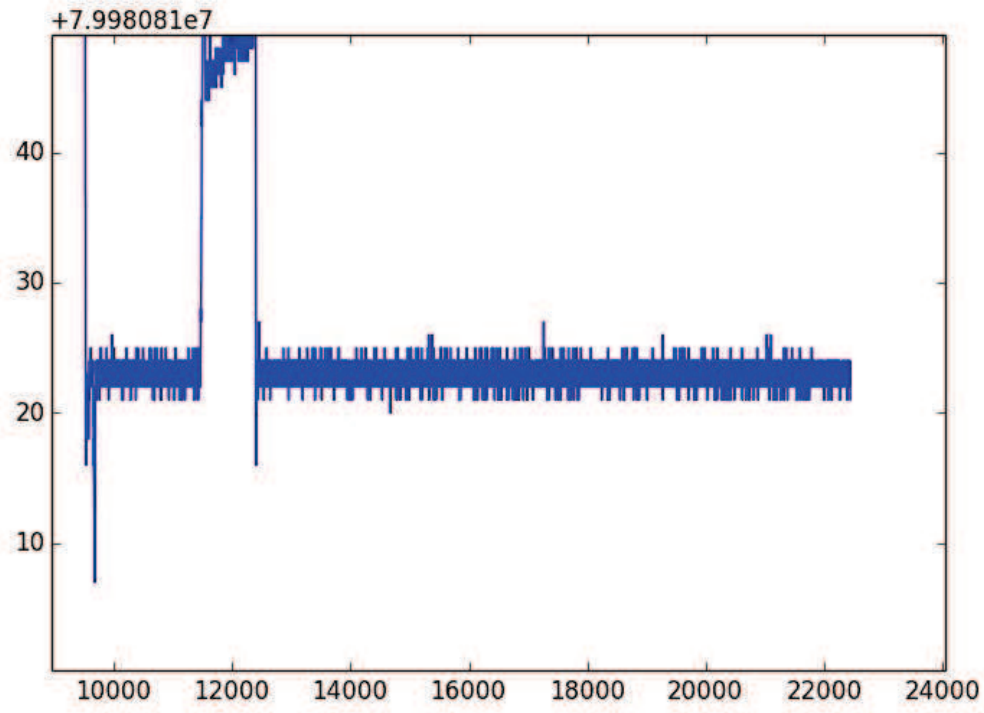

Figure 3.3: A plot of pump laser repetition rate in Hz versus time in seconds. The apparent repetition rate variation of ∼5 Hz here is actually due to the 1 second gate time of the frequency counter. The excursion at 12000 seconds was due to setting the pump slow PID to a non-ideal setpoint. This data was taken over a time period of 3 hours with $f_M = 79.980833$ MHz.

3.3 Acquisition of THz-TDS Spectra

Once the lasers are on and their repetition rates are under PID control, the system may be used to obtain THz spectra for samples of interest. Systems for generation and detection of THz radiation are described in Subsections 3.3.1 and 3.3.2. The operation of data acquisition hardware and software is described in Subsections 3.3.3 and 3.3.4. Additionally the implications of the ASOPS time scaling factor for data obtained with the current system setup are explored.

3.3.1 THz Generation

A GaAs photoconductive interdigitated emitter is used to generate pulses of THz radiation. The performance of this device is extremely sensitive to both the spatial and temporal characteristics of the 800 nm laser pulses incident on it. The user manual calls for a 300 μm spot size on the face

of the emiter to optimize the density of carriers liberated by an incident laser pulse for maximum THz bandwidth. In practice it is difficult to measure the spot size at the exact plane of incidence on the emitter. As such, a beam profiler is used to measure the spot size to ensure that it is in the correct ballpark. Then a translation stage is used for fine adjustments of the emitter along the axis of propagation of the laser beam, while monitoring the intensity of the THz radiation.

The pulse duration at the emitter is also critical to the bandwidth of the emitted THz radiation. High-bandwidth ultrafast laser pulses from the pump and probe lasers are highly susceptible to GVD, and will be temporally broadened after interaction with dispersive optics. An example of reduction in bandwidth due the use of high GVD doublet achromats is shown in Figure 3.4. Even with the use of low GVD optics, the addition of a pulse compressor can further improve THz bandwidth.

To use the GaAs emitter in our setup to generate THz radiation, we apply a 15 V accelerating voltage to the emitter electrode array with an external DC power supply. The emitter will sustain damage due to resistive heating if a CW power dissipation of 0.75 W is exceeded. This equates to a maximum photocurrent of 50 mA at 15 V, but for optimal focusing conditions using a Coherent Micra pump laser a photocurrent of closer to 25 mA is induced at 15 V. The device may be safely biased up to 30 V if the CW power dissipation requirements are met. Always operate the device while measuring the CW current with a multimeter to avoid resistive heating damage. To power up the emitter, simply dial up the voltage to 15 V while watching the current reading. Since water vapor in the atmosphere is highly absorptive of THz radiation, the purge box must be purged with dry nitrogen to avoid attenuation of the detected THz radiation.

3.3.2 THz Detection

A ZnTe or GaP crystal may be employed to detect THz radiation via electro-optic sampling with a 800 nm probe laser. To achieve efficient sampling, good temporal and spatial overlap of probe pulses with THz pulses is required. Due to the difference in the index of refraction for ZnTe or GaP at optical wavelengths versus THz wavelengths, each type of radiation will propagate through the crystal at a slightly different speed. The thicker the crystal, the longer the beam path and the

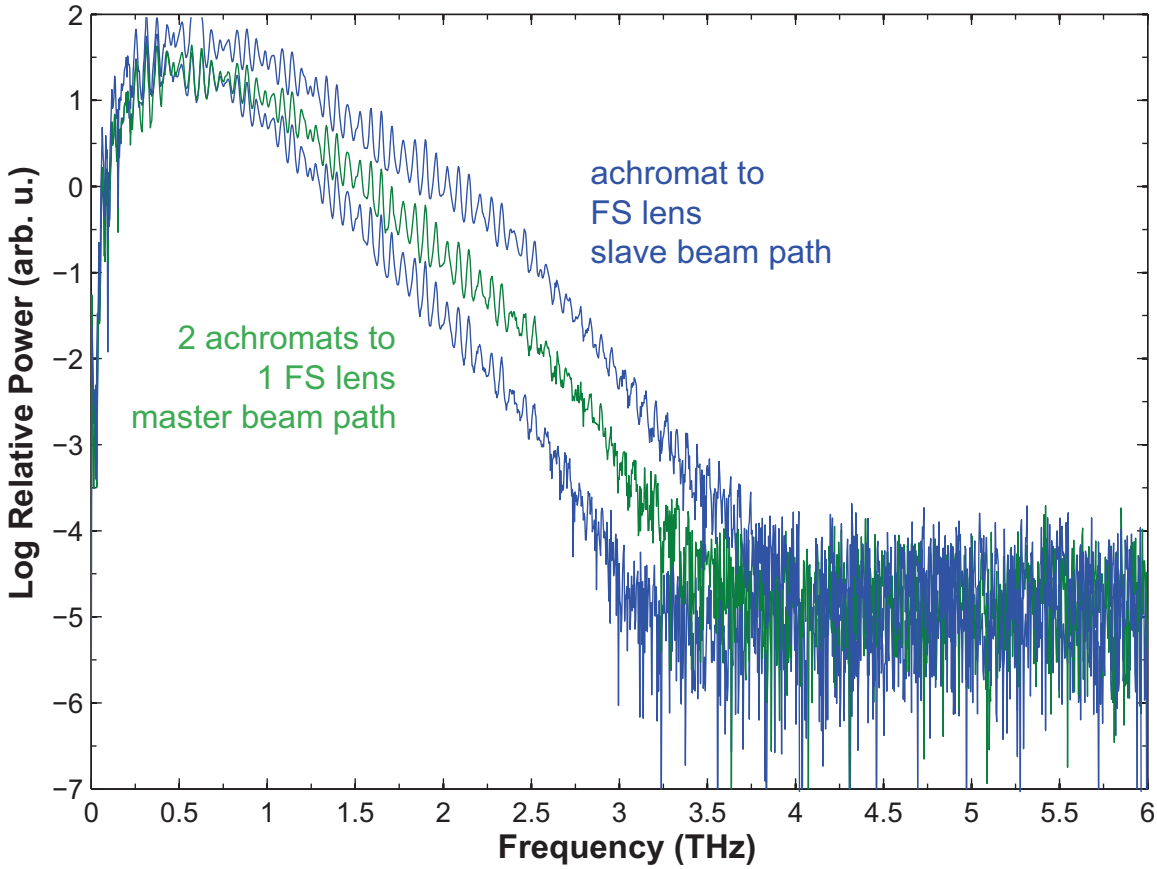

Figure 3.4: A plot of the THz bandwidth improvement obtained by exchanging achromats made of high GVD materials for low GVD fused silica (FS) lenses. The lowest bandwidth blue trace has high GVD optics along both the pump and probe beam paths. To achieve the green trace, two high GVD achromats were replaced with a single low GVD FS lens along the pump beam path leading to the emitter. To achieve the highest bandwidth blue trace, a high GVD achromat was replaced with a low GVD FS lens along the probe beam path, in addition to the replacements made along the pump beam path. Further improvements can be made by the addition of pulse compressors to the pump and probe beam paths

more temporal distortion added by the refractive index mismatch. This effect is illustrated in Figure 3.5 which compares the use two different thicknesses of ZnTe for the EO detection of THz pulses. As expected, the thin crystal achieves slightly better bandwidth, at the expense of EO conversion efficiency. However, ZnTe has phonon modes at 5 THz and 8 THz that fundamentally limit its THz EO detection capabilities above 4 THz. To determine whether the current instrument bandwidth is limited by the EO detection crystal or by the duration of the laser pulses themselves, EO detection using a 0.4 mm thick GaP crystal was tested.

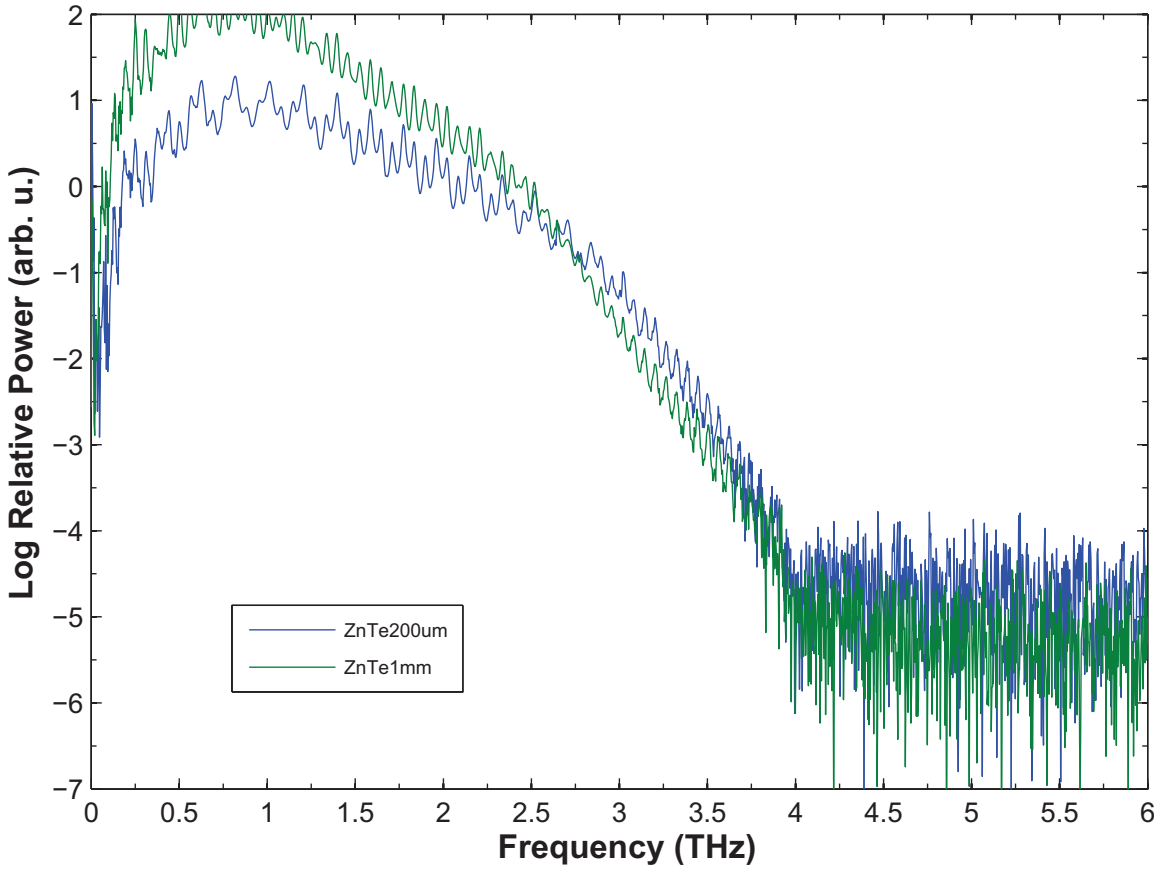

Figure 3.5: A plot showing the effect of decreased phonon absorption for a 1 mm thick ZnTe crystal versus a 0.2 mm thick ZnTe crystal. High frequency signal improves slightly but the thinner ZnTe crystal has a lower overall conversion efficiency.

A plot of detected bandwidth with GaP vs ZnTe is shown in Figure 3.6. The use of GaP instead of ZnTe for THz EO detection has advantages and disadvantages. One advantage is that the first phonon mode of GaP is past 8 THz, enabling higher bandwidth detection. Additionally, the index of refraction mismatch for optical and THz radiation in GaP is smaller than in ZnTe, resulting in less temporal distortion. However, a significant disadvantage is that the EO effect is roughly three times less efficient in GaP. For the current detection limits of our system, we see no improvement in bandwidth when using GaP for EO detection. To determine whether we are in a regime where the optical pulse width could limit our EO detection we take the inverse of the detected 3.3 THz bandwidth, which is approximately 300 fs. This corresponds to the pulse width at which our EO sampling pulse is too broad to measure frequency content higher than our bandwidth. According

to Drude-Lorentz simulations, a 200 fs pump laser optical pulse duration would limit our emitter bandwidth to 3 THz, so the fact that we detect THz bandwidth past 3 THz implies that our pulses are at most 200 fs broad.[10] This in turn implies that we can accurately sample frequencies of at least 5 THz using EO sampling.

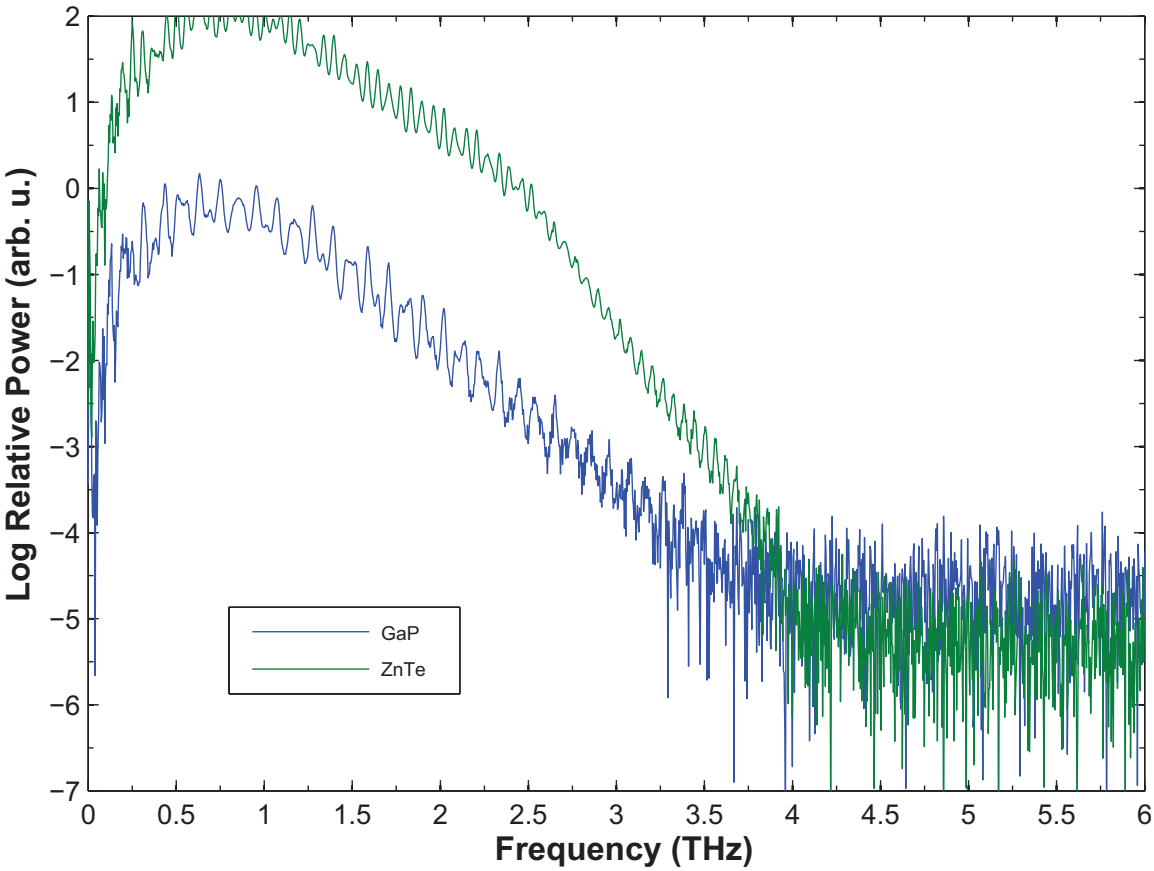

Figure 3.6: A plot showing the effect of the decreased EO coefficient of GaP versus ZnTe. The THz bandwidth obtained via EO detection with a 1 mm thick ZnTe crystal and with a 0.4 mm thick GaP crystal is equivalent for our current setup. An absorption shoulder due to the ZnTe phonon mode at 5 THz is visible starting at 2.5 THz, whereas for GaP the drop off in signal is linear (on a log plot) until it drops below the noise floor.

As far as the spatial alignment of the THz and optical beams on the EO detection crystal is concerned, a poor alignment can have a significant impact on observed bandwidth, as shown in Figure 3.7. Since higher frequency THz radiation will have a smaller focused beam diameter, a good alignment is critical for observation of high frequency THz content. An optimal technique for initial alignment of the THz beam through the OAPMs is to remove the THz emitter from its mount and

replace it with a ground glass beam diffuser. Be extremely cautious when handling the emitter, as static discharge or mechanical shock could easily damage the device. The diffuser will cause the optical beam to diverge in a similar fashion to the THz radiation propagating from the emitter. One can then optimize the shape of the focused beam to as close to circular as possible and estimiate its rough position of incidence on the EO detection crystal. Once a visual overlap of the focused probe and pump beams is achieved, reinsert the emitter. Ensure that the pump beam does not focus onto the area surrounding the emitter as it may melt the plastic or ablate debris onto the active emitter surface.

Once the emitter is properly aligned and powered up, it is time for the final alignment of the EO detection crystal and optics. The rotational orientation of the EO detection crystal will determine the EO conversion efficiency. The rotational orientation is easiest to optimize once a THz signal is available. For now a rough alignment of the doublet achromat, Wollaston prism, and balanced photodetector to ensure that the component polarizations are incident on the two photodiodes of the balanced photodetector will suffice. Turn on the power supply for the balanced photodetector and when the readouts of the DC monitor channels in the ASOPS monitor program are above 10 V for both photodiodes, the alignment is good enough to proceed.

3.3.3 Data Acquisition Hardware

The 3 dB point of the detection bandwidth of the balanced photodetector is 15 MHz. As discussed in Subsection 2.1.4, this imposes a THz bandwidth roll-off based on the ASOPS time scaling factor as determined by the ratio τ_d/t_d. We can invert this ratio to obtain the frequency scaling factor, which may be multiplied by the bandwidth of the detector, to determine the THz detection bandwidth achievable with ASOPS. The predicted 3 dB roll-off values as calculated in Table 3.1 may be compared to data acquired at various offset locks as shown in Figure 3.8. The product of number of traces averaged with record length was constant across this data set, to ensure that the dynamic range and noise floor were ultimately determined by the detector bandwidth. Data sets taken at Δf = 800 and 1600 show a clear roll-off at the frequencies predicted according to the reduction

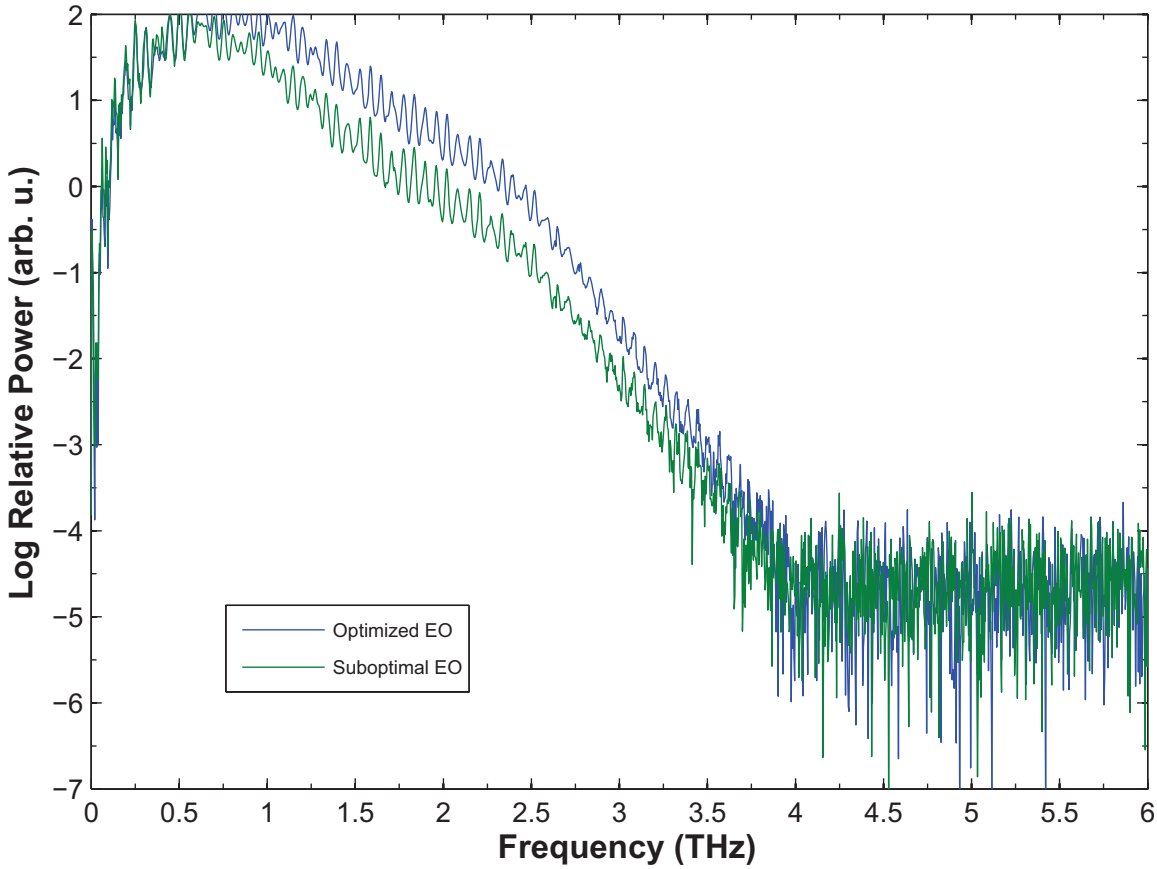

Figure 3.7: A plot showing the importance of optimized spatial overlap of the probe and THz beams to achieving maximum THz bandwidth. Note the comparable performance at lower frequencies (0.1 to 0.5 THz), but suboptimal performance at higher frequencies that leads to a decreased THz bandwidth.

in ASOPS frequency scaling factor, t_d/τ_d. This indicates that offsets between 100 and 400 Hz are suitable for acquiring THz spectra with the current setup.

We now turn our discussion towards the data card used to digitize and record the analog output of the balanced photodetector. Two important features of the digitizer card are the ability to trigger off of an external signal and to be clocked by an external reference. The onboard oscillators included with most digitizers lack sufficient precision to support high-fidelity sampling and certainly cannot match the one part in 10^{-11} accuracy of a 10 MHz Rb frequency standard. Referencing the digitizer card to our Rb frequency standard enables mHertz levels of sampling precision. Since we wish to average many traces together to improve the SNR of our data, accurate external triggering is essential. An optical cross-correlator and a PMT provide the scan triggering signal employed by our

Table 3.1: Data acquisition parameters and bandwidth limitations imposed by the balanced photodetector and theoretical maximum time delay resolution. For these conditions, only data sets taken at $\Delta f = 800$ and 1600 suffered from limited THz bandwidth

Δf (Hz)	t_d (ms)	$\Delta\tau_d$ (fs)	t_d/τ_d ($\tau_d = 12.5$ ns)	PD bandwidth 3 dB roll-off (THz)	$\Delta\tau_d$ bandwidth limit (THz)
100	10	15.6	80000	12	64
200	5.0	31.2	40000	6	32
400	2.5	62.4	20000	3	16
800	1.25	124.8	10000	1.5	8
1600	0.625	249.6	5000	0.75	4

system. To take averaged data, turn on the current preamplifier and then turn on the PMT power supply. The alignment of the optical cross-correlator is similar to the alignment for EO detection, requiring spatial and temporal overlap of the pump and probe pulses within a nonlinear optical crystal, BBO in the case of the cross-correlator.

The third important feature of the digitizer card is fast sampling, at a rate of 80 MSa/s or higher. This is important to individually sample each incoming laser pulse. Undersampling will effectively convolute a given probe pulse with neighboring probe pulses. For example, sampling at a rate of 40 MSa/s will only extract the information content of each pair of probe pulses, effectively halving N_s and increasing the coarseness of the time delay resolution by a factor of two. This effect will only be noticeable if the pulse width and timing jitter support the maximum theoretical time delay, $\Delta\tau_d$, of the system. For our system, a probe pulse width of approximately 150 fs means that we are effectively convolving the information content of 10 pulses as we take time delay steps of 15.6 fs from each pulse to the next. The effective time delay resolution limit imposed by the probe pulse width will limit sampling to 6.7 THz of bandwidth. Since we are convolving 10 pulses together we will not notice a decrease in THz bandwidth until we sample at rates of 8 MSa/s or slower. Future pulse compression of our laser pulses to 15 fs would exploit the maximum theoretical time delay resolution of 15.6 fs at an offset lock of 100 Hz, ensuring that the information content of each probe pulse is unique. In this case, sampling at a rate lower than 80 MSa/s would limit THz bandwidth. We discuss how to choose triggering and sampling settings using digitizer software settings in the following section.

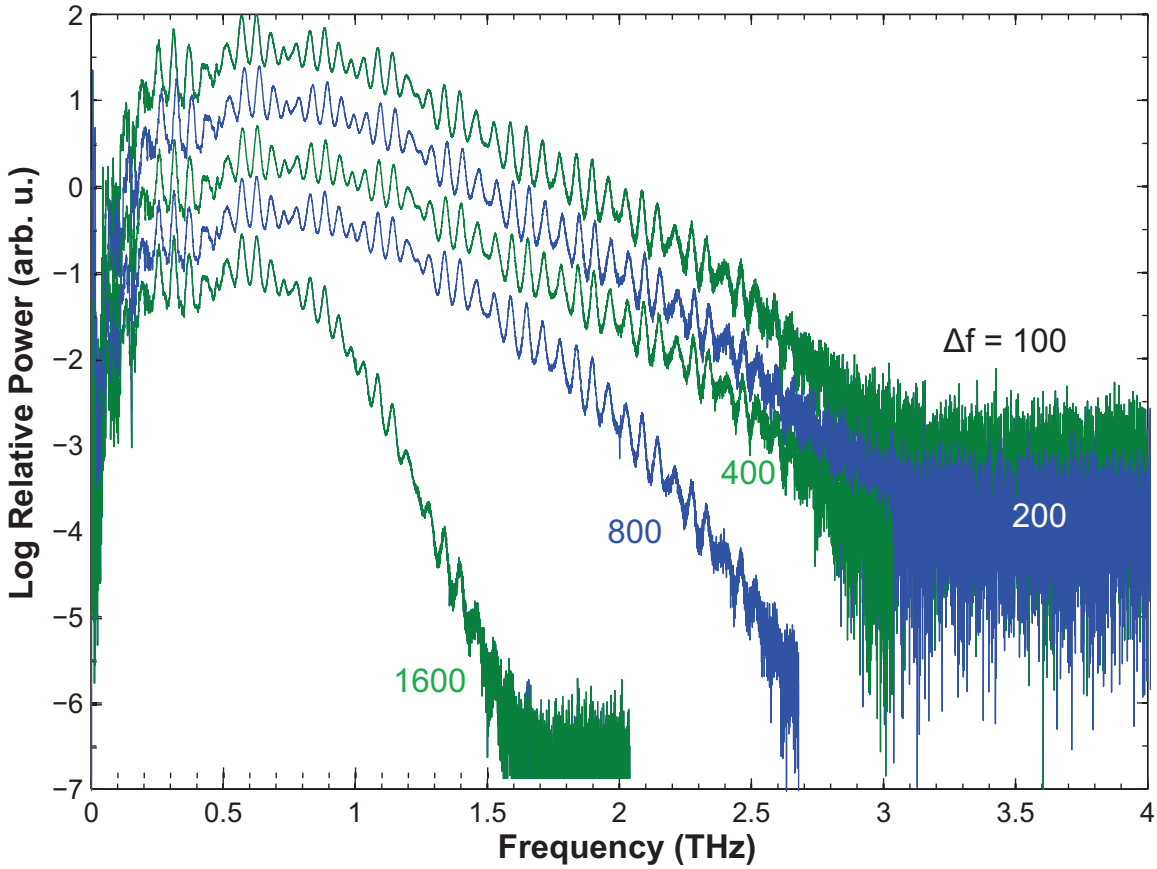

Figure 3.8: A plot showing the effect of decreasing the ASOPS factor on the THz bandwidth. For $\Delta f = 100$, 200, and 400 the bandwidth is unaffected, but for $\Delta f = 800$ and 1600 the limited bandwidth of the 15 MHz balanced photodetector is no longer sufficient to cover the full THz bandwidth.

3.3.4 Data Acquisition Software

To take data, and to adjust sampling, triggering, and reference settings we use the AlazarTech control software included with the digitizer card. This software functions like a virtual oscilloscope, with the display and control options modeled after those commonly found on stand alone digital sampling oscilloscopes. To open the software, double click on the icon found on the desktop. In the upper left hand corner of the black display panel, the number of samples per record is displayed. In the upper right hand corner the sampling rate and reference settings are displayed. In the lower left hand corner, the time per division is given and in the lower right hand corner, the V or mV per division for each channel is given (Ch 1 = pink, Ch 2 = green). To adjust any of these values,

double click the displayed number. Along the right hand side of the display is an arrow indicating the current triggering channel and level.

For ASOPS-THz-TDS or static comb data, we set the samples per record to 1.6 MSa and the sample rate to 160 MSa/s. This matches the scan rate of 100 Hz, so that the digitizer collects 100 records per second. We trigger off of channel 1, which is connected to the trigger signal from the PMT. The trigger level should be set to ∼75% of the trigger pulse peak height. The structure of the digitizer card onboard memory stores groups of records as acquisitions. We set the number of records per acquisition to 10. There is an averaging app within the control software, we use this to select the number of acquisitions to average to obtain our final waveform. For the data discussed in Chapter 4, we select 20000 acquisitions for a total of 200000 averages. At a rate of 0.01 s per record, this should take 35 minutes of averaging time. After adjusting all of the parameters necessary for data acquisition, click the acquire button to collect a sample. In order to fine tune the THz alignment and peak up the THz power, select 10 or 100 acquisitions, and select the acquire until stop option. This will give a real time readout of the THz time domain signal, ideal for seeing the results of alignment changes in real time.

3.3.5 Sample Preparation

Before clicking the acquire button to being averaging data, the sample cell and purge box should be prepared. It is ideal to flush the purge box with dry nitrogen for 30-60 min before beginning a scan to remove residual water vapor from the purge box. To maintain dry conditions within the box, leave the lid on the purge box unless it needs to be removed to align or modify optics within the box. For normal day to day operation, the optics inside of the box should not require adjustment.

A homebuilt sample cell fashioned from an aluminum tube with Topas windows epoxied onto its ends is the primary cell used for spectroscopy with the system. The 12.5 cm path length is short, but is sufficient for measurement of molecules with sufficiently large dipole moments. For ASOPS-THz-TDS measurements, a pressure in the range from 0.1 to 10 Torr will maximize the signal to noise ratio (SNR). Pressure broadening is dominant relative to Doppler broadening in this pressure

range and will result in a linewidth comparable to the FWHM of the comb teeth of the static comb, 80 MHz. Matching linewidth to comb tooth size will optimize SNR by only filling one frequency bin.

The sample cell is typically operated as a flow cell maintaining a static equilibrium pressure. A glass bulb is loaded with the sample of interest, usually a liquid with moderate to high vapor pressure. Before dosing the cell with sample, the valve leading to the glass bulb is shut, allowing the cell to be evacuated using a vacuum pump (Edwards RV5) or the house vacuum line. It is good practice to always leave the sample cell under vacuum when not in use to help purge residual sample between scans. This ensures quick pump down times since the pump will only have to remove the sample residue from a single scan. Once the cell has reached a pressure of 0.01 Torr or below and is holding to within ±5 mTorr a background scan may be acquired.

Typically averaging between 100000 and 500000 traces yields an ideal bandwidth and SNR for ASOPS-THz-TDS data. Once a background trace has been acquired and saved, the cell is dosed with a flow of sample by opening the gate valve on the glass bulb. Before attempting to stabilize the sample pressure be sure to pump down on the sample for several minutes to ensure complete outgassing of dissolved air. Once the sample pressure is near the desired pressure, reduce the flow of sample by partially closing the gate valve. By adjusting the pumping gate valve and sample gate valve a steady state flow may be obtained. For pressures of several Torr, sample will be consumed rapidly so reduce pumping speed while keeping the sample gate valve fully open for best results. Turn on the Variac to heat the resistive heating tape wrapped around the sample dosing line to avoid unwanted spikes in pressure caused by sample condensing and blocking the sample gate valve. Upon stabilizing the sample pressure to within ±5 mTorr, a sample scan may be taken. Now that we have covered the procedures necessary to operate the spectrometer, we may discuss the analysis of gas-phase spectra acquired with the instrument.

Chapter 4

Analysis of THz-TDS Spectra

Parts of this chapter are reproduced from "A decade-spanning high-resolution asynchronous optical sampling terahertz time-domain and frequency comb spectrometer," by J.T. Good, D.B. Holland*, I.A. Finneran, P.B. Carroll, M.J. Kelley, and G.A. Blake, Review of Scientific Instruments **86**, 103107 (2015). [* Co-first author]*

Once a background and sample scan have been acquired with the same acquisition parameters, as described in Chapter 3, they may be analyzed to extract frequency content and to produce relative absorbance data. In this chapter the performance of our high-resolution ASOPS based THz-TDS system is characterized via the comparison of experimentally measured water vapor and acetonitrile rotational transition energies to the values listed by the JPL molecular spectroscopy database. Data processing techniques to yield optimal spectra are discussed along with the relation between the time-domain and frequency-domain data.

4.1 Processing Time-Domain and Frequency-Domain Data

The raw data acquired provide a time-domain measurement of the THz electric field as a function of time delay, as shown in Figure 4.1. Since the polarization shift induced by the EO sampling process is linearly proportional to the electric field of the THz pulses incident on the EO detection crystal, this is a direct measurement of the THz waveform. As such, a quantitative measurement of THz pulse power could be used to calibrate the units of the THz electric field in terms of absolute electric

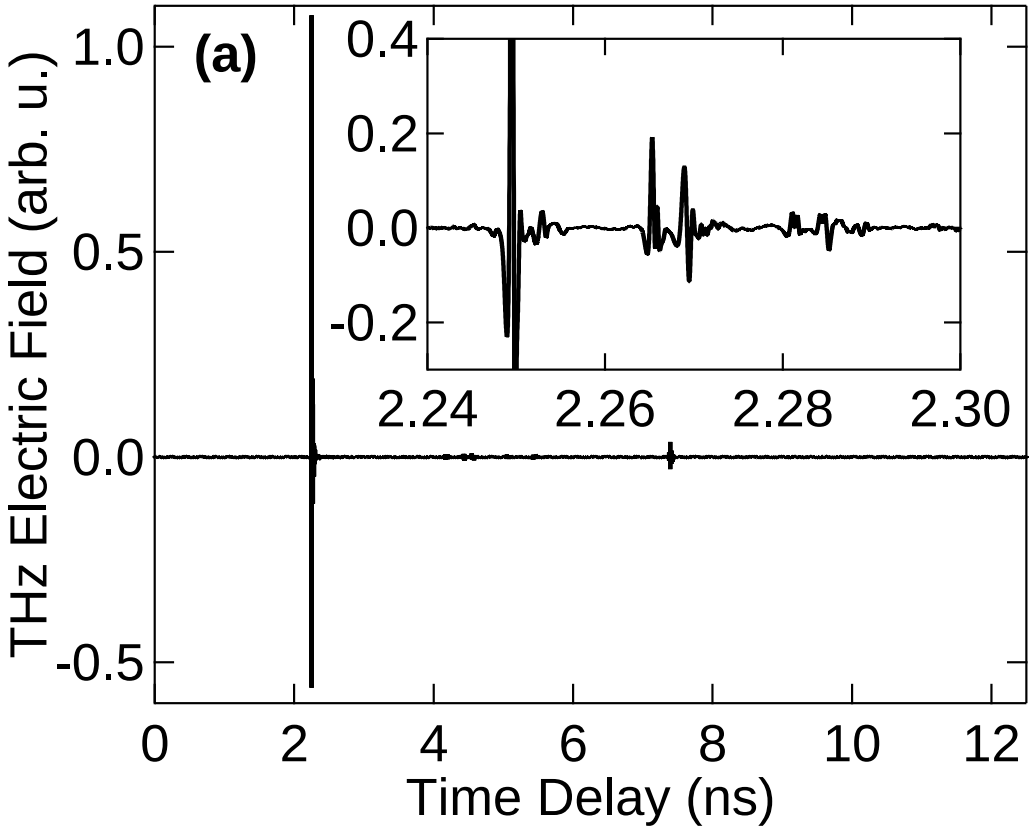

Figure 4.1: THz time-domain trace acquired over 70 min (200000 averages) at a sample cell pressure of 0.01 Torr (blank scan with no sample) and under dry nitrogen purge inside of the purge box. The inset detail shows the electric field oscillations of the THz pulse.

field magnitude. However, since we are ultimately interested in a relative intensity measurement, the absolute intensity is unimportant and we may leave this axis in terms of arbitrary units.

Similarly, while we could calibrate the time delay axis as in Figure 2.5, we are ultimately interested in extracting the frequency-domain information from the THz pulse. Since the frequency content is the same regardless of the absolute time delay of the axis, we leave the time axis in terms of arbitrary time delay. The smaller pulse visible at around 7.5 ns is an etalon due to the reflection of THz pulses off of two parallel reflective surfaces. This adds path length to the THz pulses, much like the air-spaced etalon discussed in Section 2.3.1, except that this THz etalon is an unwanted source of noise. Here, approximately 5.2 ns of time delay was added relative to the main pulse, which implies that the distance between the reflective surfaces responsible is $\sim$0.8 m, assuming a

single round trip reflection is responsible the etalon. Since this corresponds to the distance between the detector and emitter, this etalon could likely be eliminated by dithering the emitter (slowly rotating or translating the emitter back and forth by a small amount) during the measurement to misalign the reflective surfaces of the emitter and detector relative to each other.

An alternative method for eliminating the unwanted frequency content of the etalon is to cut the time domain trace to a 5 ns window centered on the THz pulse out to just before the etalon. This will eliminate noise contributions from the etalon. However, this processing has the side effect of limiting the frequency resolution obtained from the data once it is Fourier transformed. Since the record is only 5 ns long, our comb teeth will be broadened to 200 MHz. The comb tooth spacing will remain at 80 MHz. We can mitigate the effects of comb tooth broadening by zero-padding our data. We zero-pad the data to the nearest power of 2, and then to 8 additional powers of 2. This will yield 512 FFT frequency bins with a width of 0.39 MHz for each 200 MHz wide comb tooth frequency bin. This will improve our ability to resolve absolute frequencies below the limit imposed by our comb tooth frequency bin width. However, this technique cannot resolve peaks that are spaced more closely than 200 MHz since both peaks will fill the same comb tooth frequency bin.

Once an FFT is applied, the zero-padded time-domain data are effectively interpolated in the frequency-domain, yielding a power spectrum of the THz frequency content. A power spectrum acquired after 70 min with 1 Torr of water vapor is shown in Figure 4.2. The SNR obtained is 50 dB measured from the peak of the power spectrum to the noise floor. Since the comb tooth width is greater than the comb tooth spacing for this measurement, no adjustment of f_M is required to cover the entire spectral range. The frequency of the pump laser was locked to 79.980833 MHz to ensure that the comb teeth remained static while acquiring these data. No features due to molecular absorptions are visible in the blank spectrum at this background pressure and averaging time. A few spurious peaks show up in the low frequency end of the spectrum due to etalons or other sources of interference, but they appear at consistent frequencies and are subtracted out when the sample and the background scans are compared.

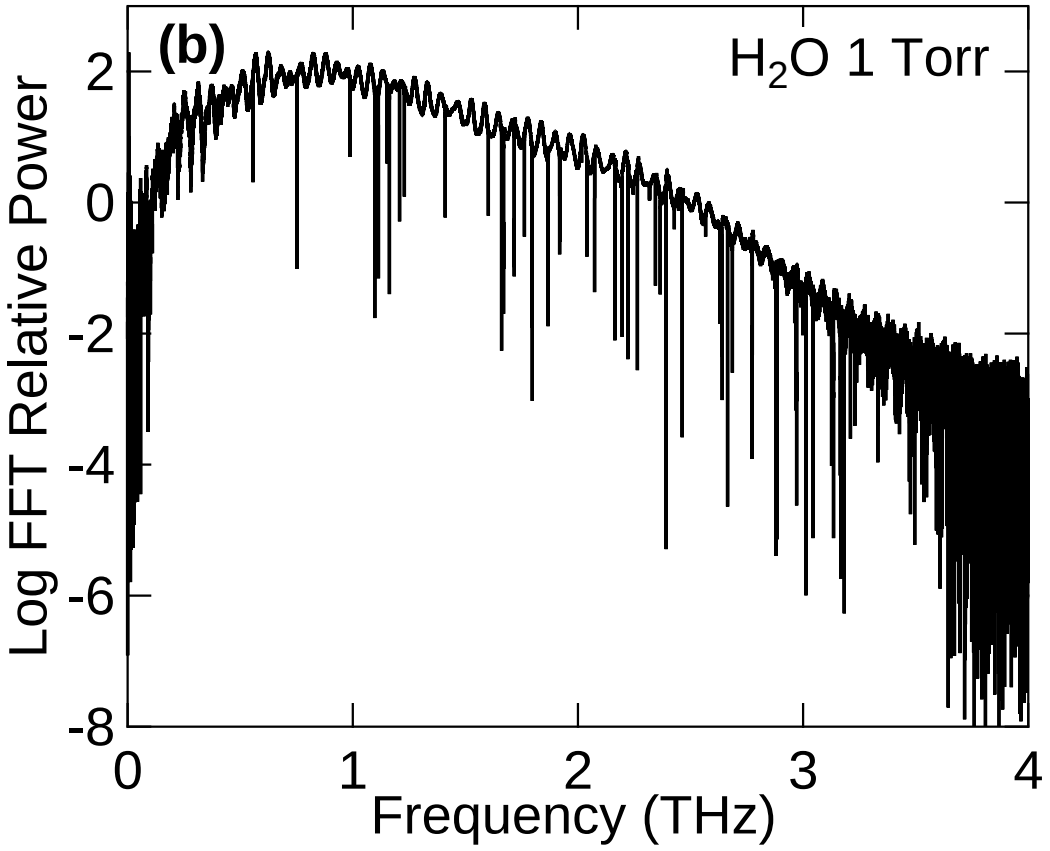

Figure 4.2: FFT relative power spectrum of a THz time-domain trace acquired over 70 min with H_2O vapor in the sample cell at a pressure of 1 Torr.

4.2 Water Relative Absorbance Data

Relative absorbance data is obtained by taking the ratio of the relative power of the 1 Torr water vapor data shown in Figure 4.2 and the blank power spectrum obtained by taking an FFT of the blank time domain trace to account for the variations in the power spectrum intrinsic to the instrument. The resulting relative absorbance data are shown in Figure 4.3. Many sharp peaks are visible due to rotational transitions of molecular water. At a pressure of 1 Torr these peaks have a high SNR, which enables the extraction of their center frequencies a precision better than the 200 MHz comb tooth precision. However, at a pressure of 1 Torr the linewidths are pressure broadened to a linewidth of ∼110 MHz as shown in Figure 4.4. As such our ability to accurately determine peak centers will be limited under these experimental conditions.

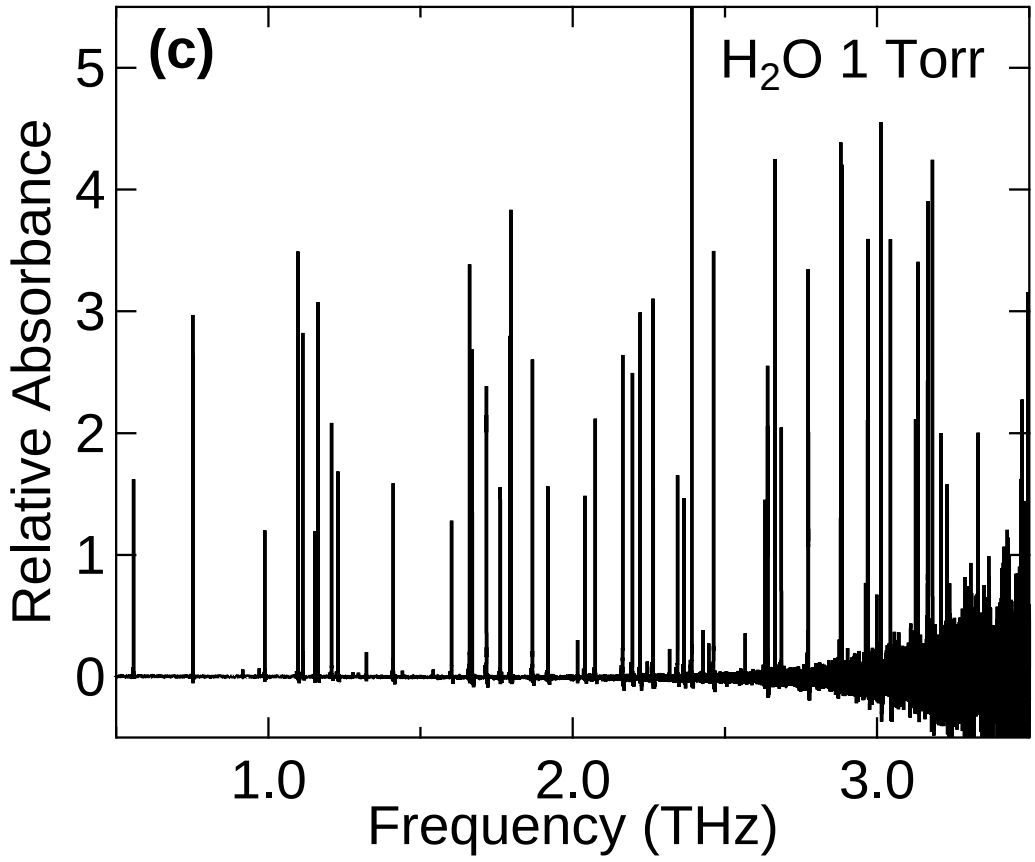

Figure 4.3: Relative absorbance plot showing water vapor rotational transitions up to 3.35 THz.

Once processed to obtain relative absorbance values, accurate values for line center frequencies are obtained with a simple peak picking algorithm. Relative absorbance data were acquired at water vapor pressures of 1 and 0.2 Torr to test the dynamic range of the system. See Table 4.1 for the acquisition parameters and analysis results of each data set. To compare to THz spectral line catalogs, we calculated the sensitivity floor of the instrument in terms of the intensity units used by the JPL database, namely the base 10 logarithm of the integrated line intensity in units of nm^2 x MHz.[33] Intense water absorption peaks for the 1 Torr data set begin to saturate, limiting the accuracy of this data set. A composite data set was therefore compiled using 34 lines with intensities between -2.68 and -0.80 from the 1 Torr data set and 32 lines with intensities above -0.80 from the 0.2 Torr data set. One line that was still saturated at 0.2 Torr was omitted. The full suite of water measurements achieved an RMS deviation of 14.6 MHz and a mean deviation of 11.6 MHz

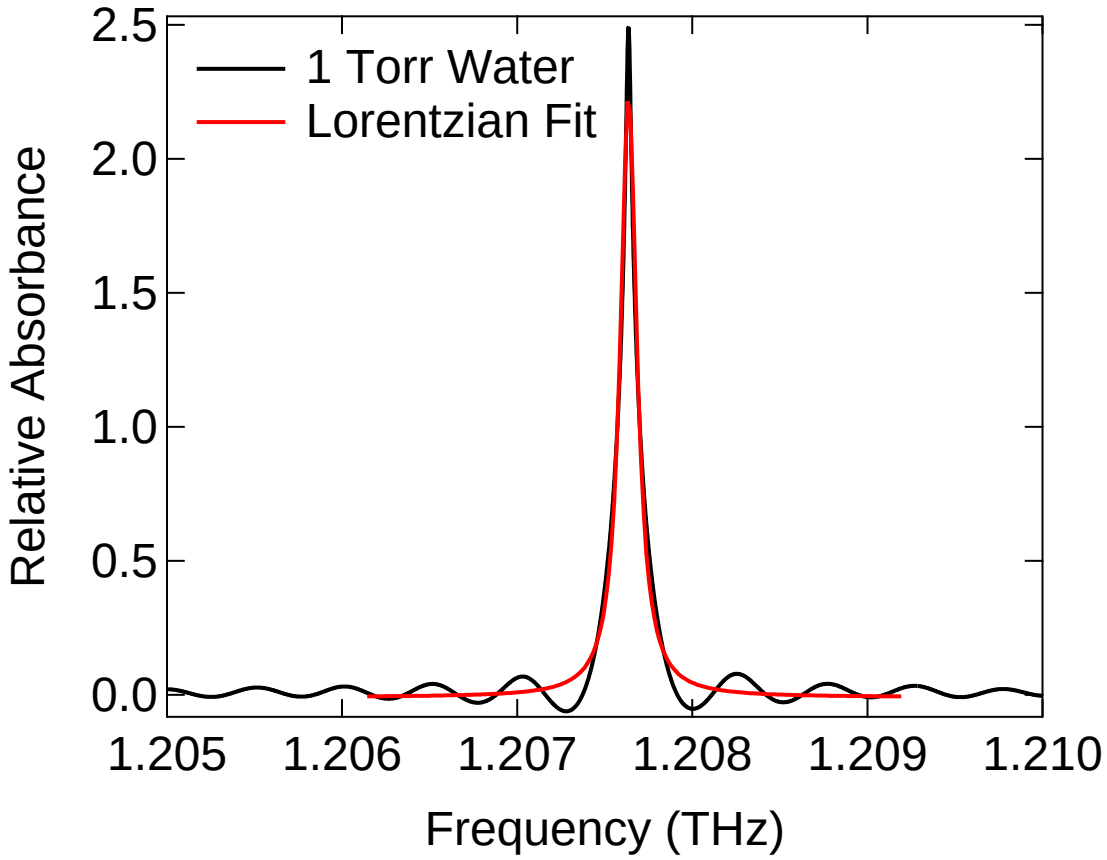

Figure 4.4: Detail of a single water transition from Figure 4.3 Water at 1 Torr is significantly pressure broadened and therefore we observe a Lorentzian line shape. The oscillations around the peak are structure introduced by zero-padding the FFT.

for the composite data set acquired over 140 minutes. For the individual spectral data sets the mean frequency deviations were 14.9 and 23.3 MHz at 0.2 and 1 Torr, respectively.

Generally, the RMS accuracy of absorption peak centers determined by a spectrometer equals half the FWHM of the peak measured divided by the square root of the SNR of the peak measured (RMS = FWHM/$2\sqrt{SNR}$). Taking the peak shown in Figure 4.4 as an example, the FWHM is 112 MHz and the SNR is 100:1, so the expected measurement accuracy for this peak is 5.6 MHz. This relation only holds true for peaks that are not saturated. By using a composite data set to boost the SNR of weak peaks and to attenuate saturated peaks, we maximize the overall accuracy of the system to the limit of the SNR limited measurement accuracy.

Table 4.1: Summary of water vapor absorption data acquisition parameters and analysis results. The detection and saturation thresholds were determined by using the reported intensity values in the JPL database which are given as the base 10 logarithm of the integrated intensity in units of nm^2 x MHz. Row 3 is the composite data set.

Acquisition Time (min)	H_2O Pressure (Torr)	Lines Assigned	Detection Threshold	Saturation Threshold	RMS Dev (MHz)	Mean Dev (MHz)
70	**0.2**	**32**	**-1.00**	**-0.46**	**19.9**	**14.9**
70	1	34	-2.68	-0.80	33.2	23.3
70, 70	**0.2**, 1	66	-2.68	**-0.46**	14.6	11.6

4.3 Acetonitrile Relative Absorbance Data

Water lacks strong rotational transitions below 0.55 THz and so, to test the low frequency performance of the instrument, the rotational spectrum of acetonitrile was measured. For our spectrometer with a 12.5 cm path length sample cell, acetonitrile absorbtions are not saturated at 2 Torr. Relative absorbance data for CH_3CN (99.5% ACS grade, Mallinckrodt) at 2 Torr are shown in Figure 4.5. This data shows the ability of the instrument to accurately measure the relative intensity of rotational transitions across a decade of bandwidth, down to 0.13 THz.

Acetonitrile is a prolate symmetrical top and the frequencies of rotational transitions involving the moment of inertia perpendicular to the symmetry axis will increase linearly as the rotational quantum number along this axis, J, increases. However, with increasing J, increasing centrifugal distortion will slightly perturb the rotational inertia of the rotor. The predicted energies of rotational transitions along the unique axis are given by Equation (4.1):

$$E(J) = B_e J(J+1) - D_{ej} J^2 (J+1)^2, \tag{4.1}$$

where $E(J)$ is the predicted energy of the transition, B_e is the rotational constant of the molecule as a rigid rotor, J is the rotational quantum number of the lower state, $J+1$ is the rotational quantum number of the upper state, and D_{ej} is the centrifugal distortion constant associated with the molecular rotation. We observe a Boltzmann distribution of states in Figure 4.5 since we are not

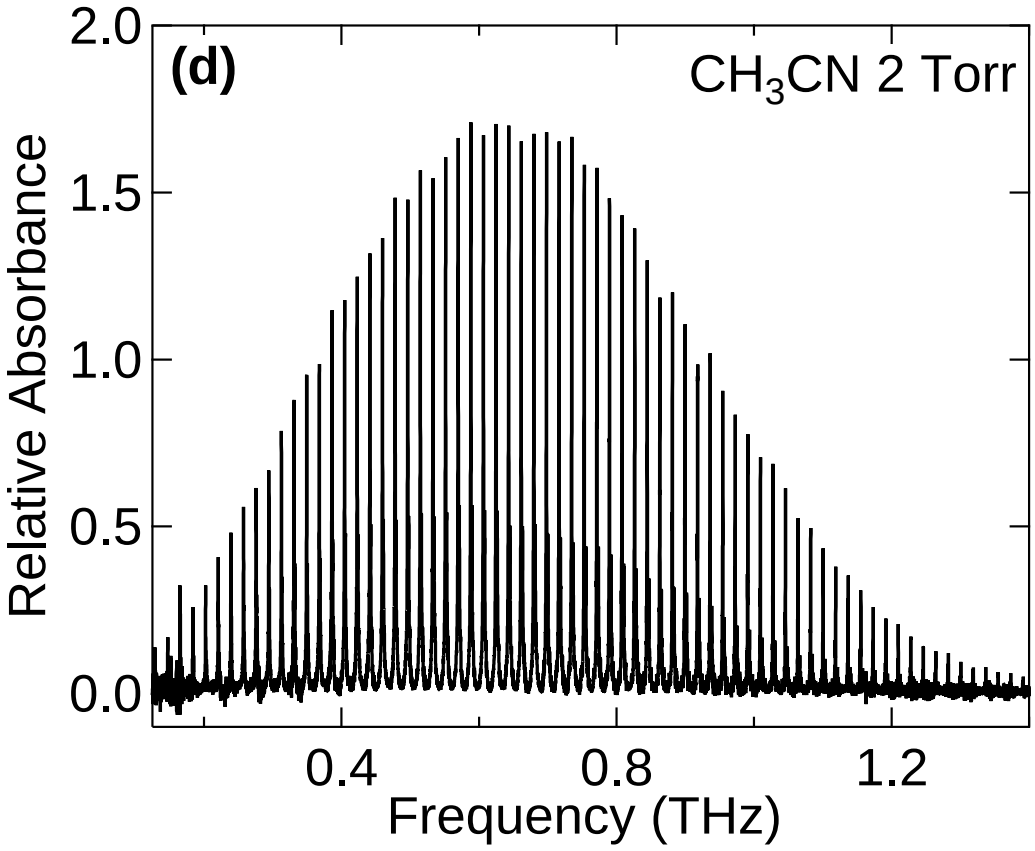

Figure 4.5: Relative absorbance plot acquired at an acetonitrile (CH_3CN) vapor pressure of 2 Torr showing rotational transitions down to 0.13 THz.

probing the system with sufficient THz power to shift the distribution of states away from thermal equilibrium.

For each parent transition along the unique axis, the moment of inertia associated with rotation about the C_{3v} axis will shift the transition away from its parent position according to Equation (4.2):

$$E(J,K) = B_e J(J+1) - D_{ej} J^2 (J+1)^2 + (A_e - B_e) K^2 - D_{ek} K^4 - D_{ejk} J(J+1) K^2, \qquad (4.2)$$

where K is the rotational quantum number associated with the degenerate axes, A_e is the moment of inertia about the C_3 axis, D_{ek} is the centrifugal distortion constant associated with the degenerate axes, and D_{ejk} is a centrifugal distortion coupling constant between all of the axes. The predicted

peak splitting for acetonitrile K-stacks is as low as a few MHz. Due to our large comb tooth width, we cannot expect to resolve individual line structure for acetonitrile K-stacks in ASOPS-THz-TDS mode. The wide frequency bins are filled by multiple transitions, resulting in the blurring of the predicted features, as shown in Figure 4.6. Nevertheless, we fully resolve each $\Delta J = 1$ rotational transition. Despite achieving the best reported resolution for an ASOPS based THz-TDS system over the covered bandwidth from 0.13-3.35 THz, the system is fundamentally limited by a resolution of 80 MHz in static comb mode. Part III describes a method for increasing the resolution of the instrument through acquisition of longer records to decrease the comb tooth width, and interleaving of the resulting narrow comb teeth to cover the spectral range of interest.

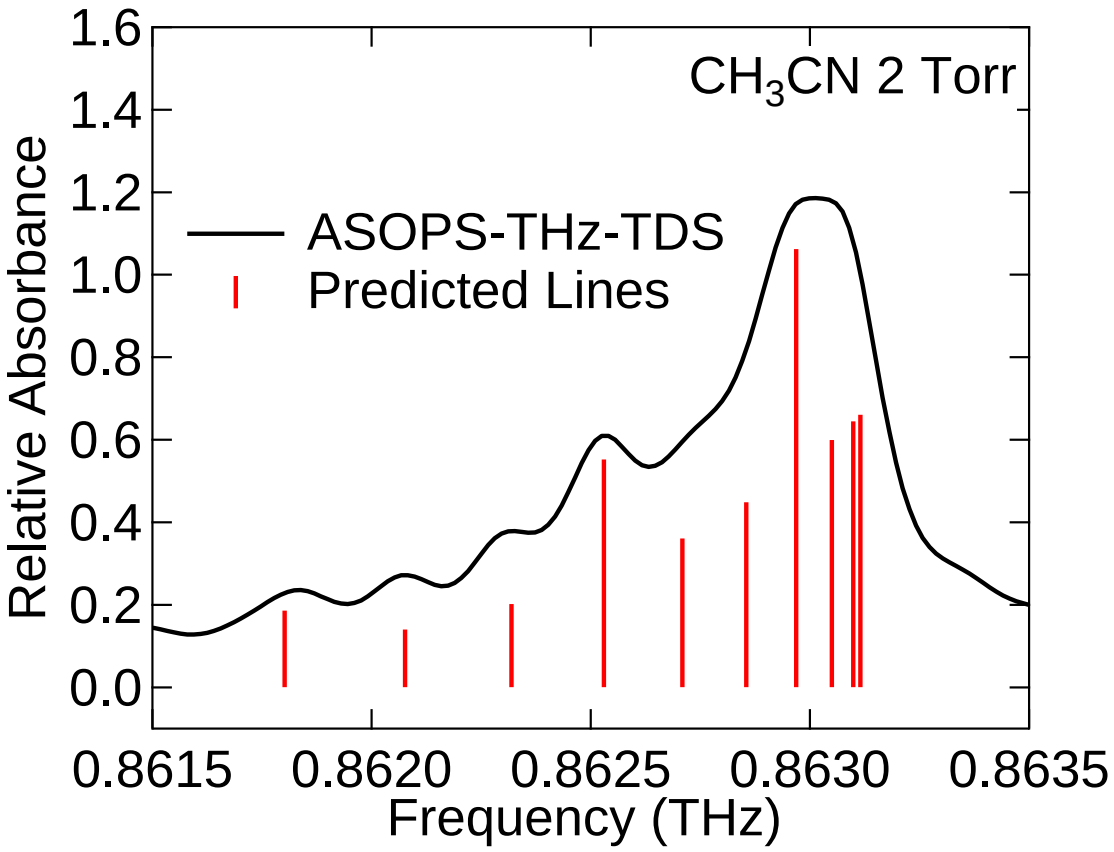

Figure 4.6: Relative absorbance plot for data acquired at an acetonitrile (CH_3CN) vapor pressure of 2 Torr. Predicted transitions are plotted as red vertical lines to show unresolved K stack structure underneath the envelope of the data plotted as a black solid line.

Part III

Interleaved Terahertz Frequency Comb Spectroscopy

Chapter 5

Acquisition of THz-FCS Spectra

Portions of this chapter are reproduced from "A decade-spanning high-resolution asynchronous optical sampling terahertz time-domain and frequency comb spectrometer," by J.T. Good, D.B. Holland*, I.A. Finneran, P.B. Carroll, M.J. Kelley, and G.A. Blake, Review of Scientific Instruments* ***86****, 103107 (2015). [* Co-first author] or "Decade-spanning high-precision terahertz frequency comb," by I.A. Finneran, J.T. Good, D.B. Holland, P.B. Carroll, M.A. Allodi, and G.A. Blake, Physics Review Letters* ***114****, 163902 (2015).*

Mode-locked Ti:Sapphire oscillators exhibit extremely precise repetition rates due to the rigorous selection of cavity modes. As such acquisition of data in THz-FCS mode only requires minor changes to the operating settings used in Part II. In this chapter we discuss the operation of the system in THz-FCS mode. The process of interleaving narrow comb teeth to cover the entire spectral range of interest is detailed, and additionally stabilization of the pump laser repetition rate and its effect on the performance of the spectrometer is discussed.

5.1 Collection of Longer Records

THz-FCS is enabled by the high stability of the repetition rate of the pump laser, which ensures that time delay between adjacent THz pulses remains constant across long THz pulse trains. If the time axis is cut into a 12.5 ns windows and processed by a FFT, we obtain the ASOPS-THz-TDS data shown in Figure 4.2. Alternatively, multiple pulses may be selected in a window that is an

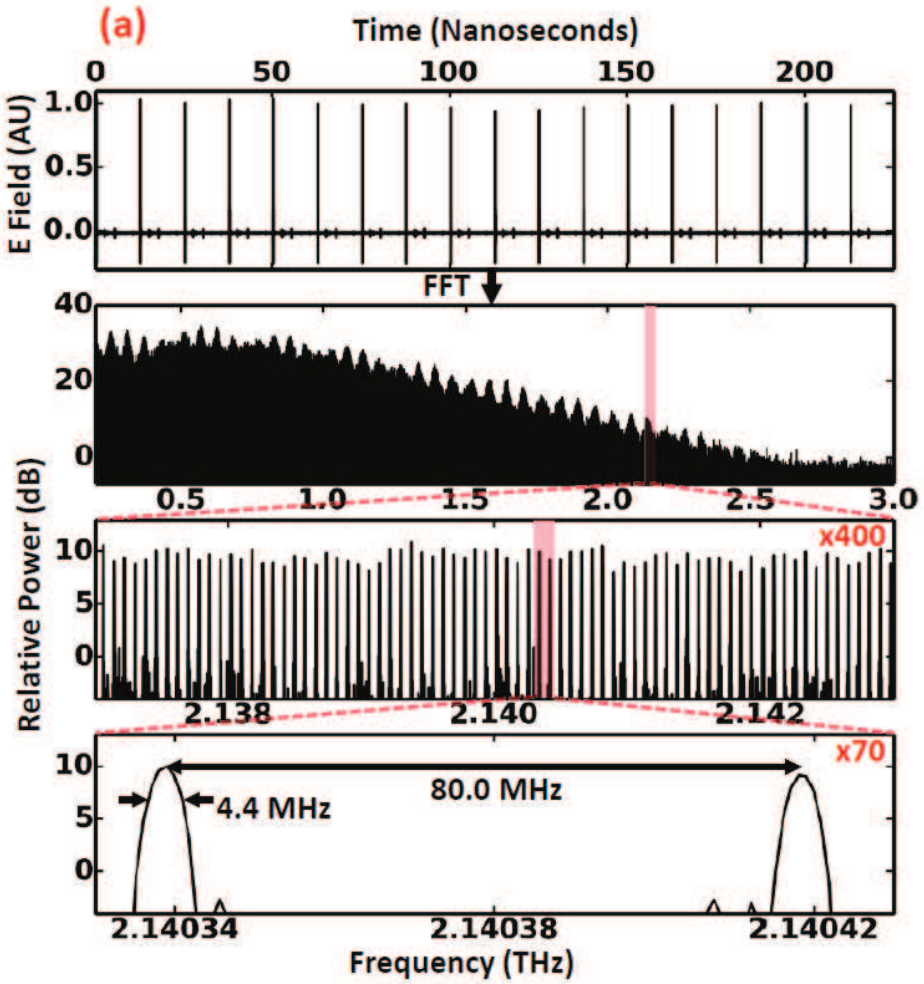

Figure 5.1: Diagram showing 4.4 MHz wide comb teeth produced by acquiring a record containing 18 THz pulses. Note that the spacing of the comb teeth is still 80 MHz, leading to the need to interleave the comb teeth in order to cover the full spectral range.

integer multiple of 12.5 ns. When that entire window is processed by a FFT, the frequency content from all of the pulses within the window is extracted. Each time the record length is doubled, the comb tooth width of the resulting frequency comb is halved. Fundamentally, the only limitation to the comb tooth width is the stability of the pump laser over the measurement time scale of interest. As long as the pump laser repetition rate is stable, the tooth width is limited only by the number of THz pulses included in the FFT. As such, the resolution of the instrument is readily adjustable in THz-FCS mode.

To collect longer records, no additional hardware is required. Follow the same startup procedures outlined in Chapter 3. However, some changes to the data acquisition software parameters are required. Previously, a sampling rate of 160 MSa/s was used, along with an offset lock of 100 Hz, chosen to ensure sampling of only one pulse per scan. There are three ways to increase the number pulses sampled in a single scan. The first is to increase the number of samples per scan at a given sampling rate, increasing the length of time sampled. The second is to decrease the sampling rate for a fixed number of samples. The third is to increase the offset lock frequency, decreasing the number of probe pulses used to sample each THz pulse, and increasing the scan rate. The first method increases the sampling time required, and so it is best to increase the number of pulses sampled using the second and third methods, if possible.

As discussed in Subsection 3.3.3, the offset lock may be increased up to 400 Hz without adversely affecting the current bandwidth of the system. We may offset lock the pump and probe repetition rates at $\Delta f = 400$ Hz by setting the output frequency of the probe DDS to 70.0240 MHz. For this offset, the time required to complete a scan is 2.5 ms. At a sampling rate of 160 MSa/s and a record length of 1.6 MSa, the digitizer card will acquire a total of 4 THz pulses over 10 ms. This will decrease the comb tooth width to 20 MHz. At our current bandwidth of 3.5 THz we do not require a sampling rate of 160 MSa/s. As such, we may decimate the digitizer card sampling rate by a factor of 4 to 40 MSa/s. Leaving the record length at 1.6 MSa, this will expand the sampling window of the digitzer to 40 ms. At an offset of 400 Hz and a sampling rate of 40 MSa/s, 16 comb teeth may be acquired, decreasing the comb tooth width to 5 MHz.

Our first comb generated with the instrument employed a record length of 1.8 MSa, a sample rate of 180 MSa/s, and an offset lock of 100 Hz. The resulting time-domain record contained 18 consecutive THz pulses, and when processed by a FFT yielded a 4.4 MHz comb tooth width. However, such an increase in spectral resolution comes at a price. At a spacing of 80 MHz, we no longer cover the full spectral range with a 4.4 MHz comb tooth width at a single pump repetition rate as shown in Figure 5.1. In the following section we discuss methods for interleaving narrow comb teeth to produce complete high resolution spectra across the entire bandwidth of the instrument.

5.2 Interleaving Narrow Comb Teeth

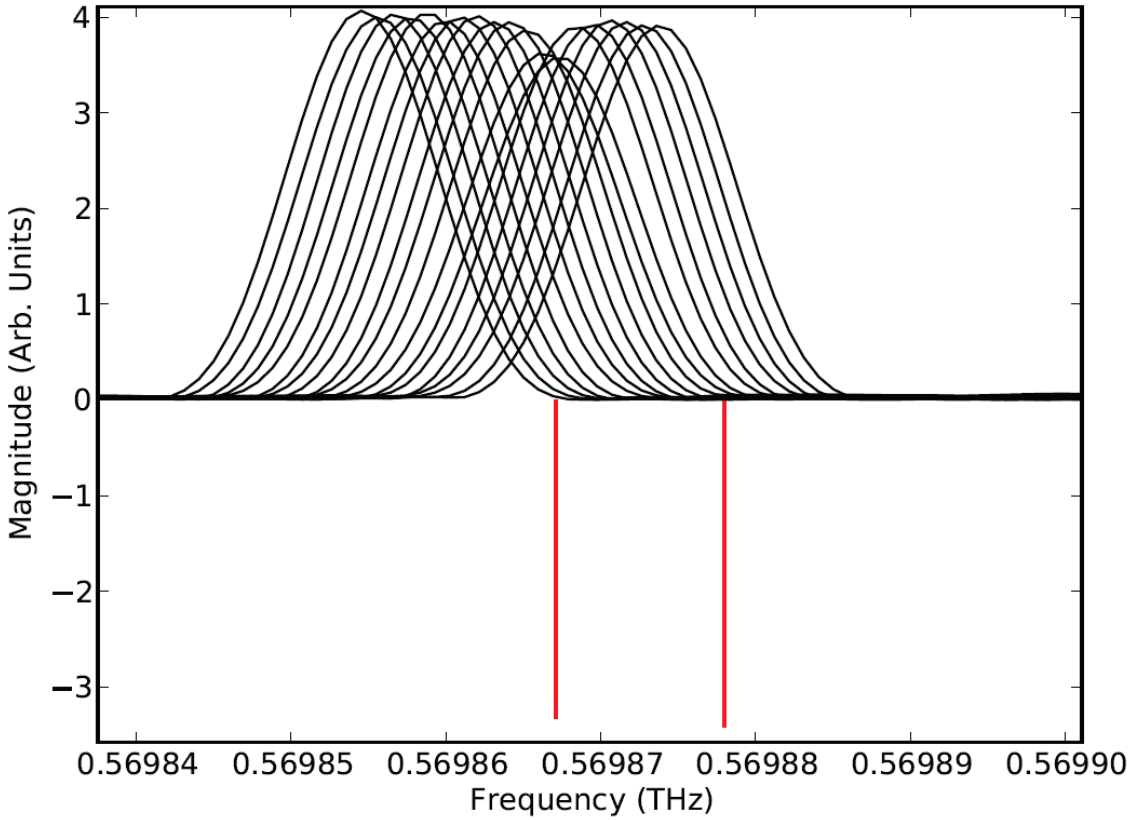

Figure 5.2: Diagram showing the use of interleaved comb teeth to perform absorbtion spectroscopy. Each black Gaussian curve represents an individual comb tooth and the two vertical red lines are plotted at the predicted positions of two acetonitrile absorptions at 0.5698671036 THz and 0.5698779816 THz. Note that only a few unique comb teeth are attenuated by each absorption.

In order to apply the improved resolution of our narrow comb teeth to Doppler-limited spectroscopy, we must step the comb accurately to achieve the desired spectral resolution. The minimum interleaving required is to step the comb a total of N times at a step size of $1/N$ MHz, where N is the number of THz pulses included in the FFT. At each step, a separate scan must be taken. This means that the scanning time required to obtain a fully interleaved spectrum with a given SNR increases linearly with the number of frequency steps taken. To step the comb teeth accurately, we may apply a control voltage to the pump slow PZT using the pump slow PID controller. This may be done by adjusting the manual voltage control on the pump slow PID controller. Such a voltage step will slightly increase or decrease the pump laser cavity length, shifting f_{pump}

Since the spacing of the comb teeth is given by the repetition rate of the pump laser, f_{pump}, any shift in f_{pump} will induce a shift in the comb teeth. The absolute frequency of the N^{th} comb tooth, $f_{comb}(N)$, is given by $f_{comb}(N) = N \cdot f_{pump}$. A shift of the pump repetition rate, Δf_{pump}, will shift the absolute frequency of the N^{th} comb tooth by $\Delta f_{comb}(N) = N \cdot \Delta f_{pump}$. For a repetition rate of 80 MHz, the 10000^{th} comb tooth is at 0.8 THz and the 20000^{th} comb tooth is at 1.6 THz. If we apply a shift of 100 Hz, the 10000^{th} comb tooth will shift by 1 MHz, meanwhile the 20000^{th} comb tooth will shift by 2 MHz. As such, $\Delta f_{comb}(N)/f_{comb}(N)$ is constant and the sampling resolution in the frequency domain can be matched to Doppler-limited spectral linewidths across the entire bandwidth of the comb. The amplification of small repetition rate shifts to large comb tooth shifts enables precise interleaving of THz comb teeth to cover the 80 MHz gap in between comb teeth.

To generate a full spectrum, we must interleave the comb teeth, preferably at a reproducible step size until the entire spectral range is covered. A scan must be taken for each step of the comb teeth. Since this process must be repeated many times, it is advantageous to automate the process. We employ the program sim.py located in the freq_counter_code directory. This simple program repetitively sweeps the control voltage on the pump slow PID controller from its lower limit at -5 V to its upper limit at +5 V and back down to the lower limit again. It does so in a series of voltage steps, with the size of the steps adjustable within the program (the current step size is 175 mV). To use the program, manually step the control voltage on the pump slow PID down to -5 V in 0.1 V steps to avoid destabilizing the probe slow PID controller. Open the AlazarTech control software and set the scan parameters to collect the desired number of THz pulses as discussed in Section 5.2. The automation software makes use of mouseclicker.py so ensure that the AlazarTech software is maximized and that no other windows or popups are blocking the screen.

You may now call sim.py from the command prompt. The software will wait for several seconds and then begin a scan using the AlazarTech software. Once the scan completes, the software will save the averaged time domain trace. Then it will increase the control voltage on the pump slow PID by 175 mV shifting the repetition rate of the pump laser down by 100 Hz. After waiting for the pump laser to settle to the new repetition rate, the program will begin a new scan. This process is

repeated stepwise 58 times across the entire -5 V to +5 V range of the pump slow PID, scanning the pump laser repetition rate across a frequency range of 5.8 kHz. Over the course of these scans, the comb teeth are interleaved at a step size of 1.4 MHz. The program will then decrease the control voltage stepwise by 175 mV until it returns to -5 V, and then back upwards to +5 V until the user stops the program with a Ctrl + C command. The resulting effect on the pump laser repetition rate is shown in Figure 5.3.

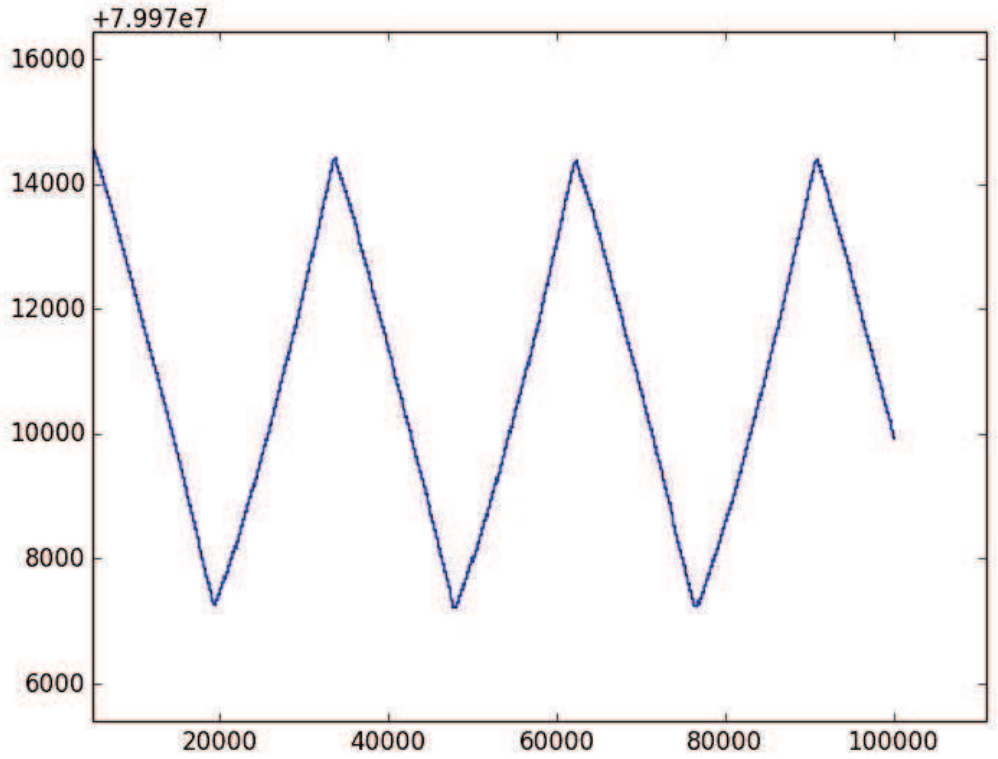

Figure 5.3: Plot of the pump laser repetition rate in Hertz versus time in seconds. The zig-zag pattern is produced by stepping the control voltage back and forth between -5 V and +5 V.

5.3 Stabilization of the Pump Laser Repetition Rate

This stepping program does not, however, lock the pump laser repetition rate once a voltage step is applied. In unlocked mode, over the course of 5-30 minutes, the pump repetition rate is subject to

sinusoidal oscillations of up to ±30 Hz. Over longer periods of time, systematic variations in room temperature can contribute systematic shifts as well, as is shown in Figure 3.2. These variations of 60 Hz peak-to-peak amplitude in f_{pump} will lead to a 1.2 MHz broadening of the 20000^{th} comb tooth, but no net displacement in its absolute position. Since this is commensurate with the width of comb tooth desired, it is not necessary to lock the pump laser repetition rate for short scans while there are no systematic deviations in f_{pump}. For more precise measurements requiring sub-MHz comb tooth widths, the pump laser repetition rate may be locked to the precisely desired value once the voltage step is applied. To lock the pump laser repetition rate the program freq_counter.py issues commands to the synthesizer that generates the reference signal for pump laser stabilization and automatically switches between PID control during scans and manual control to apply voltage steps.

To test the fundamental precision of the comb with our current hardware, we locked the repetition rate of the pump laser to 79.980833 MHz and set the offset to 200 Hz. We adjusted the sampling rate of the digitizer card to 20 MSa/s, the record length to 1.8 MSa, and used the stream to disk data acquisition mode. This mode may only be accessed by running the additionally included AlazarTech C code (the standard AlazarTech control software supports a maximum record length of 225 ns at 40MSa/s). When this C code is run, the digitizer begins sampling in a single unbroken stream of data for the specified record length upon receiving trigger signal. We specified 107 s of data acquisition, to acquire a total of 21,470 THz pulses. At this record length, the transform limited pulse width is 3.73 kHz. At a sampling rate of 20 MSa/s, this data set contained over 2 billion data points and was too computationally intensive for a conventional computer running a standard FFT algorithm.

We therefore ran the FFTW algorithm in MATLAB on our multi-core Linux cluster and finally obtained the frequency-domain data. The measured comb tooth width, shown in Figure 5.4, is 3.7 kHz. However, to obtain such narrow comb teeth is prohibitively time consuming given the current bottlenecks in data processing and scanning throughput. Fortunately, for Doppler-limited spectroscopy the narrowest tooth width required is ∼100 kHz, which is yielded by the acquisition of a train of ∼795 THz pulses. Such pulse trains are be readily acquired by our system, but require use

of the additional AlazarTech C code included with the digitizer. For Doppler-limited spectroscopy of acetonitrile, a train of 16 THz pulses provides a tooth width of 5 MHz, matching the spectral linewidth of the rotational transitions. Such data is recorded using the standard AlazarTech control software and is analyzed readily on a personal computer and sufficiently resolves the entire rotational spectrum of acetonitrile.

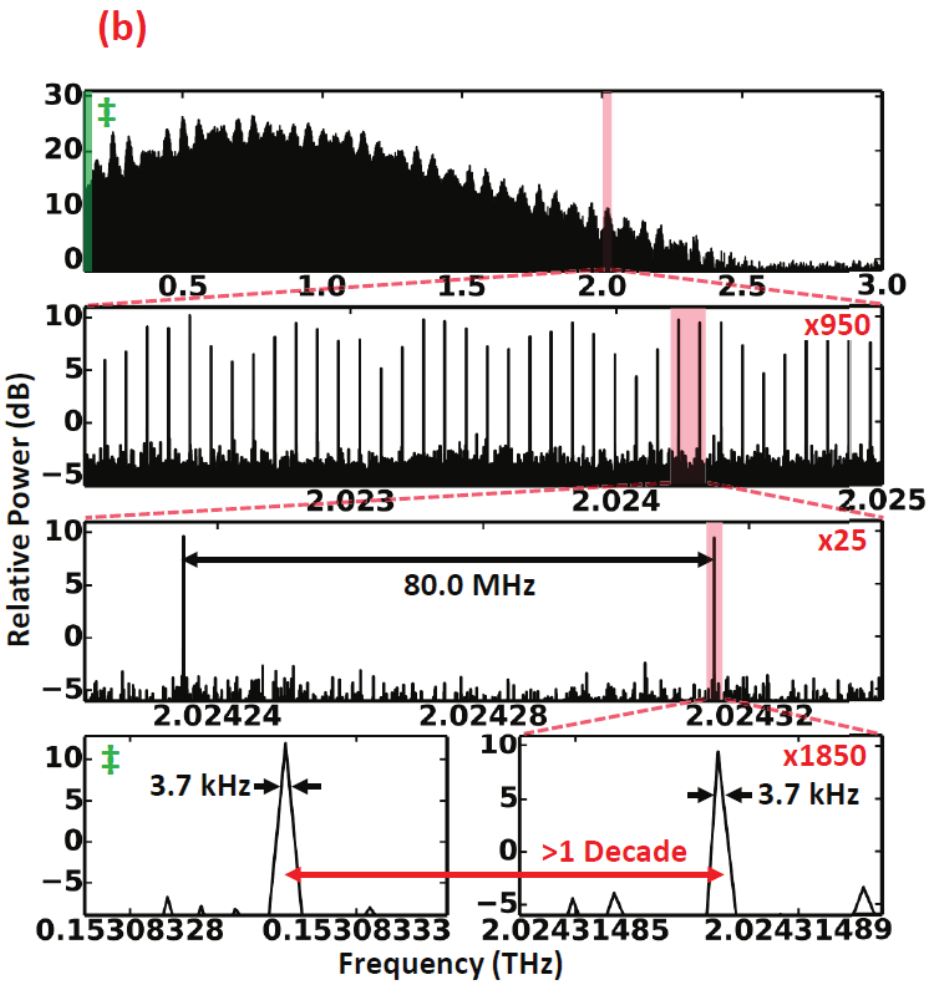

Figure 5.4: Diagram showing 3.7 kHz wide comb teeth produced by acquiring a very long record containing 795 THz pulses. Even at such narrow tooth widths, the instrument still produces a decade-spanning frequency comb with the frequency resolution determined by the FFT length.

Chapter 6

Analysis of THz-FCS Spectra

Portions of this chapter are reproduced from "A decade-spanning high-resolution asynchronous optical sampling terahertz time-domain and frequency comb spectrometer," by J.T. Good, D.B. Holland*, I.A. Finneran, P.B. Carroll, M.J. Kelley, and G.A. Blake, Review of Scientific Instruments* ***86****, 103107 (2015). [* Co-first author] or "Decade-spanning high-precision terahertz frequency comb," by I.A. Finneran, J.T. Good, D.B. Holland, P.B. Carroll, M.A. Allodi, and G.A. Blake, Physics Review Letters* ***114****, 163902 (2015).*

Although the generation of a broadband frequency comb with interleaved comb teeth featuring 5 MHz resolution is not impressive from a metrology standpoint, the gas-phase spectroscopy applications of such a comb are numerous. In this chapter we present Doppler-limited spectroscopy of water at 10 mTorr using 4.4 MHz wide comb teeth. Additionally, we present data in which the rotational structure of acetonitrile at 150 mTorr is fully resolved using 5 MHz wide comb teeth. Due to the need to collect multiple scans to cover the full spectral range, the collection of background data for each scan becomes prohibitive. As such, data processing techniques are employed to generate synthetic background spectra without the explicit collection of background data. The effect of these data processing techniques on the quality of spectra produced is explored.

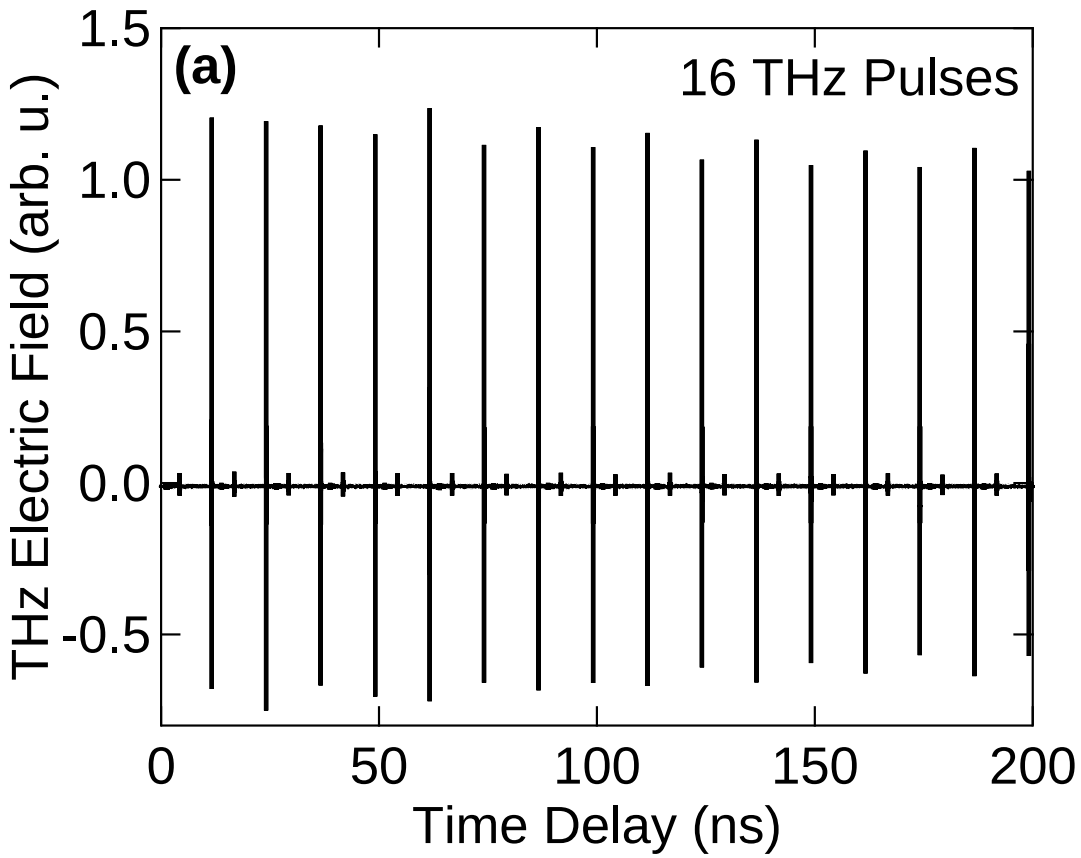

Figure 6.1: THz time-domain trace including 16 THz pulses. These data were acquired over 3.33 min at an acetonitrile vapor pressure of 150 mTorr.

6.1 Raw Data Processing

In static comb mode, the acquisition of a single background scan and a single sample scan are sufficient for the generation of relative absorbance spectra. With the interleaving of combs, a background scan and a sample scan is required for each comb tooth step. For large numbers of steps, the total scanning time and processing time for all of the individual files becomes prohibitive. Also, due to the narrow bin size, the sensitivity of the spectrometer is vastly improved, making the removal of sample for the collection of background scans challenging. As such we have developed a data processing method to generate synthetic background spectra.

For acetonitrile data, the sample cell was run as a flow cell at the desired pressure of 150 mTorr. The program sim.py was used to ramp the control voltage once from -5 V to + 5 V. We set the

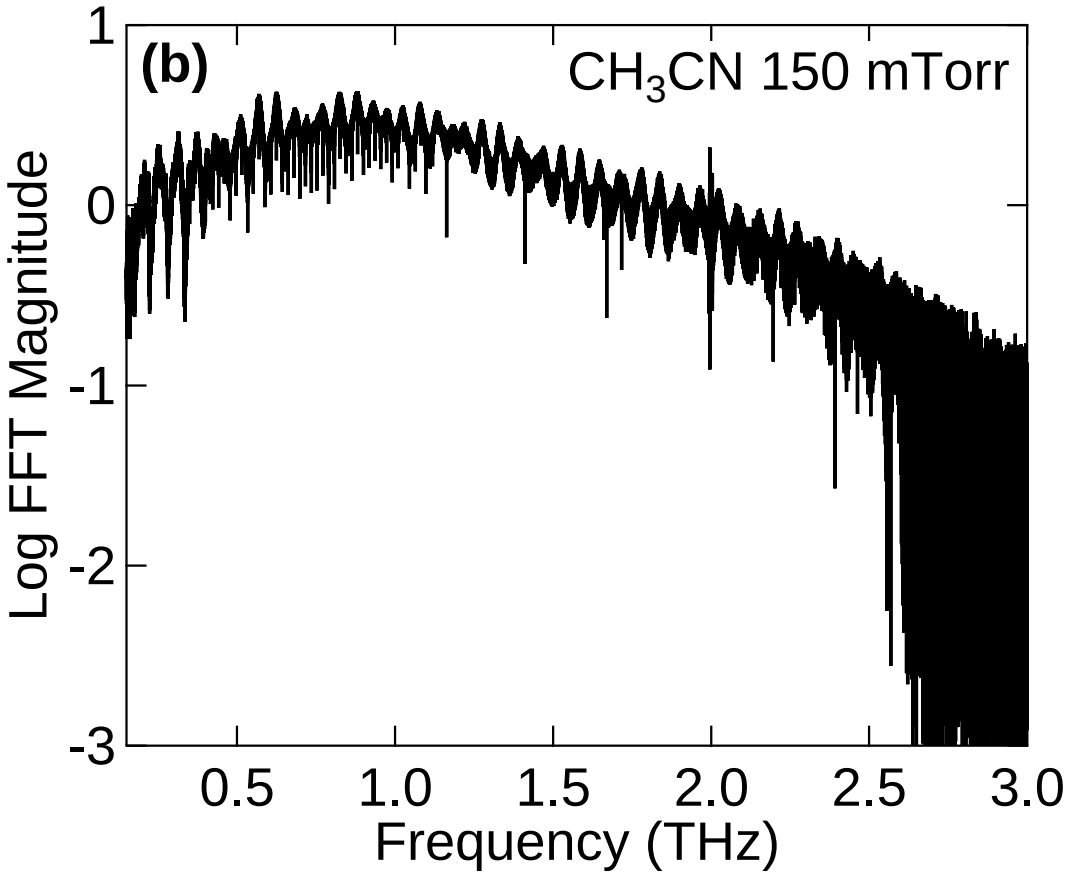

Figure 6.2: FFT relative power spectrum of the peak picked comb tooth intensities extracted from all 58 time-domain traces acquired an acetonitrile (CH_3CN) vapor pressure of 150 mTorr.

record length to 1.6 MSa, the sampling rate to 40 MSa/s, and the offset to 400 Hz. For each of the 58 voltage steps, a total of 5000 traces are averaged together requiring 3.33 min of integration time, with an example of the resulting time-domain data for a single step shown in Figure 6.1. We apply a FFT to the time domain trace acquired for each voltage step, generating a frequency comb with a tooth spacing of 80 MHz and a tooth width of 5 MHz for each repetition rate step. When these individual combs collected at each voltage step are interleaved together at an interval equal to the comb tooth width, the comb teeth cover the entire spectral range between comb teeth.

Since we are performing frequency comb spectroscopy, we measure relative absorbance by the attenuation of each individual comb tooth. To extract this information, we employ a peak picking algorithm to measure the peak intensity of each comb tooth. Attenuation of comb teeth appear

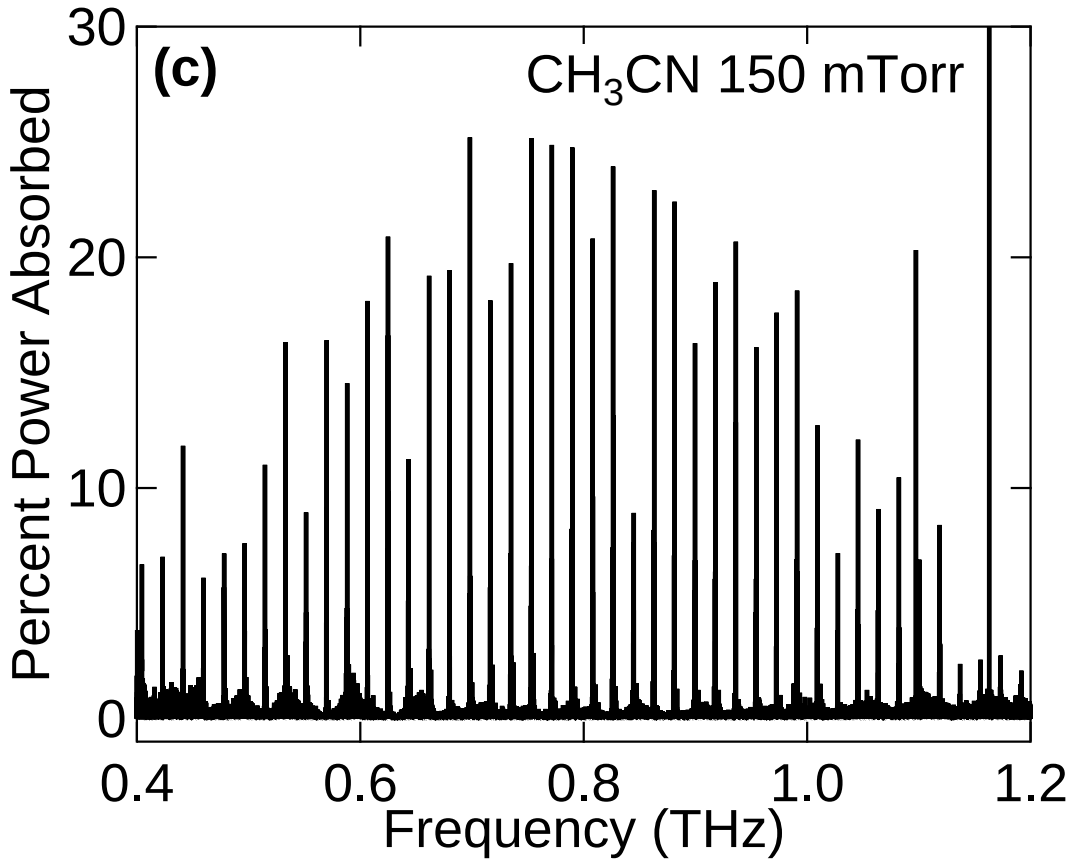

Figure 6.3: Percent power absorbance plot showing acetonitrile rotational transitions. The features shown here are actually K-stacks, each of which is fully resolved to the detection limits of the instrument, as shown in Figure 6.4.

as absorptions in the raw FFT magnitude spectrum shown in Figure 6.2. Once these values have been acquired, a 50 point boxcar average of the peak intensities is taken. This boxcar average effectively calculates a background spectrum by ignoring the attenuation of individual comb teeth by absorptions. This backgrounding method works best for the sparse spectra shown here and care should be taken in applying such an algorithm to denser spectra. Some empirical optimization of the number of points included in the boxcar average is required to find a value that effectively ignores sharp features due to absorptions while simultaneously reproducing the broad features due to etalons in the background spectrum. The present THz-FCS implementation of the instrument only achieves 2.5 THz bandwidth due to the limited SNR when using only 5000 averages, but has an enhanced resolution of 5 MHz across this entire bandwidth.

6.2 Acetonitrile Percent Power Absorption Data

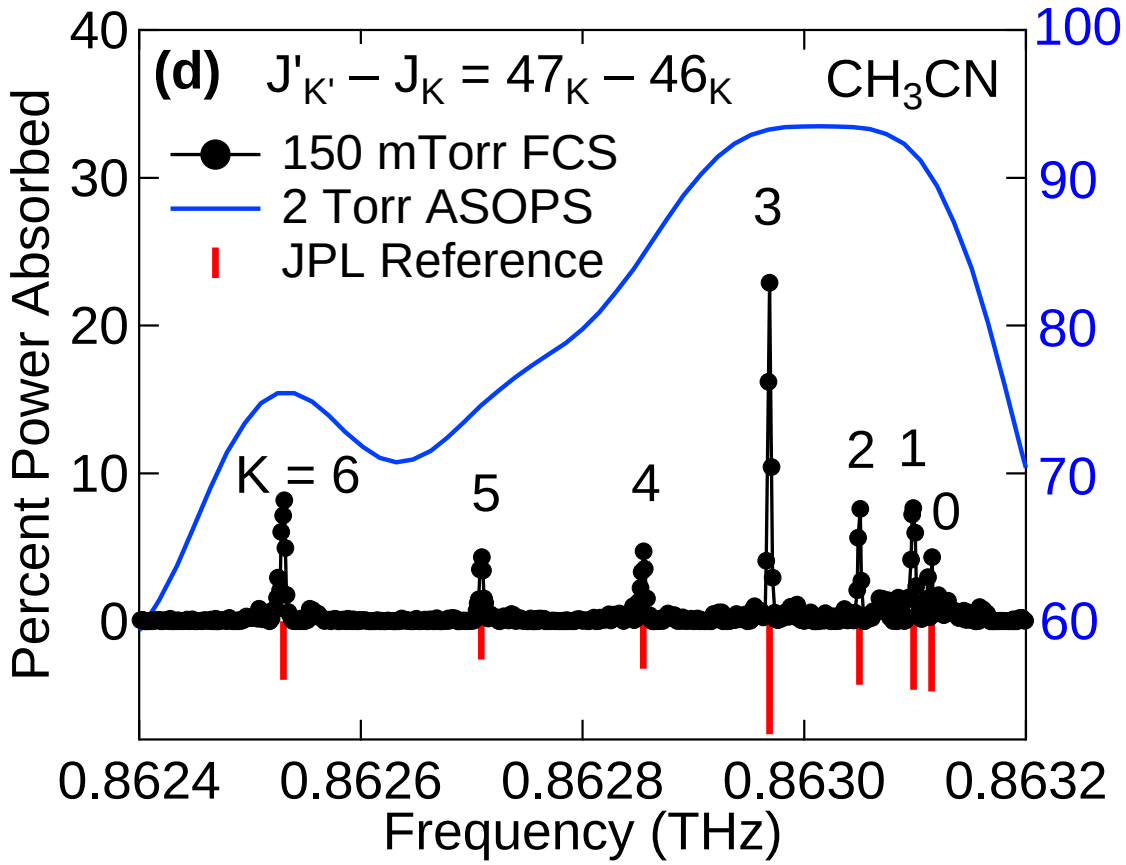

Figure 6.4: Detail of acetonitrile percent power absorbance plot showing the ability of the interleaved comb to resolve Doppler limited lines with 5 MHz resolution. Data points acquired via peak picking raw data are plotted as black points. The comparable data set from Figure 4.6 converted to units of percent power absorbed is plotted as a blue line highlighting that the instrument is only able to resolve these transitions in THz-FCS mode. Predicted line positions from the JPL reference catalog are plotted as vertical red lines with height scaled to the predicted linear absorbance intensity. Lines are labeled with their associated quantum numbers.

The background comb tooth intensities obtained by the boxcar average are then used to calculate a percent power absorbance value for each comb tooth, and these values are plotted in the percent power absorbance spectrum shown in Figure 6.3. Once again, we observe the equally spaced parent pseudo-diatomic transition manifolds. However, in THz-FCS mode, each parent manifold is fully resolved as a K-stack with the enhanced spectral resolution of 5 MHz. Figure 6.4 compares data taken in THz-FCS mode with data taken in ASOPS-THz-TDS mode. It should be noted that the linewidth for the ASOPS-THz-TDS trace is fundamentally limited by the instrument in this

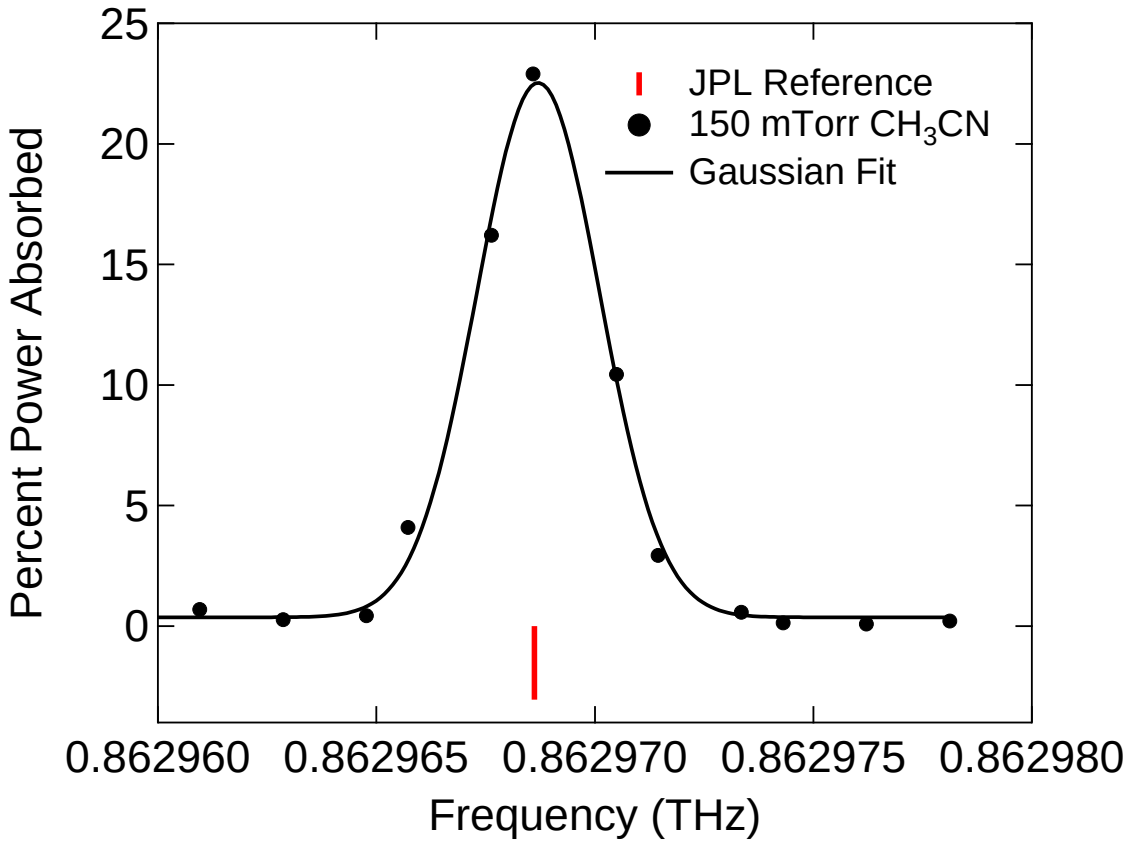

Figure 6.5: Detail of the K-stack shown in Figure 6.4. At this level of frequency resolution a single acetonitrile rotational transition with K = 3 is visible, demonstrating that the frequency accuracy of the instrument is not limiting the measurement of the transition frequency, as we have reached the Doppler-limit. This is evidenced by the Gaussian lineshape of the measured transition.

experiment and not by pressure broadening. The pressure of 2 Torr was chosen to maximize the number of lines resolved in the spectrum shown in Figure 4.3. As such, this instrument represents a nearly ideal compromise between fast-scanning systems with low resolution and slow-scanning systems with high-resolution, switching seamlessly between ASOPS-THz-TDS mode and THz-FCS mode.

Figure 6.5 is a detailed plot of the transition with K = 3 that is part of the K-stack plotted in Figure 6.4. The FWHM is 4.68 MHz and the lineshape is Gaussian, indicating the line is primarily Doppler broadened. The SNR of this peak is 115:1 and so the expected measurement accuracy is 220 kHz. For this transition with K = 3, the actual measurement accuracy of 85 kHz exceeds the expectation. The RMS accuracy of measured transitions across the entire K-stack is 150 kHz.

However, for higher SNR Doppler-limited absorptions, the accuracy of the instrument in THz-FCS mode will exceed 100 kHz, as discussed in the following section.

6.3 Water Percent Power Absorption Data

The initial demonstration of THz-FCS involved spectroscopy of water at pressures of 100 mTorr and 10 mTorr. Acquisition of these data predated direct PID control of the repetition rate of the pump laser. As such these data were obtained by shifting the set point temperature of the water chiller. This method of repetition rate control is limited by the 0.1 °C set point temperature control provided by the chiller. Each 0.1 °C step produced a ∼150 Hz step in repetition rate. The time required to reach thermal equilibrium with a new chiller temperature vastly increases instrument dead time between repetition rate steps. As such 0.5 °C steps were employed to collect broadband 100 mTorr data. As shown in Figure 6.6(a), this density of sampling (15 MHz step size for the 20000th comb tooth at 1.6 THz) was enough to provide at least one data point per absorption line. The RMS of the measured transitions here was 2.0 MHz due to the coarse sampling.

We obtained improved accuracy and resolved the line shape of water absorptions by taking fine steps of 0.1 °C over the range of three selected transitions, producing a step size of 3 MHz for the 20000th comb tooth. This step size was commensurate with the tooth width of 4.4 MHz. Over the three transitions shown in Figure 6.6(b)(c)(d), the RMS deviation from the predicted line positions was 92 kHz. At 10 mTorr these lines are Doppler broadened and well matched to a Gaussian line shape. These data demonstrate the excellent performance of the instrument as applied to Doppler-limited spectroscopy, even without stabilization of the pump laser repetition rate. Additionally, these experiments emphasize the importance of repetition rate control of the pump laser. For any experiment, the resolution of the comb is limited by the ability to step the comb accurately to cover the full spectral range. By employing longer scans with pump laser stabilization, the instrument resolution may be tuned to any desired value between 80 MHz and 3.7 kHz.

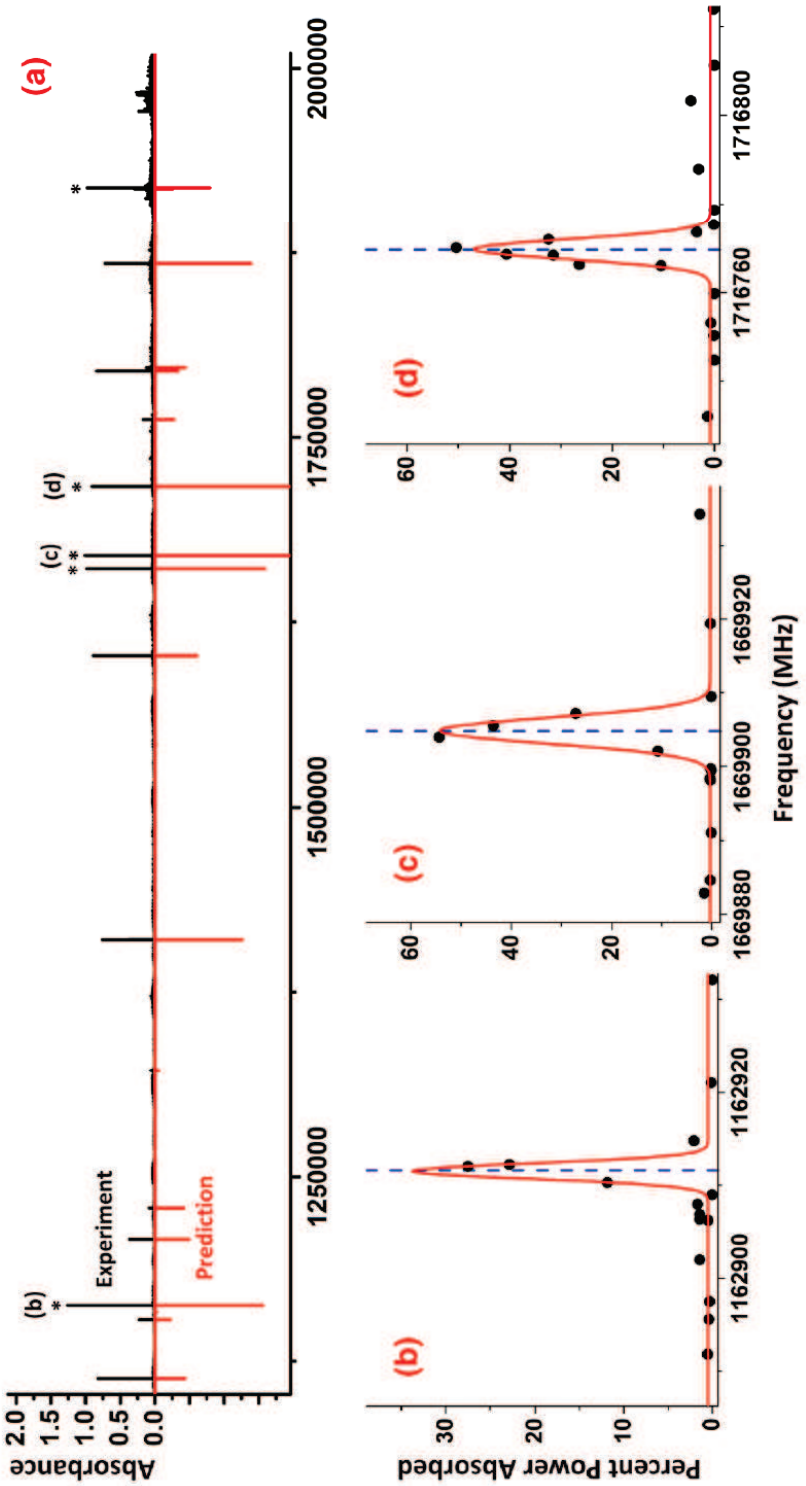

Figure 6.6: (a) Relative absorbance plot showing absorbtion spectroscopy of water at 100 mTorr across 1 THz of bandwidth, from 1 THz to 2 THz. The predicted spectrum is scaled to arbitrary units and inverted and plotted in red for clarity. (b)(c)(d) Percent power absorption plots showing individual water rotational transitions measured at 10 mTorr. Individual data points are plotted, along with a Gaussian fit in red and the predicted line center as a blue dotted line.

Chapter 7

THz-FCS of Methanol and MeOD

Up until this point, the spectra presented here have served a diagnostic role in characterizing the performance of the THz-FCS instrument. The THz spectra of water and acetonitrile are well studied and modeled, and the lines for water and acetonitrile reported in this thesis match assigned transitions predicted by existing models based on Doppler-limited data. Since measurements made by the spectrometer match previous data to ∼100 kHz precision, THz-FCS spectra generated by the spectrometer are suitable for assigning quantum numbers for rotational transitions of small molecules with incomplete or non-existent THz spectral data.

7.1 THz Spectroscopy of Methanol and Its Isotopologues in the Literature

Methanol and its isotopologues are ubiquitous throughout the interstellar medium (ISM). The ratios of deuterated isotopologues to normal MeOH may be used to determine the history of the conditions within molecular clouds.[34] At the low temperatures of the ISM the lower zero-point energy of deuterium relative to hydrogen in chemical bonds drives the exchange of hydrogen for deuterium in both gas phase molecules and molecules adsorbed on the icy mantles of dust grains, enriching the local abundance of deuterated species in cold molecular clouds relative to the average D/H abundance ratio throughout the universe. Furthermore, D/H branching ratios may be used to place constraints on formation of MeOH and its deuterated isotopologues through sequential H/D addition

to CO molecules adsorbed to ice grains. The $[CH_2DOH]/[CH_3OD]$ ratio is particularly useful for determining the probability of deuteration at the CH_3 site versus the OH site for methanol.[35] Different probability ratios are expected for each sequential deuteration step of methanol depending on the mechanism of deuteration. In addition to providing information about the chemistry of the ISM, the study of interstellar methanol has been used to place constraints on the drift of the proton-to-electron mass ratio over the history of the universe. Comparison of measurements of methanol absorptions in distant galaxies to laboratory measurements provides an excellent probe due to the extreme sensitivity of the energies of the mixed rotational-torsional transitions in MeOH to changes in the proton-to-electron mass ratio.[36] MeOH is also the molecule with the largest number of different maser transitions. MeOD has been predicted as a likely maser candidate due to favorable energy levels for IR pumping and high column densities relative to other MeOH isotopologues.[37]

Methanol is also an important molecule in developing the application of quantum mechanics to the prediction of rotational spectra, as it is the smallest molecule to contain an internal methyl rotor. This makes MeOH an important prototype for the study of the rotational spectra of molecules with C_{3v} internal rotors. As such much effort has been invested in the acquisition and analysis of MeOH spectra over the past several decades. A tunable far-infrared (TuFIR) spectrometer was used to measure MeOH absorptions from 1.5 to 6.5 THz with 20 kHz precision.[38] Far-infrared (FIR) synchrotron based FT spectroscopy was employed to measure MeOH absorptions from 1.8 to 11 THz with a precision of 1.5 MHz.[39] A global analysis from 0.15 to 1.0 THz was performed using an internal axis method (IAM) Hamiltonian to account for the internal rotation, resulting in a fit with a RMS deviation of 1.2 MHz.[40] A global analysis of a much larger data set has been refined into a superior fit that models the ground torsional state to an acuracy of 50 kHz.[41] Further analysis treated a data set including the torsionally excited states with a rho-axis method (RAM) Hamiltonian to obtain predictions limited by the accuracy of the measured lines.[42; 43] The predictive power of the model was recently evaluated using THz data from a JPL FMSS configuration covering the range from 2.48 to 2.77 THz.[44] The JPL FMSS instrument is capable of generating broadband, high-precision THz reference spectra for small molecules, with some caveats as discussed

in Section 7.3. The result of the extensive spectroscopy and modeling work with MeOH has yielded a high quality reference catalog of predicted transition frequencies and intensities available on the JPL molecular spectroscopy website.

A much smaller effort has gone towards acquiring and modeling spectra for MeOD. A high-resolution FT-IR spectrum from 0.5 to 6.1 THz has been acquired at a resolution of 6 MHz and a fit obtained for the torsionally excited states to an accuracy of 24 MHz.[45; 46; 47] However, the accuracy of this fit is ultimately limited by the accuracy of the data. A global analysis incorporating microwave and FT-IR data using a RAM Hamiltonian to treat the torsionally excited states resulted in a more accurate fit limited by the measurement uncertainty of the data.[48] The most recent global analysis fit the microwave and the FT-IR data separately, obtaining an RMS of 150 kHz for the microwave data and an RMS of 8.1 MHz for the FT-IR.[49] As such, future fits of MeOD can greatly benefit from THz data with an accuracy of 500 kHz or better, that is an order of magnitude more precise than the 6 to 8 MHz precision of the previous data.

7.2 THz-FCS of Methanol

As covered in the previous section, the THz spectrum of MeOH is well studied and serves as an excellent molecule to test the limits of the THz-FCS capabilities of the instrument. The predicted pure rotational spectrum of MeOH exceeds the useful bandwidth of the THz-FCS instrument, and the magnitude of the dipole is sufficient for detection of absorptions even in a short path length cell. Due to the hindered internal methyl rotor, the spectrum is exceedingly dense and provides an ideal test case for the combined high resolution and high bandwidth of the instrument. Data were acquired using the parameters described in Section 6.2. The sample cell was dosed with a steady flow of spectroscopic grade MeOH (99.9%, Sigma-Aldrich) resulting in a constant pressure of 140 mTorr. However, rather than stopping the data acquisition after a single cycle from -5V to +5V and back to -5V, the acquisition was allowed to run through multiple cycles as shown in Figure 5.3. These extra passes contribute additional data points improving the Gaussian fit of the absorptions and help to average out noise in the spectrum due to fluctuations in the power of the comb teeth

from scan to scan. The data set produced by stepping 68 times over the voltage range from -5V to +5V, back and forth 4 times for a total of 272 individual scans, for MeOH at 140 mTorr is explored in detail in this section.

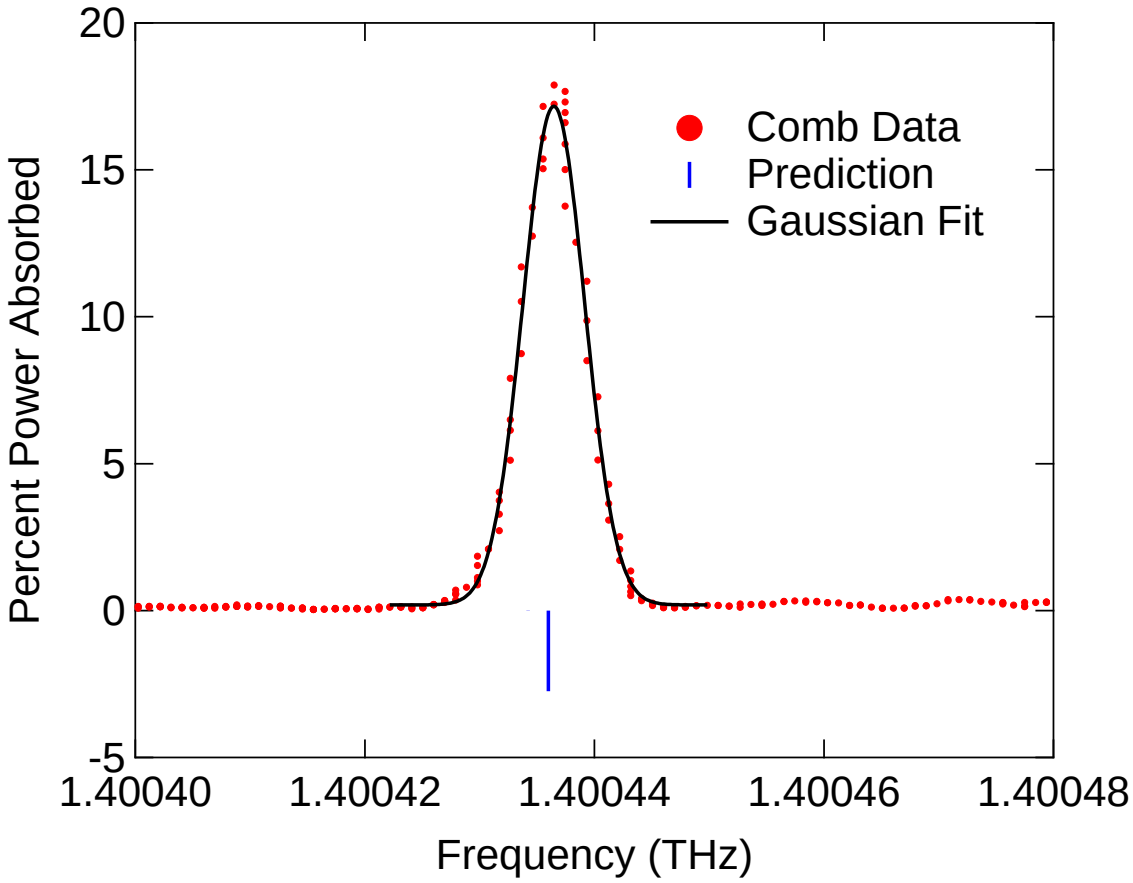

Figure 7.1: Detail of MeOH percent power absorption plot showing a strong absorption with a 120:1 SNR . The observed minus calculated error is 468 kHz with a Gaussian peak shape. THz-FCS data points are plotted as red points. Predicted MeOH absorptions are plotted as vertical blue lines. A Gaussian fit of the data is plotted as a bold black line.

Figure 7.1 shows a Gaussian fit of one of the strong absorptions in this data set. The Gaussian fit to the data is good with an uncertainty in the fit on the frequency axis of 30.5 kHz. Following the rule of $RMS\ error = FWHM/2\sqrt{SNR}$ for a FWHM of 8.98 MHz and SNR of 120:1 for this peak it should be possible to measure the center frequency of the absorption to an accuracy of 410 kHz. Indeed, the observed minus calculated (OMC) error for this peak is 468 kHz, close to the SNR limited accuracy. Since the uncertainty in the fit is an order of magnitude lower than the OMC

error, peaks with a good quality Gaussian fit will have a SNR limited measurement accuracy. Figure 7.2 shows a Gaussian fit of a weaker absorption where the quality of the fit is contributing to the error in resolving the center frequency. The peak clearly has an asymmetric shape, skewed towards higher frequencies, and the uncertainty in the fit on the frequency axis is 100 kHz. This peak has a FWHM of 8.60 MHz and a SNR of 20:1 with an expected measurement error of 960 kHz. The OMC error of 918 kHz is quite close to this value. At 1.933 THz we are at the 24160^{th} comb tooth and so we can expect a drift of 10 Hz in the pump laser repetition rate during a scan to correspond to a drift of 242 kHz in the comb teeth around 1.933 THz. In the unlocked mode of scanning the pump repetition rate, such 10 Hz drifts are expected and can be a contributing factor to the error in peak measurement. In the conclusion, an improvement to the scanning routine is discussed that will eliminate these drifts by locking the pump laser during scans.

Figure 7.3 shows a multi-peak Gaussian fit of a K-stack of MeOH absorptions. This K-stack highlights the limitations imposed by the Doppler limit at 140 mTorr, and the chosen 5 MHz resolution of the THz-FCS instrument. Since the tooth width was 5 MHz when this data was acquired, the data will not resolve splittings less than or equal to 5 MHz. For MeOH at 140 mTorr, 298 K, and 1.933 THz, the expected Doppler broadened FWHM is 4.2 MHz and the expected pressure broadened FWHM is 4.4 MHz. This means that even if the tooth width were smaller, the broadened lines will blend together, making it impossible to resolve splittings smaller than $\sim$5 MHz. With this knowledge we set the instrument resolution to 5 MHz, knowing that any increase in resolution would be wasted due to the Doppler limit. The first two MeOH absorptions in Figure 7.3 are predicted at 1.588594756 THz and 1.588587991 THz, a splitting of 3.2 MHz. In the multi-peak fit, it was impossible to fit two peaks accurately to the data without fixing one of the peaks to the predicted value for one of the absorptions. By fixing the second peak at 1.588587991 THz, it was possible to fit the position of the first peak to an error of 730 kHz. All of the other peaks in the K-stack have splittings of greater than 5 MHz, and are sufficiently resolved for fitting.

A list of selected MeOH absorptions detected by the instrument is given in Table 7.1. The RMS error for these absorptions is 402 kHz, which decreases to 303 kHz when excluding low SNR peaks

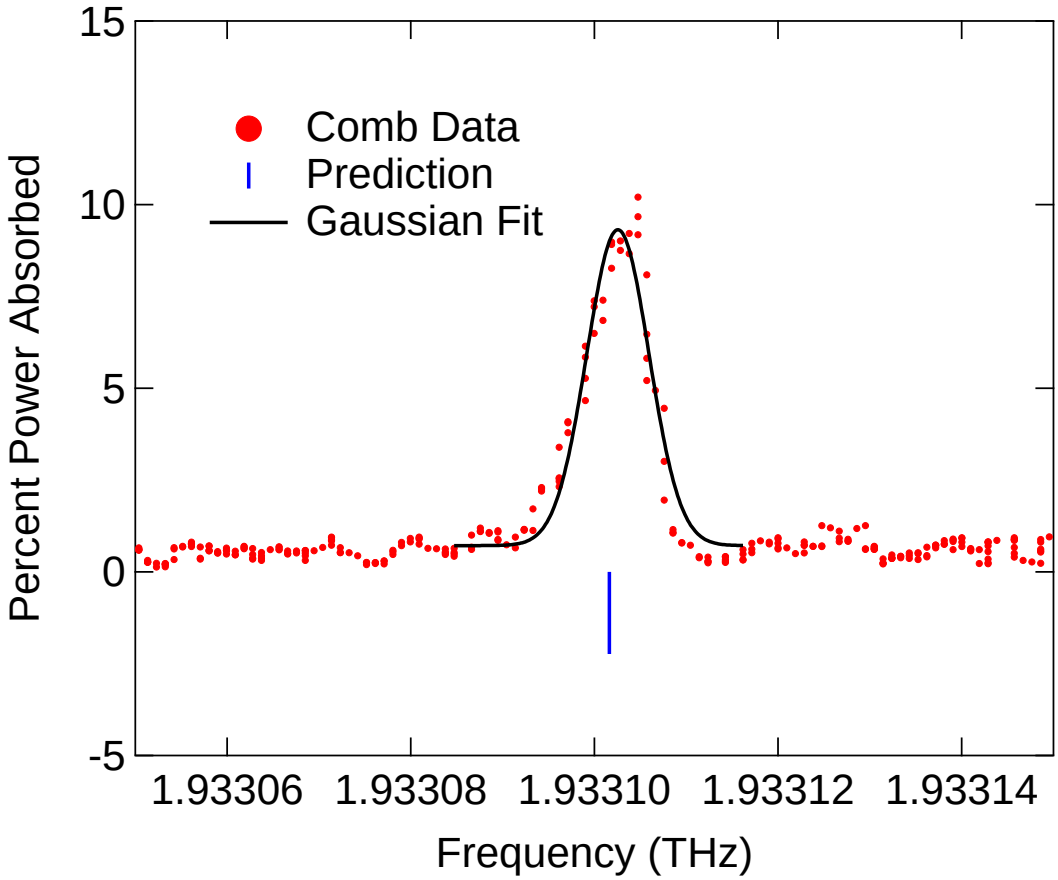

Figure 7.2: Detail of MeOH percent power absorption plot showing a weaker absorption with a 20:1 SNR. The OMC error is 918 kHz with a distorted Gaussian peak shape. THz-FCS data points are plotted as red points. Predicted MeOH absorptions are plotted as vertical blue lines. A Gaussian fit of the data is plotted as a bold black line.

and a few peaks with obvious errors in fitting. Overall, there is no correlation between the error contribution from fitting and the total error in the accuracy of the measurement of the peak center. This indicates that a sufficient number of data points were acquired at a sufficient SNR for accurate fitting of the data. Cases involving peak asymmetry are easily identified via visual inspection of the fit and confirmed by a poor fitting factor on the frequency axis. There is also no correlation between measurement error and FWHM, indicating that the main limiting factor for measurement accuracy is SNR.

The relative intensity performance of the instrument may be evaluated by plotting the base 10 logarithm of the integrated intensities obtained by the instrument versus the reference intensity

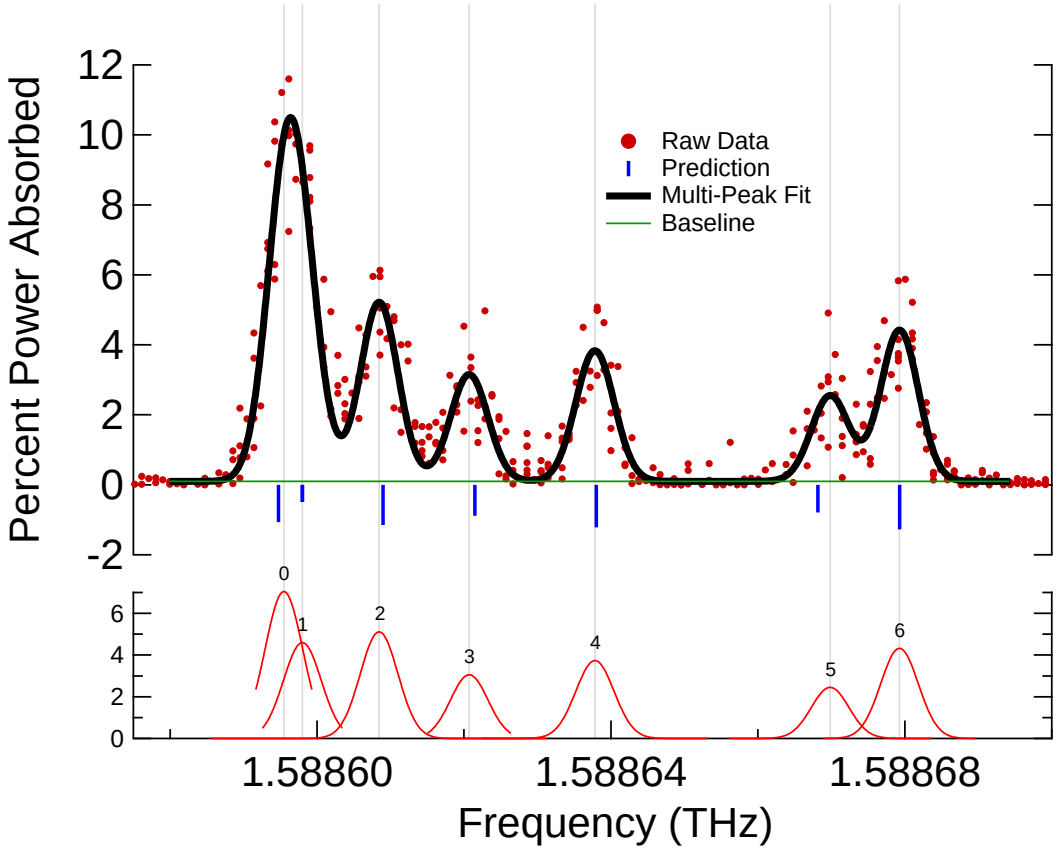

Figure 7.3: Detail of MeOH percent power absorbance plot showing the ability to resolve Doppler limited lines with 5 MHz resolution. Data points acquired via peak picking raw data are plotted as red points. Predicted MeOH absorptions are plotted as vertical blue lines. A multi-peak Gaussian fit of the data is plotted as a bold black line. The baseline is plotted as a green line. The individual fit peaks are plotted separately below the data.

values in the JPL catalog. As shown in Figure 7.4, the intensity response of the instrument correlates linearly with JPL intensity values plotted on a linear axis. The spread of intensity values for the instrument increases for lower intensity absorptions, indicating that power noise is present in the data. To obtain absolute intensity information the trend line parameters may be used to calibrate the intensity data obtained by the instrument.

With a benchmark of the system performance in hand, it is possible to confidently assign new absorptions for molecules of interest. Since the absorptions detected are generally SNR limited, it is possible to estimate the measurement accuracy for a given absorption and weight it accordingly when generating a model spectrum from measured absorptions. When assigning quantum numbers

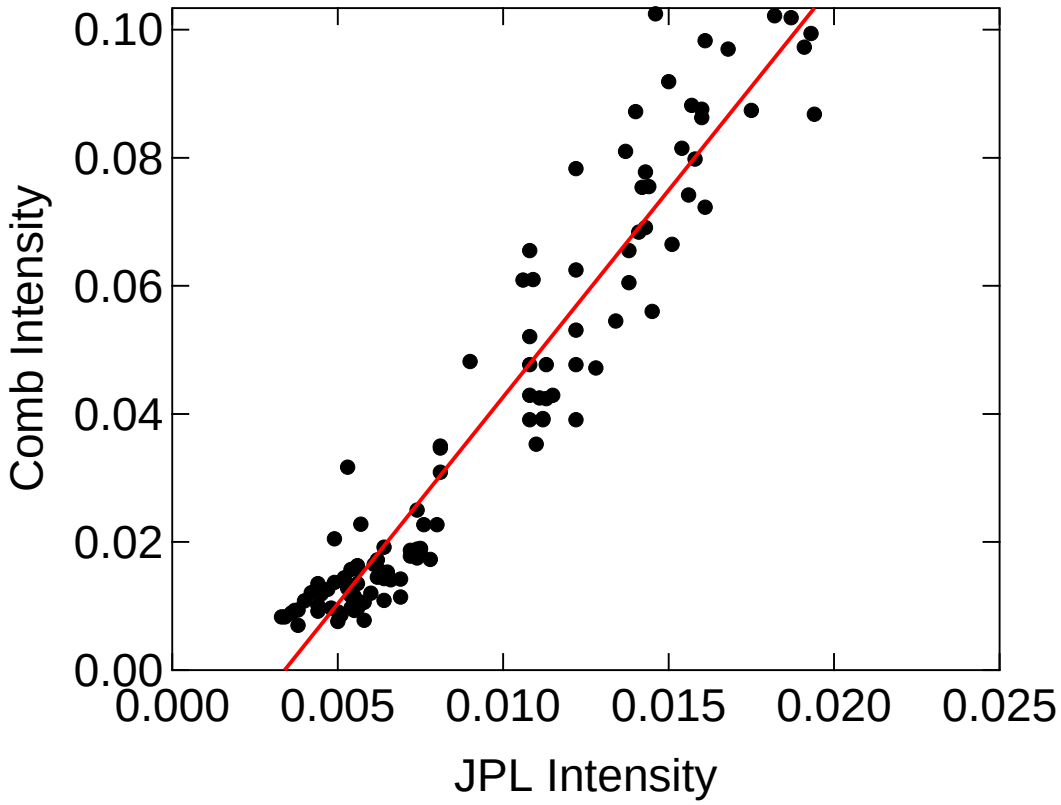

Figure 7.4: Plot of JPL intensity values versus comb intensity values as black dots with the linear correlation in the data plotted as a red line. The equation of the line is y = 6.459x - 0.022 with an uncertainty of ±0.185 in the slope and an uncertainty of ±0.002 in the y-intercept (R^2 = 0.9177). This corresponds to a 3% error in measuring the intensity of absorptions for the instrument.

to transitions in the THz region, an RMS error of 100 kHz or lower is generally preferred. This corresponds to a measurement accuracy of 0.1 ppm at 1 THz. As such, future efforts at improving the SNR of the instrument should aim to bring down the current RMS of the THz-FCS instrument by a factor of 5, requiring a factor of 25 improvement in SNR.

Table 7.1: List of absorptions of MeOH at 140 mTorr between 1.33 and 2.0 THz detected by the instrument in THz-FCS mode. Data associated with the measured absorptions is listed as Comb, reference data from the JPL molecular spectroscopy catalog is labeled JPL. The observed minus calculated (OMC) error in the measured absorptions is listed under Comb-JPL is provided as a diagnostic of the comb performance. The uncertainty of the Gaussian fit in kHz along the frequency axis is listed as Comb σ. The integrated intensity under the measured absorptions is calculated using the FWHM (in units of THz) and the height (in units of absorbance) of the Gaussian fit. The units of percent power absorbed used on the vertical axis of Figures 7.1, 7.2, and 7.3 plots were converted to units of absorbance and then the base 10 logarithm of the comb integrated intensity is taken for comparison of comb intensity values to JPL intensity values in Figure 7.4 and in this table. The RMS error in the measured MeOH absorptions versus reference values was 402 kHz including all measured absorptions and 303 kHz when excluding low SNR data.

Comb (THz)	JPL (THz)	Comb-JPL (MHz)	Comb σ (kHz)	Comb FWHM	Comb Height	Comb Inten	Comb Log Int	JPL Log Int
1.330500881	1.330500286	0.595	43.5	10.14	0.0126	0.137	-0.86	-2.33
1.344611643	1.344611377	0.266	41.1	10.08	0.0172	0.185	-0.73	-2.21
1.380430436	1.380430609	-0.173	53.0	9.76	0.0096	0.100	-1.00	-2.25
1.392327829	1.392328126	-0.297	48.3	8.30	0.0086	0.076	-1.12	-2.29
1.392897606	1.392897576	0.030	38.7	10.20	0.0153	0.167	-0.78	-2.18
1.400436466	1.400435998	0.468	30.5	8.98	0.0810	0.776	-0.11	-1.86
1.428691710	1.428691984	-0.274	69.8	11.12	0.0108	0.128	-0.89	-2.25
1.433126620	1.433126888	-0.268	87.2	11.33	0.0082	0.099	-1.01	-2.75
1.441042325	1.441042061	0.264	49.4	9.26	0.0983	0.971	-0.01	-1.79
1.441143242	1.441143445	-0.203	57.8	8.94	0.0142	0.135	-0.87	-2.16
1.448657956	1.448657561	0.395	42.2	10.03	0.0872	0.933	-0.03	-1.85
1.453115217	1.453115618	-0.401	35.1	8.34	0.1025	0.912	-0.04	-1.83
1.462661034	1.462661560	-0.526	61.6	11.14	0.0157	0.186	-0.73	-2.25
1.469946714	1.469946550	0.164	66.5	7.93	0.0143	0.121	-0.92	-2.19
1.489338619	1.489338349	0.270	69.5	10.49	0.0178	0.199	-0.70	-2.15
1.489380884	1.489380620	0.264	34.0	9.99	0.0970	1.034	0.01	-1.78
1.496857850	1.496857503	0.347	43.5	10.15	0.0754	0.816	-0.09	-1.85

Comb (THz)	JPL (THz)	Comb-JPL (MHz)	Comb σ (kHz)	Comb FWHM	Comb Height	Comb Inten	Comb Log Int	JPL Log Int
1.501412622	1.501412900	-0.278	50.4	9.21	0.0919	0.903	-0.04	-1.82
1.506143484	1.506143383	0.101	57.2	8.61	0.0101	0.093	-1.03	-2.35
1.510747320	1.510747284	0.036	85.1	10.87	0.0135	0.156	-0.81	-2.25
1.518122877	1.518123510	-0.633	72.2	11.37	0.0109	0.132	-0.88	-2.19
1.522091721	1.522091204	0.517	58.1	11.89	0.0157	0.200	-0.70	-2.27
1.525231735	1.525231284	0.451	59.7	13.38	0.0097	0.138	-0.86	-2.26
1.532395243	1.532395509	-0.266	87.1	13.99	0.0091	0.136	-0.87	-2.31
1.537470140	1.537470487	-0.347	78.2	13.39	0.0189	0.270	-0.57	-2.13
1.537705935	1.537705595	0.340	59.0	11.07	0.0874	1.031	0.01	-1.76
1.545035322	1.545035068	0.254	51.2	10.57	0.0778	0.878	-0.06	-1.84
1.549690487	1.549691099	-0.612	48.5	10.02	0.0815	0.871	-0.06	-1.81
1.554394740	1.554394426	0.314	102.0	9.47	0.0121	0.122	-0.91	-2.38
1.566287811	1.566288264	-0.453	65.1	9.70	0.0154	0.159	-0.80	-2.20
1.569653367	1.569653051	0.316	66.0	8.31	0.0115	0.102	-0.99	-2.26
1.585526920	1.585526901	0.019	40.9	10.41	0.0190	0.211	-0.67	-2.13
1.586013180	1.586013008	0.172	34.3	12.16	0.1022	1.325	0.12	-1.74
1.588595486	1.588594756	0.730	71.5	8.57	0.0317	0.290	-0.54	-2.27
1.588597991	1.588597991	0.000	0.0	8.56	0.0205	0.187	-0.73	-2.31
1.588608450	1.588608982	-0.532	102.8	8.54	0.0228	0.208	-0.68	-2.24
1.588620710	1.588621485	-0.775	172.6	8.48	0.0135	0.122	-0.91	-2.35
1.588637823	1.588638007	-0.184	143.7	8.67	0.0165	0.153	-0.82	-2.21
1.588669835	1.588668167	1.668	237.0	8.54	0.0108	0.098	-1.01	-2.40
1.588679276	1.588679307	-0.031	120.8	8.55	0.0192	0.175	-0.76	-2.20
1.593189923	1.593189562	0.361	49.7	10.36	0.0755	0.834	-0.08	-1.84
1.597947062	1.597947024	0.038	76.7	9.63	0.0882	0.906	-0.04	-1.80

Comb (THz)	JPL (THz)	Comb-JPL (MHz)	Comb σ (kHz)	Comb FWHM	Comb Height	Comb Inten	Comb Log Int	JPL Log Int
1.606782404	1.606782040	0.364	82.4	8.41	0.0116	0.104	-0.98	-2.27
1.614442299	1.614442036	0.263	68.0	10.43	0.0145	0.162	-0.79	-2.21
1.617029219	1.617029687	-0.468	117.0	10.42	0.0100	0.111	-0.96	-2.26
1.633493129	1.633493496	-0.367	71.7	11.40	0.0180	0.218	-0.66	-2.12
1.634298513	1.634298405	0.108	39.4	11.54	0.1019	1.255	0.10	-1.73
1.641320412	1.641320359	0.053	34.0	10.43	0.0691	0.769	-0.11	-1.84
1.643454904	1.643454999	-0.095	49.5	10.16	0.0609	0.660	-0.18	-1.97
1.646177000	1.646177219	-0.219	28.0	10.86	0.0863	1.000	0.00	-1.80
1.654722932	1.654722284	0.648	80.7	13.81	0.0144	0.212	-0.67	-2.28
1.662586735	1.662586230	0.505	74.5	9.92	0.0120	0.127	-0.90	-2.22
1.662847995	1.662847210	0.785	36.9	9.85	0.0350	0.368	-0.43	-2.09
1.664194028	1.664193757	0.271	77.5	11.36	0.0163	0.197	-0.70	-2.26
1.681355052	1.681355068	-0.016	95.3	14.05	0.0189	0.283	-0.55	-2.13
1.682557173	1.682556856	0.317	34.8	12.08	0.0973	1.254	0.10	-1.72
1.689426920	1.689426893	0.027	46.7	10.12	0.0684	0.738	-0.13	-1.85
1.691768616	1.691768189	0.427	54.7	8.95	0.0610	0.583	-0.23	-1.96
1.694377855	1.694377964	-0.109	40.4	9.85	0.0723	0.760	-0.12	-1.79
1.702604956	1.702604914	0.042	65.3	8.55	0.0076	0.069	-1.16	-2.30
1.710722784	1.710722430	0.354	101.0	11.51	0.0078	0.096	-1.02	-2.24
1.711024381	1.711023981	0.400	64.5	10.10	0.0309	0.333	-0.48	-2.09
1.711117710	1.711117441	0.269	65.3	9.71	0.0093	0.096	-1.02	-2.26
1.718473926	1.718473478	0.448	58.1	8.08	0.0119	0.103	-0.99	-2.35
1.725801247	1.725800981	0.266	71.4	10.01	0.0094	0.100	-1.00	-2.43
1.726230532	1.726228794	1.738	75.0	8.24	0.0093	0.082	-1.09	-2.43
1.726762268	1.726761901	0.367	82.8	12.81	0.0089	0.122	-0.91	-2.45

Comb (THz)	JPL (THz)	Comb-JPL (MHz)	Comb σ (kHz)	Comb FWHM	Comb Height	Comb Inten	Comb Log Int	JPL Log Int
1.729095372	1.729095336	0.036	83.8	12.13	0.0175	0.226	-0.65	-2.13
1.730783205	1.730782964	0.241	37.3	11.01	0.0994	1.168	0.07	-1.71
1.737508968	1.737508664	0.304	50.1	10.32	0.0605	0.666	-0.18	-1.86
1.740069026	1.740068615	0.411	54.5	12.25	0.0425	0.556	-0.26	-1.96
1.742544898	1.742545274	-0.376	57.7	11.56	0.0876	1.080	0.03	-1.80
1.759174076	1.759173476	0.600	31.8	7.77	0.0347	0.287	-0.54	-2.09
1.776696884	1.776696991	-0.107	38.5	9.62	0.0187	0.192	-0.72	-2.14
1.778970553	1.778970864	-0.311	49.2	12.75	0.0868	1.180	0.07	-1.71
1.785565127	1.785565236	-0.109	48.6	10.92	0.0545	0.635	-0.20	-1.87
1.788354271	1.788354322	-0.051	51.7	11.50	0.0393	0.482	-0.32	-1.95
1.790674330	1.790674899	-0.569	42.0	12.02	0.0798	1.023	0.01	-1.80
1.804132753	1.804132942	-0.189	99.4	7.95	0.0128	0.108	-0.97	-2.27
1.807294439	1.807294030	0.409	58.4	9.09	0.0227	0.220	-0.66	-2.10
1.817752377	1.817752285	0.092	38.8	10.12	0.0783	0.845	-0.07	-1.91
1.822898077	1.822898448	-0.371	32.0	8.95	0.0655	0.625	-0.20	-1.97
1.824141303	1.824141748	-0.445	109.0	11.06	0.0114	0.135	-0.87	-2.16
1.833159398	1.833159051	0.347	73.1	11.04	0.0083	0.098	-1.01	-2.48
1.833596156	1.833596237	-0.081	27.2	10.69	0.0472	0.538	-0.27	-1.89
1.834358282	1.834358504	-0.222	83.2	9.13	0.0083	0.081	-1.09	-2.47
1.836623468	1.836623223	0.245	35.7	10.36	0.0424	0.468	-0.33	-1.95
1.838761955	1.838762330	-0.375	37.3	10.62	0.0742	0.840	-0.08	-1.81
1.855101288	1.855101602	-0.314	149.0	9.18	0.0097	0.095	-1.02	-2.32
1.855384528	1.855383941	0.587	77.8	9.74	0.0173	0.179	-0.75	-2.11
1.866031205	1.866031258	-0.053	45.6	10.76	0.0625	0.717	-0.14	-1.91
1.871183032	1.871183728	-0.696	44.3	9.00	0.0521	0.500	-0.30	-1.97

Comb (THz)	JPL (THz)	Comb-JPL (MHz)	Comb σ (kHz)	Comb FWHM	Comb Height	Comb Inten	Comb Log Int	JPL Log Int
1.871410419	1.871410427	-0.008	87.4	10.34	0.0141	0.156	-0.81	-2.18
1.881601537	1.881601359	0.178	52.0	11.61	0.0391	0.484	-0.32	-1.91
1.884873116	1.884873108	0.008	56.3	9.82	0.0477	0.500	-0.30	-1.95
1.886802949	1.886802804	0.145	48.5	10.47	0.0665	0.743	-0.13	-1.82
1.895862590	1.895862726	-0.136	76.9	9.27	0.0137	0.135	-0.87	-2.31
1.901719811	1.901719349	0.462	106.0	10.62	0.0070	0.079	-1.10	-2.42
1.903224860	1.903225247	-0.387	116.0	13.45	0.0092	0.132	-0.88	-2.35
1.903441816	1.903441472	0.344	83.3	8.45	0.0227	0.205	-0.69	-2.12
1.914297224	1.914297382	-0.158	38.4	10.90	0.0531	0.617	-0.21	-1.91
1.919447824	1.919449123	-1.299	71.3	9.56	0.0429	0.437	-0.36	-1.97
1.929580505	1.929580359	0.146	76.6	11.09	0.0429	0.507	-0.29	-1.94
1.933102557	1.933101639	0.918	100.0	11.35	0.0391	0.473	-0.33	-1.95
1.934791276	1.934791275	0.001	71.9	11.44	0.0560	0.684	-0.17	-1.84
1.951464840	1.951464848	-0.008	70.7	10.15	0.0250	0.271	-0.57	-2.13
1.962550235	1.962550047	0.188	28.5	10.85	0.0477	0.552	-0.26	-1.91
1.965338157	1.965338919	-0.762	106.0	12.69	0.0106	0.143	-0.85	-2.24
1.967691129	1.967691350	-0.221	30.9	10.31	0.0477	0.525	-0.28	-1.97
1.970934236	1.970933840	0.396	54.1	8.61	0.0482	0.442	-0.35	-2.04
1.977532909	1.977533063	-0.154	69.3	12.29	0.0391	0.512	-0.29	-1.97
1.981305968	1.981306350	-0.382	70.2	10.90	0.0353	0.410	-0.39	-1.96
1.982722164	1.982722415	-0.251	52.7	12.00	0.0655	0.838	-0.08	-1.86

7.3 THz-FCS of MeOD

Despite the apparent similarity between MeOH and MeOD, the increase in mass of the hydroxy group induced by the substitution of deuterium for hydrogen is significant. Indeed, the torsional energy manifold defined by the perturbation of the internal rotation is significantly altered. As a result there is no simple relation between the THz rotational spectra of MeOH and MeOD and a completely revised version of the model Hamiltonian used for MeOH is needed to predict the spectrum of MeOD. The overall increase in the mass of MeOD favorably shifts the peak of the rotational spectrum to a lower frequency, better overlapping with the bandwidth of the THz-FCS instrument. THz-FCS data for MeOD were acquired using the same parameters as for MeOH. The sample cell was dosed with a steady flow of MeOD (99%, Cambridge Isotope Labs) resulting in a constant pressure of 80 mTorr. Under these conditions the expected Doppler broadened FWHM is 4.2 MHz and the expected pressure broadened FWHM is 2.5 MHz. However, the average measured FWHM for MeOD absorptions was 9.6 MHz. This indicates that some other broadening process is occurring that did not occur for the CH_3CN absorptions measured in Section 6.2, which had FWHM values averaging 5.7 MHz. Methanol is a notoriously sticky molecule and so the likely source of additional broadening that the actual cell pressure is higher than the pressure reported by our gauge due to MeOH and MeOD sticking to the walls of the sample cell. This is further discussed later on in this section.

There is no entry in the JPL molecular spectroscopy catalog for MeOD and so reference data was generously provided by Shanshan Yu of the JPL molecular spectroscopy group for comparison with the comb spectrum. The JPL data is plotted alongside the comb data in Figure 7.5. Since the JPL data was acquired by a frequency multiplier submillimeter spectrometer (FMSS), the error in the measurement of the absorption centers is largely Doppler-limited and highly accurate. The drawback to this instrument is that electronic frequency multipliers are used to multiply microwave frequencies up to THz frequencies. These frequency multipliers are limited in frequency range and as a result a series of different multiplier configurations must be used to cover the entire THz region of interest. For example, a JPL data set for MeOD acquired in 24 hours of integration time is shown

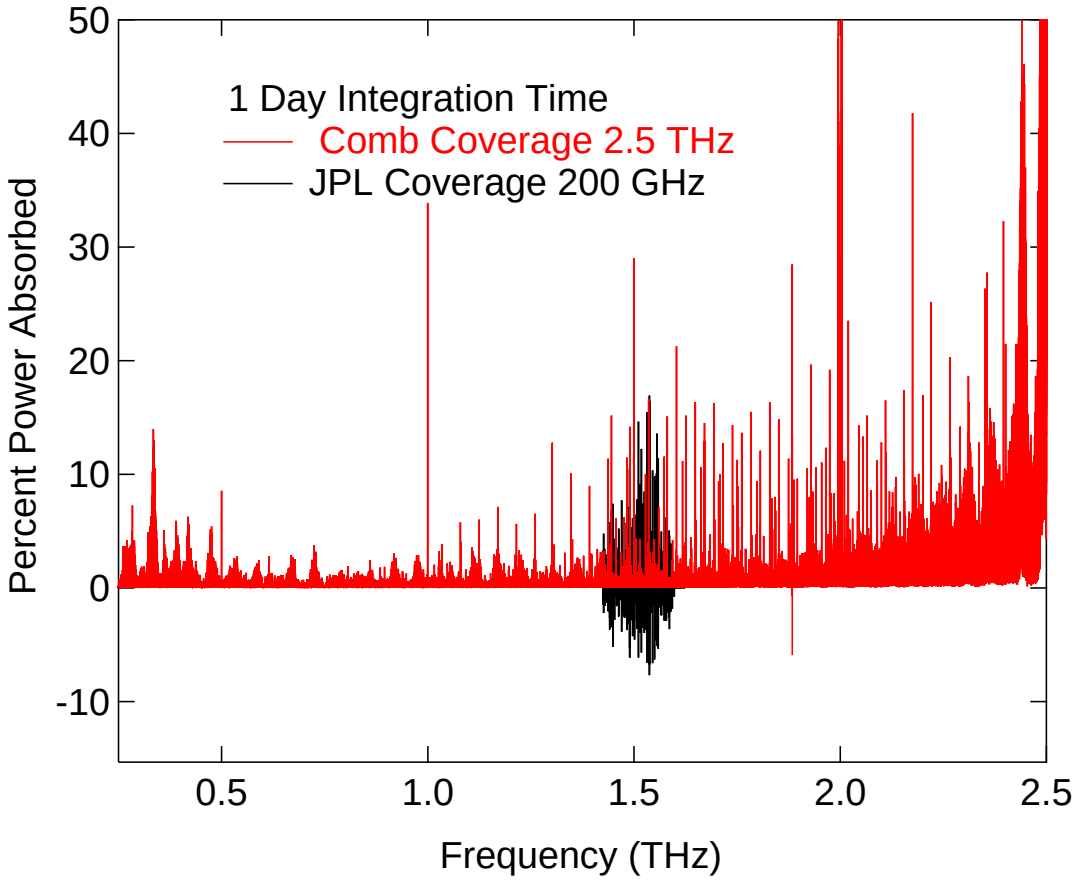

Figure 7.5: Plot of JPL FMSS absorption data set from 1.43 to 1.60 THz (black lines) and comb absorption data set from 1.1 THz to 2.1 THz (red lines) for MeOD at ∼100 mTorr. The JPL spectrum intensity values are scaled for comparison to the comb values. Both data sets took approximately 24 hours (1 day) of integration time. Note the superior bandwidth of the THz-FCS comb data set.

in Figure 7.5 along with the THz-FCS comb data set acquired in 24 hours of integration time for MeOD. The comb covers the entire range from 1.0 to 2.5 THz (1.5 THz bandwidth) in 24 hours of integration time, while the JPL FMSS instrument only covers the range from 1.43 to 1.6 THz (0.17 THz bandwidth). The frequency comb instrument is roughly an order of magnitude faster than the JPL instrument when generating broadband THz reference spectra. The JPL FMSS instrument may be configured to cover the following ranges: 1.0 to 1.2 THz, 1.33 to 1.43 THz, 1.43 to 1.6 THz, 1.6 to 1.8 THz, and 1.8 to 2.0 THz. There is an additional range of coverage from 2.5 to 2.8 THz but this exceeds the current bandwidth of the THz-FCS instrument.[50] Each of these scans requires a different configuration of frequency multipliers with a characteristic response function across the

frequency range of the scan. As such, extracting relative intensity information from the data requires individual calibration of each multiplier configuration.[51]

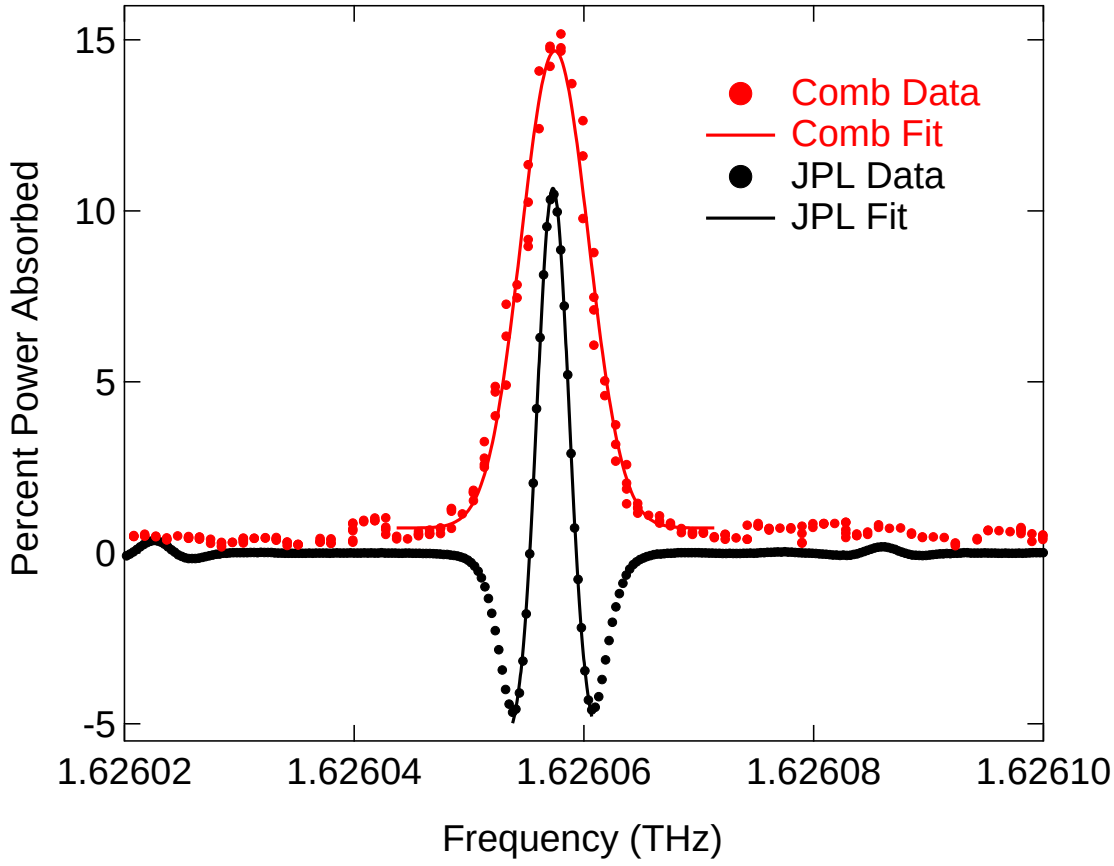

Figure 7.6: Detail of JPL absorption spectrum and comb absorption spectrum showing individual data points for a MeOD absorption. The comb data are plotted as red points with a Gaussian fit plotted as a red line. The JPL data have been scaled for comparison and are plotted as black points with a Gaussian fit to the data plotted as a black line. Note the superior SNR of the JPL data, further emphasizing that the current accuracy of the comb data is SNR limited.

As shown in Figure 7.6, the JPL FMSS data exhibit excellent sensitivity and high SNR. The peaks in the baseline for the JPL data to the left and right of the main peak are actually low intensity absorptions. The rest of the baseline is essentially flat due to the high SNR of the JPL measurement. The SNR is 1500:1 with a FWHM of 9.52 MHz (the FWHM of the JPL data appears narrower because this data is plotted as a second derivative, the FWHM of the comb data and the JPL data are nearly identical when both are plotted normally). This corresponds to a SNR limited measurement accuracy of 120 kHz with an uncertainty in the Gaussian fit of 5.4 kHz. In comparison,

the comb measurement of the same MeOD absorption has a SNR of 75:1 with a FWHM of 9.80 MHz. This corresponds to a SNR limited measurement accuracy of 560 kHz with an uncertainty in the Gaussian fit of 47 kHz. However, the comb measurement is able to acquire the entire spectrum from 1.0 to 2.5 THz in a single acquisition with an easily calibrated relative intensity response across the entire spectrum as shown previously in Figure 7.4. This fills in the gaps in available JPL FMSS data from 1.2 to 1.33 THz and from 2.0 to 2.38 THz. Overall, the RMS discrepancy between comb measured and JPL measured MeOD absorptions was 474 kHz. The RMS was reduced to 342 kHz when excluding low SNR comb data. Table 7.2 provides a full listing of MeOD absorptions detected by the THz-FCS instrument. This high resolution THz-FCS data may be used along with JPL FMSS data to refine the existing fits of MeOD to generate a high quality catalog suitable for analysis of astronomy data. Such efforts are presently underway both in the JPL Molecular Spectroscopy Group and in the Blake Group.

Table 7.2: List of absorptions of MeOD at 80 mTorr detected by the instrument in THz-FCS mode. Data associated with the detected absorptions is listed as Comb, reference data fitted from JPL frequency multiplier submillimeter spectra is labeled as JPL. The difference between the measured absorptions for the two different instruments is listed under Comb-JPL. The uncertainty in the Gaussian fit in kHz along the frequency axis is listed as Comb σ. The integrated intensity under the measured absorptions is calculated using the FWHM (in units of THz) and the height (in units of absorbance) of the Gaussian fit. JPL data for MeOD was available from 1.33 THz to 2 THz and as such absorptions detected by the comb outside of this range are reported without comparison. The RMS discrepancy between the of the comb measured and JPL measured MeOD absorptions was 474 kHz including all measured absorptions and 342 kHz when excluding low SNR comb data.

Comb (THz)	JPL (THz)	Comb-JPL (MHz)	Comb σ (kHz)	Comb FWHM	Comb Height	Comb Inten	Comb Log Int
1.207455276			89.0	16.11	0.0056	0.097	-1.01
1.210050307			78.1	12.65	0.0050	0.067	-1.17
1.212130487			55.7	8.88	0.0122	0.116	-0.94
1.215052818			43.2	11.84	0.0231	0.291	-0.54
1.252305093			96.4	12.01	0.0056	0.072	-1.14
1.257449713			44.3	8.88	0.0106	0.100	-1.00

Comb (THz)	JPL (THz)	Comb-JPL (MHz)	Comb σ (kHz)	Comb FWHM	Comb Height	Comb Inten	Comb Log Int
1.260306877			29.4	11.61	0.0265	0.328	-0.48
1.261284534			108.0	10.48	0.0084	0.094	-1.03
1.272951070			55.8	7.29	0.0055	0.043	-1.37
1.299631911			76.2	6.57	0.0067	0.047	-1.33
1.301728065			28.1	7.35	0.0533	0.418	-0.38
1.302762425			61.2	9.53	0.0132	0.134	-0.87
1.305537262			76.1	9.49	0.0159	0.161	-0.79
1.320801649			61.8	9.26	0.0079	0.078	-1.11
1.332810501	1.332809906	0.595	44.3	10.24	0.0122	0.133	-0.88
1.346990488	1.346990152	0.336	32.6	8.30	0.0432	0.383	-0.42
1.348068261	1.348068471	-0.210	59.2	10.31	0.0100	0.110	-0.96
1.350739511	1.350736641	2.870	49.3	13.42	0.0172	0.246	-0.61
1.350739511	1.350741922	-2.411	49.3	13.42	0.0172	0.246	-0.61
1.351794312	1.351794129	0.183	64.3	8.38	0.0057	0.051	-1.29
1.377866863	1.377866693	0.170	71.5	8.36	0.0096	0.085	-1.07
1.392230379	1.392230496	-0.117	28.9	10.28	0.0404	0.443	-0.35
1.393367070	1.393367278	-0.208	46.9	8.23	0.0101	0.089	-1.05
1.395904400	1.395903937	0.463	106.0	13.08	0.0111	0.155	-0.81
1.395915649	1.395914751	0.898	93.3	10.93	0.0119	0.139	-0.86
1.397021692	1.397021624	0.068	73.1	11.21	0.0074	0.088	-1.06
1.397753651	1.397753284	0.367	60.8	9.11	0.0122	0.119	-0.92
1.411243301	1.411242615	0.686	64.6	8.29	0.0128	0.113	-0.95
1.422860595	1.422860616	-0.021	101.0	9.42	0.0119	0.119	-0.92
1.437443375	1.437443416	-0.041	26.2	8.97	0.0490	0.469	-0.33
1.438658740	1.438658506	0.234	34.2	7.81	0.0136	0.114	-0.94

Comb (THz)	JPL (THz)	Comb-JPL (MHz)	Comb σ (kHz)	Comb FWHM	Comb Height	Comb Inten	Comb Log Int
1.441031550	1.441031695	-0.145	99.3	10.89	0.0071	0.082	-1.08
1.441052384	1.441052652	-0.268	78.1	8.76	0.0087	0.081	-1.09
1.442227503	1.442228153	-0.650	103.0	12.52	0.0067	0.089	-1.05
1.443064180	1.443063638	0.542	32.6	8.17	0.0158	0.138	-0.86
1.445311561	1.445311664	-0.103	32.1	8.50	0.0638	0.578	-0.24
1.456424887	1.456424886	0.001	90.5	8.67	0.0172	0.159	-0.80
1.467781321	1.467781320	0.001	43.0	6.18	0.0124	0.082	-1.09
1.482625967	1.482625941	0.026	28.1	9.18	0.0473	0.463	-0.33
1.486151204	1.486151910	-0.706	83.7	9.94	0.0102	0.108	-0.97
1.488367806	1.488367773	0.033	77.7	11.32	0.0143	0.172	-0.76
1.490538663	1.490538693	-0.030	25.4	8.61	0.0621	0.570	-0.24
1.501576520	1.501577212	-0.692	69.3	8.83	0.0119	0.112	-0.95
1.505162884	1.505162696	0.188	56.4	10.67	0.0173	0.197	-0.71
1.512620371	1.512619913	0.458	60.7	6.92	0.0074	0.054	-1.27
1.514736403	1.514736134	0.269	48.4	7.63	0.0173	0.141	-0.85
1.527772880	1.527772911	-0.031	20.5	10.55	0.0422	0.475	-0.32
1.529217190	1.529216989	0.201	48.7	8.47	0.0105	0.095	-1.02
1.531142509	1.531142635	-0.126	64.7	10.38	0.0067	0.074	-1.13
1.531207594	1.531208236	-0.642	70.1	11.82	0.0086	0.108	-0.97
1.533665224	1.533665062	0.162	45.7	8.05	0.0149	0.128	-0.89
1.535741105	1.535740806	0.299	36.7	10.16	0.0694	0.752	-0.12
1.546696248	1.546696300	-0.052	92.1	12.26	0.0114	0.150	-0.83
1.549436469	1.549435015	1.454	52.5	9.14	0.0159	0.155	-0.81
1.559988595	1.559988108	0.487	53.6	8.03	0.0274	0.235	-0.63
1.572879144	1.572879433	-0.289	31.5	13.42	0.0481	0.689	-0.16

Comb (THz)	JPL (THz)	Comb-JPL (MHz)	Comb σ (kHz)	Comb FWHM	Comb Height	Comb Inten	Comb Log Int
1.578955111	1.578955503	-0.392	44.5	10.07	0.0159	0.171	-0.77
1.580914805	1.580914919	-0.114	30.3	8.76	0.0696	0.650	-0.19
1.591778274	1.591778439	-0.165	71.3	10.36	0.0097	0.107	-0.97
1.593634182	1.593633798	0.384	53.7	9.03	0.0148	0.142	-0.85
1.602007467	1.602007162	0.305	115.0	13.14	0.0108	0.151	-0.82
1.603168336	1.603168653	-0.317	56.3	9.27	0.0894	0.884	-0.05
1.605220838	1.605220965	-0.127	107.0	8.14	0.0109	0.094	-1.03
1.617939847	1.617939926	-0.079	60.2	11.27	0.0435	0.523	-0.28
1.619740175	1.619740501	-0.326	103.0	15.23	0.0138	0.224	-0.65
1.621003645	1.621003981	-0.336	86.8	10.12	0.0078	0.085	-1.07
1.624239450	1.624238602	0.848	68.1	9.53	0.0148	0.151	-0.82
1.626057470	1.626057309	0.161	47.1	9.80	0.0654	0.684	-0.17
1.636819409	1.636819866	-0.457	61.5	10.10	0.0097	0.105	-0.98
1.637784793	1.637784226	0.567	53.1	9.32	0.0164	0.163	-0.79
1.639534889	1.639533912	0.977	78.8	6.23	0.0110	0.073	-1.13
1.648439884	1.648439899	-0.015	40.7	9.28	0.0724	0.717	-0.14
1.650432778	1.650432531	0.247	33.1	8.43	0.0245	0.220	-0.66
1.662948615	1.662948521	0.094	34.2	9.90	0.0449	0.474	-0.32
1.664988528	1.664988112	0.416	100.0	11.32	0.0096	0.116	-0.94
1.669515361	1.669514298	1.063	91.9	12.03	0.0152	0.196	-0.71
1.671164489	1.671164358	0.131	59.4	9.82	0.0591	0.619	-0.21
1.684613252	1.684613904	-0.652	101.0	12.57	0.0152	0.204	-0.69
1.693698199	1.693697844	0.355	34.7	10.05	0.0700	0.750	-0.12
1.695620395	1.695620199	0.196	89.4	8.36	0.0224	0.200	-0.70
1.704987208	1.704987066	0.142	52.4	10.33	0.0380	0.418	-0.38

Comb (THz)	JPL (THz)	Comb-JPL (MHz)	Comb σ (kHz)	Comb FWHM	Comb Height	Comb Inten	Comb Log Int
1.707899117	1.707898809	0.308	69.8	9.89	0.0388	0.409	-0.39
1.708035094	1.708034878	0.216	81.6	8.36	0.0282	0.252	-0.60
1.710226502	1.710225585	0.917	97.9	9.81	0.0132	0.138	-0.86
1.714783048	1.714782502	0.546	91.3	10.66	0.0145	0.165	-0.78
1.716232287	1.716232113	0.174	52.5	10.42	0.0517	0.575	-0.24
1.720916247	1.720917677	-1.430	112.0	8.45	0.0104	0.093	-1.03
1.726053173	1.726053388	-0.215	117.0	12.13	0.0098	0.127	-0.90
1.726765351			163.0	14.31	0.0113	0.172	-0.76
1.729615468	1.729615728	-0.260	95.4	9.49	0.0136	0.138	-0.86
1.738941349	1.738941073	0.276	81.1	9.68	0.0604	0.623	-0.21
1.740782084	1.740781614	0.470	80.5	8.38	0.0274	0.245	-0.61
1.750237785	1.750238377	-0.592	71.8	8.08	0.0440	0.379	-0.42
1.752783777	1.752784022	-0.245	64.1	10.60	0.0356	0.403	-0.39
1.753210746	1.753210611	0.135	104.0	12.03	0.0219	0.281	-0.55
1.760043081	1.760043144	-0.063	73.7	8.07	0.0115	0.099	-1.00
1.761256425	1.761256262	0.163	52.8	10.56	0.0560	0.631	-0.20
1.770232988	1.770234175	-1.187	74.1	10.89	0.0122	0.141	-0.85
1.771659424	1.771659495	-0.071	76.8	8.10	0.0101	0.088	-1.06
1.778773784	1.778773501	0.283	95.1	6.70	0.0090	0.064	-1.19
1.784168437	1.784168173	0.264	38.7	9.64	0.0667	0.686	-0.16
1.785913719	1.785913965	-0.246	69.0	9.49	0.0170	0.172	-0.76
1.795475567	1.795475935	-0.368	114.0	8.89	0.0152	0.145	-0.84
1.797596523	1.797597030	-0.507	73.0	10.83	0.0337	0.389	-0.41
1.798356769	1.798356498	0.271	53.4	8.76	0.0362	0.338	-0.47
1.805295775	1.805296233	-0.458	122.0	9.93	0.0182	0.193	-0.72

Comb (THz)	JPL (THz)	Comb-JPL (MHz)	Comb σ (kHz)	Comb FWHM	Comb Height	Comb Inten	Comb Log Int
1.806231838	1.806232336	-0.498	63.5	10.43	0.0477	0.531	-0.28
1.814489643	1.814489648	-0.005	69.9	7.46	0.0159	0.127	-0.90
1.829378252	1.829377389	0.863	46.7	9.16	0.0711	0.695	-0.16
1.831014307	1.831014346	-0.039	70.4	9.30	0.0168	0.167	-0.78
1.834832868	1.834832903	-0.035	55.9	8.69	0.0301	0.279	-0.55
1.840698781	1.840698843	-0.062	68.8	10.48	0.0205	0.229	-0.64
1.842330577	1.842330192	0.385	87.2	10.12	0.0311	0.335	-0.47
1.850518275	1.850517843	0.432	109.0	6.11	0.0070	0.046	-1.34
1.850541268	1.850541749	-0.481	171.0	11.55	0.0088	0.108	-0.97
1.851155740	1.851155544	0.196	68.0	8.33	0.0555	0.493	-0.31
1.851383590	1.851384294	-0.704	130.0	5.41	0.0114	0.066	-1.18
1.858855448	1.858854961	0.487	130.0	8.07	0.0110	0.095	-1.02
1.874568186	1.874568096	0.090	70.2	8.29	0.0434	0.383	-0.42
1.876079446	1.876079538	-0.092	114.0	7.41	0.0155	0.122	-0.91
1.880025396	1.880024801	0.595	115.0	8.94	0.0177	0.169	-0.77
1.883947183	1.883946888	0.295	55.2	8.43	0.1180	1.061	0.03
1.885905632	1.885906602	-0.970	84.0	8.12	0.0214	0.185	-0.73
1.888544716	1.888545498	-0.782	74.2	7.63	0.0362	0.295	-0.53
1.895779923	1.895779797	0.126	110.0	9.93	0.0097	0.102	-0.99
1.896021357	1.896021021	0.336	65.0	10.45	0.0381	0.425	-0.37
1.919737561	1.919737946	-0.385	69.7	9.70	0.0448	0.463	-0.33
1.921104959	1.921106314	-1.355	100.0	10.57	0.0128	0.144	-0.84
1.925192356	1.925191775	0.581	83.0	7.34	0.0273	0.214	-0.67
1.929201152	1.929201071	0.081	64.7	8.90	0.0794	0.753	-0.12
1.931098416	1.931098401	0.015	105.0	8.95	0.0269	0.257	-0.59

Comb (THz)	JPL (THz)	Comb-JPL (MHz)	Comb σ (kHz)	Comb FWHM	Comb Height	Comb Inten	Comb Log Int
1.931520796	1.931520327	0.469	136.0	8.60	0.0186	0.171	-0.77
1.933581483	1.933581501	-0.018	143.0	9.89	0.0273	0.288	-0.54
1.940823467	1.940823502	-0.035	60.2	7.94	0.0395	0.335	-0.48
1.954887754	1.954887762	-0.008	47.1	8.00	0.0462	0.395	-0.40
1.964885752	1.964885678	0.074	51.3	9.96	0.0501	0.533	-0.27
1.966091861	1.966091122	0.739	71.6	10.31	0.0150	0.165	-0.78
1.970331510	1.970331101	0.409	117.0	13.40	0.0164	0.234	-0.63
1.974445482	1.974445140	0.342	60.2	11.10	0.0878	1.039	0.02
1.976273791	1.976273485	0.306	64.3	8.60	0.0237	0.217	-0.66
1.978572966	1.978573260	-0.294	47.4	5.50	0.0278	0.163	-0.79
1.985558162	1.985557594	0.568	111.0	11.00	0.0287	0.337	-0.47
1.986234809	1.986233807	1.002	185.0	13.10	0.0159	0.223	-0.65
2.010009754			58.0	9.63	0.0403	0.414	-0.38
2.015440293			76.7	7.67	0.0201	0.165	-0.78
2.019679558			37.8	8.36	0.1070	0.954	-0.02
2.021430276			66.6	7.68	0.0175	0.143	-0.84
2.023517149			73.2	9.30	0.0181	0.179	-0.75
2.030217777			66.0	9.44	0.0257	0.259	-0.59
2.042143775			81.1	5.91	0.0235	0.148	-0.83
2.045151312			72.8	7.58	0.0578	0.467	-0.33
2.055109452			70.2	8.31	0.0478	0.424	-0.37
2.064903890			85.0	12.36	0.0606	0.799	-0.10
2.065697289			71.3	9.22	0.0329	0.323	-0.49
2.074797948			110.0	11.32	0.0285	0.344	-0.46
2.088980529			72.1	9.61	0.0426	0.437	-0.36

Comb (THz)	JPL (THz)	Comb-JPL (MHz)	Comb σ (kHz)	Comb FWHM	Comb Height	Comb Inten	Comb Log Int
2.090236066			49.4	8.94	0.0344	0.328	-0.48
2.100179850			60.6	7.93	0.0474	0.401	-0.40
2.110118487			64.9	10.90	0.0673	0.782	-0.11
2.110336701			102.0	5.76	0.0205	0.126	-0.90
2.110936484			70.4	6.12	0.0440	0.287	-0.54
2.119292555			107.0	6.28	0.0298	0.200	-0.70
2.135286931			74.9	9.29	0.0382	0.379	-0.42
2.145225202			97.8	11.46	0.0263	0.321	-0.49
2.155322834			42.8	9.00	0.0776	0.745	-0.13
2.156164811			92.2	8.24	0.0269	0.236	-0.63
2.156791792			102.0	8.85	0.0193	0.182	-0.74
2.158011246			128.0	5.95	0.0221	0.140	-0.85
2.175740016			56.0	9.34	0.1931	1.924	0.28
2.190238118			106.0	6.69	0.0298	0.213	-0.67
2.200518328			91.5	11.61	0.0643	0.796	-0.10
2.220879715			70.6	8.34	0.1038	0.923	-0.03
2.245705561			129.0	10.39	0.0360	0.399	-0.40
2.265995621			72.5	8.94	0.0793	0.756	-0.12
2.269115232			132.0	6.71	0.0343	0.246	-0.61
2.280171168			118.0	9.74	0.0286	0.297	-0.53
2.291769802			114.0	7.09	0.0282	0.213	-0.67
2.336053838			86.6	8.75	0.0475	0.444	-0.35
2.336943316			75.6	6.35	0.0251	0.170	-0.77
2.351162006			68.3	9.02	0.1216	1.170	0.07
2.353759548			111.0	7.48	0.0451	0.360	-0.44

Comb (THz)	JPL (THz)	Comb-JPL (MHz)	Comb σ (kHz)	Comb FWHM	Comb Height	Comb Inten	Comb Log Int
2.356149051			88.8	9.48	0.0991	1.002	0.00
2.396168606			67.1	8.59	0.1385	1.269	0.10
2.401185061			133.0	7.52	0.0669	0.537	-0.27

Part IV

Conclusions and Future Directions

Chapter 8

Short-Term Improvements to the THz-FCS System

The THz-FCS system as described by this thesis is fully capable of Doppler-limited spectroscopy of several molecules of interest. However, the use of a short path length cell coupled with the low THz power per comb tooth results in a modest detection threshold for the system. This chapter outlines short-term upgrades to the system that will increase its sensitivity, precision, and bandwidth. In the interest of maximizing future investment of time and money, the most promising targets for improvement are discussed below.

8.1 Long Path Length Sample Cell

A 5 inch long single pass sample cell is quite sufficient for Doppler-limited rotational spectroscopy of molecules with large dipole moments, such as water (1.87 D), acetonitrile (3.44 D), and methanol (2.87 D). However, a longer path length sample cell is required for molecules with smaller dipole moments, especially for spectroscopy of large amplitude motions with small displacements in dipole such as pseudorotation in tetrahydrofuran. The technique of taking several scans at different pressures to cover a range of intensities for a single molecule cannot be employed because pressure broadening will degrade the Doppler-limited measurement accuracy above ∼100 mTorr. As such, employing a variable length sample cell is the superior method for tuning the sensitivity of the measurement. Unfortunately, maintaining alignment of THz radiation across long distances can be challenging.

As such a next-generation long cell design will employ a modular design consisting of Quick Flange components with an inner diameter of 38 mm (KF-40). The cell will consist of two Quick Flange tees, allowing vacuum and sample dosing connections at either end of the cell. Windows will be attached by machining grooves into polyethylene or TOPAS discs, which may then be clamped into place, interfacing with the standard Quick Flange O-ring. The two tees may be connected directly to each other, resulting in a 10 inch long cell, and any desired length of tubing may be added between the tees to extend the cell. Standard tubing lengths with Quick Flange ends are 5 inches and 12 inches. Quick Flange ends may be purchased separately and welded to any length of tubing desired to create any length sample cell required.

Additional path length may be gained by employing a double pass alignment. This configuration requires a rooftop reflector at one end of the cell rotated by 45° relative to the polarization of the incoming THz radiation. Upon reflection, the polarization of the THz radiation will be rotated by 90° and may be collected via reflection off of a THz polarizer that has been oriented to let THz radiation of native polarization pass into the cell. This double-pass alignment is substantially more challenging than a single pass alignment because a diffuse visible light guide beam will not reflect efficiently off of the THz polarizer. Also, the distance across which the THz beam collimation must be maintained will be doubled. Any linear gain in path length will manifest as a linear increase in percent absorption, providing a linear increase in SNR.

8.2 THz-FCS with Locked Pump Laser Repetition Rate

All of the THz-FCS spectra reported in this thesis were acquired using an unlocked pump laser repetition rate. This was largely due to the lack of an easily computer controlled synthesizer. With the acquisition of the Agilent E8257D frequency synthesizer, control of the synthesizer output via a GPIB interface is straightforward and an improved data acquisition routine, freq_counter.py, has been written in Python. The three main improvements over its predecessor, sim.py, are as follows: the ability to return to the same repetition rate steps with every complete scan over the range of the PID controller, the ability to lock the pump laser repetition rate after each voltage step is applied,

and the ability to select the absolute scan range and step size easily in terms of Hz. These three improvements are essential for improving the resolution of the comb beyond the 5 MHz resolution that was used to take the measurements in Chapters 6 and 7.

The current step size of 100 Hz corresponds to a comb tooth step of 1.25 MHz at 1 THz. This step size may be decreased down to 1 Hz with freq_counter.py, leading to a comb tooth step of 12.5 kHz at 1 THz. This level of precision is well matched to the 3.7 kHz measured comb tooth width for the THz-FCS system. At this level of precision, locking of the pump laser repetition rate during scans is essential. Any sinusoidal oscillations of the repetition rate during scans would broaden spectral features with kHz intrinsic line widths substantially. The current implementation of the pump stabilization circuit locks the pump laser repetition rate to milliHertz precision, so at this point the limiting factor is the ability to acquire and FFT long scans to resolve the comb teeth.

A few data processing techniques may help to alleviate the issues encountered when trying to process long record length scans. The ability to return to the same pump laser repetition rates every time a scan is run will allow straightforward co-adding of scans. If the averaging time to achieve a desired SNR is prohibitive, several scans of shorter averaging time may be co-added to achieve a comparable SNR. The need to collect multiple THz pulses to resolve narrow comb teeth may be circumvented by precisely synchronizing the sampling rate of the data card to the offset frequency of the lasers. If this condition is met, the frequency comb information may be recovered by zero-padding the data to an integer multiple of the scan length.

8.3 Pulse Compressor for Improved Bandwidth

Perhaps the most valuable improvement to the THz-FCS system at this point would be an increase in bandwidth. An expansion of the upper bandwidth limit may be achieved via pulse compression of the pump laser pulses that drive the THz emitter. As discussed in Section 3.3, efforts at reducing the GVD of the routing optics along the pump and probe beam paths led to the substantial increases in bandwidth shown in Figure 3.4. Further improvements in bandwidth may be achieved through additional compensation of dispersion by employing optics with negative GVD. The most

straightforward configuration of optics to achieve negative GVD is a prism pair. When the prisms are properly aligned with respect to each other, they act as a compressor, reversing the dispersive effect of the other optics in the system and compressing the laser pulses. The effect of the pump laser pulse width on the bandwidth of the Tera-SEDS THz emitter is predicted by Drude-Lorentz simulations. A pump pulse width of 50 fs will enable a bandwidth of 10 THz, increasing the coverage of the spectrometer to cover the entire THz region from 0.1 to 10 THz.[10]

Chapter 9

Future Spectroscopy Applications

The combination of bandwidth and resolution of the THz-FCS instrument makes this system ideal for survey scans of gas-phase spectra with complicated and dense spectra. As such, with the proper upgrades to bandwidth and sensitivity, the list of potential physical chemistry and astrochemistry applications of the system will be long enough to support many Ph.D. theses for decades to come. A few highlighted future directions for the instrument are discussed in this chapter. Both high resolution gas-phase and lower resolution condensed-phase spectroscopy applications are relevant.

9.1 Pseudorotational Modes in Tetrahydrofuran

Perhaps one of the most challenging and interesting molecules to study from a physical chemistry perspective is tetrahydrofuran (THF). THF deviates strongly from a rigid rotor due to its lowest energy conformations involving a puckered ring.[52] As the molecule moves between different conformers it must approach the energetically unfavorable planar conformation, leading to a hindered pseudorotation.[53] That is, the pucking phase rotates around the ring in order to avoid reaching the fully planar conformation of the THF molecule. [54] The barrier to pseudorotation in THF causes perturbations in the energies of the rotational transitions. These perturbations have been modeled using millimeter-wave data from 170 to 360 GHz.[55] An analysis has also been performed for microwave data from 8-35 GHz. [53] The existence of low lying vibrationally excited rotational transitions is predicted by the modeling of the microwave data and was confirmed by measurements of

the far-infrared (far-IR) spectrum of THF from 0.5 to 6 THz with a conventional FT-IR instrument. [56] Spectra of the related molecule 1,3-dioxolane also exhibited evidence of pseudorotation.

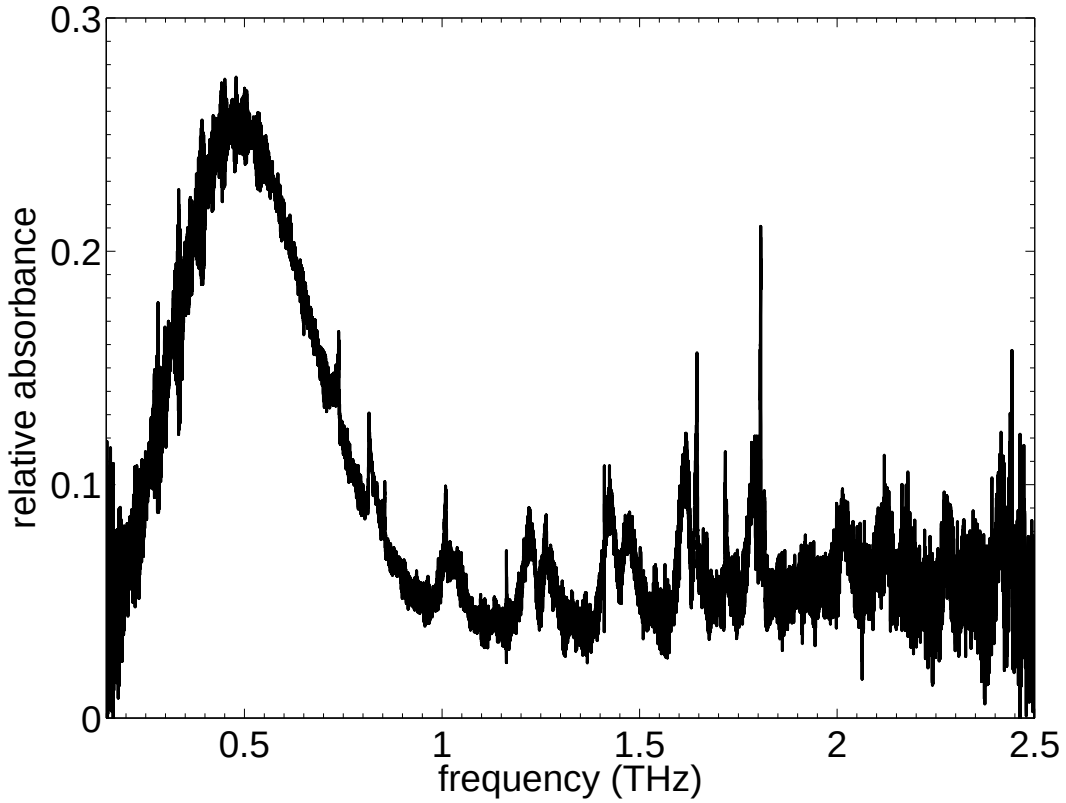

Figure 9.1: Plot of THF absorbance spectrum acquired at 5 Torr pressure and 80 MHz resolution. This resolution is insufficient to resolve individual transitions but is able to resolve the band structure of the pure rotational transitions and some low-lying vibrationally excited transitions.

These assignments were confirmed by measurements of THF at 5 Torr by our spectrometer in ASOPS-THz-TDS mode. As shown in Figure 9.1, several low lying vibrationally excited transitions are visible in addition to the ground state rotational envelope. And, Figure 9.2 demonstrates that the resolution is sufficient to determine the symmetry of the vibrationally excited bands. That is, the P and R branches are visible for each vibrationally excited band and, in cases allowed by symmetry, the Q branch is also visible. Future Doppler-limited measurements of THF made by the instrument in THz-FCS mode with a long path length sample cell would enable assignment of quantum numbers to individually resolved transitions.

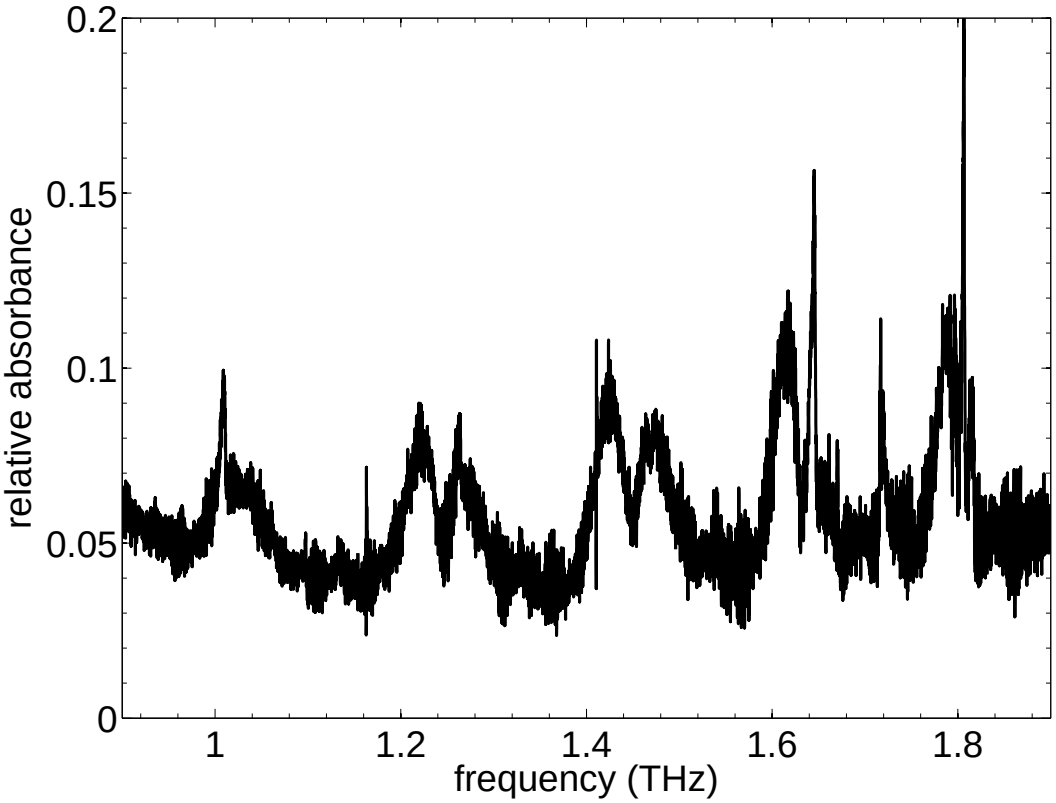

Figure 9.2: Detail of THF absorbance spectrum acquired at 5 Torr pressure and 80 MHz resolution showing the P, Q (allowed only for some bands), and R structure of some low-lying vibrationally excited transitions.

9.2 Waveguide Enhanced Spectroscopy of Polyaromatic Hydrocarbons

An exciting application of moderate resolution THz-TDS instrumentation is waveguide enhanced spectroscopy of solid-phase polyaromatic samples. In addition to the enhancement of the magnitude of the THz electric field within the waveguide, the alignment of the THz electric field coupled with the alignment of the thin film of sample deposited upon one of the plates of the waveguide can substantially narrow the observed linewidths for the sample. [57] The linewidth improvement was shown to be dependent on the crystallographic orientation of the film relative to the electric field of the THz radiation within the waveguide. [58] In the case of polycrystalline films of explosives, linewidths were reduced to 15 GHz with a combination of cooling to 11 K and waveguide

enhancement. [59] The waveguide enhanced sample provided a factor of 10 narrowing of linewidth over the linewidths measured for a pellet sample chilled to 11 K. This reduction in broadening can greatly aid identification of individual features in convoluted spectra. Reference spectra with such narrowed features would assist in the challenge of identifying interstellar ice species in a diverse array of chemical and thermal environments.

Bibliography

[1] M. Tani, R. Fukasawa, H. Abe, S. Matsuura, K. Sakai et al., "Terahertz radiation from coherent phonons excited in semiconductors," *J. Appl. Phys.*, **83**, 2473–2477 (1998), doi: 10.1063/1.367007.

[2] R. Falconer and A. Markelz, "Terahertz Spectroscopic Analysis of Peptides and Proteins," *J. Infrared Millim. THz W.*, **33**, 973–988 (2012).

[3] T. Q. Luong, P. K. Verma, R. K. Mitra, and M. Havenith, "Onset of Hydrogen Bonded Collective Network of Water in 1,4-Dioxane," *J. Phys. Chem. A*, **115**, 14462–14469 (2011), doi:10.1021/ jp204927r.

[4] H. Harde, R. A. Cheville, and D. Grischkowsky, "Terahertz studies of collision-broadened rotational lines," *J. Phys. Chem. A*, **101**, 3646–3660 (1997), doi:10.1021/jp962974c.

[5] T. G. Phillips and J. Keene, "Submillimeter astronomy," *Proc. IEEE*, **80**, 1662–1678 (1992).

[6] M. A. Allodi, S. Ioppolo, M. J. Kelley, B. A. McGuire, and G. A. Blake, "The structure and dynamics of carbon dioxide and water containing ices investigated via THz and mid-IR spectroscopy," *Phys. Chem. Chem. Phys.*, **16**, 3442–3455 (2014), doi:10.1039/c3cp53767f.

[7] S. Ioppolo, B. A. McGuire, M. A. Allodi, and G. A. Blake, "THz and mid-IR spectroscopy of interstellar ice analogs: methyl and carboxylic acid groups," *Faraday Discuss.*, **168**, 461–484 (2014), doi:10.1039/c3fd00154g.

[8] P. U. Jepsen, D. G. Cooke, and M. Koch, "Terahertz spectroscopy and imaging - Modern techniques and applications," *Laser Photon Rev.*, **5**, 124–166 (2011), doi:10.1002/lpor.201000011.

[9] D. Mittleman, *Sensing with Terahertz Radiation* (2002).

[10] P. J. Hale, J. Madeo, C. Chin, S. S. Dhillon, J. Mangeney et al., "20 THz broadband generation using semi-insulating GaAs interdigitated photoconductive antennas," *Opt. Express*, **22**, 26358–26364 (2014), doi:10.1364/oe.22.026358.

[11] B. J. Drouin, F. W. Maiwald, and J. C. Pearson, "Application of cascaded frequency multiplication to molecular spectroscopy," *Rev. Sci. Instrum.*, **76**, 10 (2005), doi:10.1063/1.2042687.

[12] S. Bartalini, L. Consolino, P. Cancio, P. De Natale, P. Bartolini et al., "Frequency-Comb-Assisted Terahertz Quantum Cascade Laser Spectroscopy," *Phys. Rev. X*, **4**, 7 (2014), doi: 10.1103/PhysRevX.4.021006.

[13] M. Rosch, G. Scalari, M. Beck, and J. Faist, "Octave-spanning semiconductor laser," *Nature Photon.*, **9**, 42–47 (2015), doi:10.1038/NPHOTON.2014.279.

[14] P. A. Elzinga, R. J. Kneisler, F. E. Lytle, Y. Jiang, G. B. King et al., "Pump/probe method for fast analysis of visible spectral signatures utilizing asynchronous optical sampling," *Appl. Opt.*, **26**, 4303–9 (1987).

[15] A. Bartels, R. Cerna, C. Kistner, A. Thoma, F. Hudert et al., "Ultrafast time-domain spectroscopy based on high-speed asynchronous optical sampling," *Rev. Sci. Instrum.*, **78**, 8 (2007), doi:10.1063/1.2714048.

[16] J. Johnson, J. A. Johnson, S. Grubel, S. Johnson, S. Graebel et al., "Distortion-free enhancement of terahertz signals measured by electro-optic sampling II Experiment," *J. Opt. Soc. Am. B*, **31**, 1035–1040 (2014).

[17] G. Klatt, R. Gebs, C. Janke, T. Dekorsy, and A. Bartels, "Rapid-scanning terahertz precision spectrometer with more than 6 THz spectral coverage," *Opt. Express*, **17**, 22847–22854 (2009).

[18] G. Klatt, R. Gebs, H. Schaefer, M. Nagel, C. Janke et al., "High-Resolution Terahertz Spectrometer," *IEEE J. Sel. Topics Quantum Electron.*, **17**, 159–168 (2011).

[19] T. Yasui, K. Kawamoto, Y. D. Hsieh, Y. Sakaguchi, M. Jewariya et al., "Enhancement of spectral resolution and accuracy in asynchronous-optical-sampling terahertz time-domain spectroscopy for low-pressure gas-phase analysis," *Opt. Express*, **20**, 15071–15078 (2012), doi:10.1364/oe.20.015071.

[20] S. A. Diddams, D. J. Jones, J. Ye, S. T. Cundiff, J. L. Hall et al., "Direct Link between Microwave and Optical Frequencies with a 300 THz Femtosecond Laser Comb," *Phys. Rev. Lett.*, **84**, 5102 (2000), doi:10.1103/PhysRevLett.84.5102.

[21] T. Udem, R. Holzwarth, and T. W. Hänsch, "Optical frequency metrology," *Nature*, **416**, 233–237 (2002), doi:10.1038/416233a.

[22] Y. D. Hsieh, Y. Iyonaga, Y. Sakaguchi, S. Yokoyama, H. Inaba et al., "Spectrally interleaved, comb-mode-resolved spectroscopy using swept dual terahertz combs," *Sci. Rep.*, **4**, 7 (2014), doi:10.1038/srep03816.

[23] S. Tammaro, O. Pirali, P. Roy, J.-F. Lampin, G. Ducournau et al., "High density THz frequency comb produced by coherent synchrotron radiation," *Nature Commun.*, **6**, 7733 (2015), doi:10.1038/ncomms8733.

[24] J. T. Good, D. B. Holland, I. A. Finneran, P. B. Carroll, M. J. Kelley et al., "A decade-spanning high-resolution asynchronous optical sampling terahertz time-domain and frequency comb spectrometer," *Rev. Sci. Instrum.*, **86** (2015).

[25] I. A. Finneran, J. T. Good, D. B. Holland, P. B. Carroll, M. A. Allodi et al., "Decade-Spanning High-Precision Terahertz Frequency Comb," *Phys. Rev. Lett.*, **114**, 5 (2015), doi:10.1103/PhysRevLett.114.163902.

[26] A. Dreyhaupt, S. Winnerl, M. Helm, and T. Dekorsy, "Optimum excitation conditions for the generation of high-electric-field terahertz radiation from an oscillator-driven photoconductive device," *Opt. Lett.*, **31**, 1546–1548 (2006), doi:10.1364/OL.31.001546.

[27] S. Matsuura, G. A. Blake, R. A. Wyss, J. C. Pearson, C. Kadow et al., "A traveling-wave THz photomixer based on angle-tuned phase matching," *Appl. Phys. Lett.*, **74**, 2872 (1999), doi:10.1063/1.124042.

[28] P. C. M. Planken, H. K. Nienhuys, H. J. Bakker, and T. Wenckebach, "Measurement and calculation of the orientation dependence of terahertz pulse detection in ZnTe," *J. Opt. Soc. Am. B*, **18**, 313–317 (2001), doi:10.1364/josab.18.000313.

[29] L. S. Ma, R. K. Shelton, H. C. Kapteyn, M. M. Murnane, and J. Ye, "Sub-10-femtosecond active synchronization of two passively mode-locked Ti : sapphire oscillators," *Phys. Rev. A*, **64**, 021802 (2001), doi:10.1103/PhysRevA.64.021802.

[30] G. Sucha, M. Fermann, D. Harter, and M. Hofer, "A new method for rapid temporal scanning of ultrafast lasers," *IEEE J. Sel. Topics Quantum Electron.*, **2**, 605–621 (1996), doi:10.1109/2944.571759.

[31] D. Holland, *Design, Construction and Applications of a High Resolution Terahertz Time-Domain ASOPS Spectrometer*, Caltech phd thesis (2014).

[32] M. Kinoshita, H. Iida, and Y. Shimada, "Frequency Calibration of Terahertz Time-Domain Spectrometer Using Air-Gap Etalon," *IEEE Trans. THz Sci. Technol.*, **4**, 756–759 (2014), doi:10.1109/tthz.2014.2357895.

[33] H. M. Pickett, R. L. Poynter, E. A. Cohen, M. L. Delitsky, and J. C. Pearson, "SUBMILLIMETER, MILLIMETER, AND MICROWAVE SPECTRAL LINE CATALOG," *J. Quant. Spectrosc. Radiat. Transfer*, **60**, 883–890 (1998).

[34] S. Charnley, A. Tielens, and S. Rodgers, "Deuterated methanol in the Orion compact ridge," *Astrophys. J.*, **482**, L203–L206 (1997).

[35] J. L. Neill, N. R. Crockett, E. A. Bergin, J. C. Pearson, and L.-H. Xu, "DEUTERATED MOLECULES IN ORION KL FROM HERSCHEL/HIFI," *Astrophys. J.*, **777** (2013).

[36] J. Bagdonaite, P. Jansen, C. Henkel, H. L. Bethlem, K. M. Menten et al., "A Stringent Limit on a Drifting Proton-to-Electron Mass Ratio from Alcohol in the Early Universe," *Science*, **339**, 46–48 (2013).

[37] K. Johns, D. Cragg, P. Godfrey, and A. Sobolev, "Class II maser candidates in substituted methanol: CH3OD, (CH3OH)-C-13, CH3 (OH)-O-18 and CH3SH," *Mon. Not. R. Astron. Soc.*, **300**, 999–1005 (1998).

[38] F. Matsushima, K. Evenson, and L. Zink, "ABSOLUTE FREQUENCY MEASUREMENTS OF METHANOL FROM 1.5 TO 6.5 THZ," *J. Mol. Spec.*, **164**, 517–530 (1994).

[39] R. M. Lees, L.-H. Xu, B. E. Billinghurst, and D. R. T. Appadoo, "Weeding the Cosmos - FIR synchrotron spectroscopy of methanol at the Canadian Light Source," *J. Mol. Struct.*, **993**, 269–276 (2011).

[40] E. Herbst, J. Messer, F. DeLucia, and P. Helminger, "A NEW ANALYSIS AND ADDITIONAL MEASUREMENTS OF THE MILLIMETER AND SUBMILLIMETER SPECTRUM OF METHANOL," *J. Mol. Spec.*, **108**, 42–57 (1984).

[41] L. Xu and J. Hougen, "GLOBAL FIT OF ROTATIONAL TRANSITIONS IN THE GROUND TORSIONAL STATE OF METHANOL," *J. Mol. Spec.*, **169**, 396–409 (1995).

[42] L. XU and J. HOUGEN, "GLOBAL FIT OF TORSIONAL-ROTATIONAL TRANSITIONS IN THE GROUND AND FIRST EXCITED TORSIONAL STATES OF METHANOL," *J. Mol. Spec.*, **173**, 540–551 (1995).

[43] L.-H. Xu, J. Fisher, R. M. Lees, H. Y. Shi, J. T. Hougen et al., "Torsion-rotation global analysis of the first three torsional states (nu(t)=0, 1, 2) and terahertz database for methanol," *J. Mol. Spec.*, **251**, 305–313 (2008).

[44] J. C. Pearson, B. J. Drouin, S. Yu, and H. Gupta, "Microwave spectroscopy of methanol between 2.48 and 2.77 THz," *J. Opt. Soc. Am. B*, **28**, 2549–2577 (2011).

[45] I. Mukhopadhyay, Y. Duan, and K. Takagi, "High resolution spectroscopy of CH3OD involving the ground and first excited torsional states in the vibrational ground state," *Spectrochim. Acta A*, **54**, 1325–1335 (1998).

[46] I. Mukhopadhyay, "High resolution spectroscopy in the second excited torsional state of CH3OD and the atlas of the Fourier transform spectrum in the range 20-205 cm(-1)," *Spectrochim. Acta A*, **55**, 1767–1791 (1999).

[47] I. Mukhopadhyay and Y. Duan, "Analysis of torsion-rotational transitions in the first three torsional states of CH3OD," *Chem. Phys.*, **257**, 91–101 (2000).

[48] M. Walsh, L. Xu, R. Lees, I. Mukhopadhyay, G. Moruzzi et al., "Millimeter-wave spectra and global torsion-rotation analysis for the CH3OD isotopomer of methanol," *J. Mol. Spec.*, **204**, 60–71 (2000).

[49] Y. Duan, I. Ozier, S. Tsunekawa, and K. Takagi, "Microwave study and global analysis of the lowest three torsional states of CH3OD," *J. Mol. Spec.*, **218**, 95–107 (2003).

[50] J. C. Pearson, B. J. Drouin, A. Maestrini, I. Mehdi, J. Ward et al., "Demonstration of a room temperature 2.48-2.75 THz coherent spectroscopy source," *Rev. Sci. Instrum.*, **82** (2011).

[51] B. J. Drouin, J. C. Pearson, S. Yu, and H. Gupta, "Characterization and Use of a 1.3-1.5 THz Multiplier Chain for Molecular Spectroscopy," *IEEE Trans. THz Sci. Technol.*, **3**, 314–321 (2013).

[52] G. Engerholm, A. Luntz, W. Gwinn, and D. Harris, "RING PUCKERING IN 5-MEMBERED RINGS .2. MICROWAVE SPECTRUM DIPOLE MOMENT AND BARRIER TO PSEUDOROTATION IN TETRAHYDROFURAN," *J. Chem. Phys.*, **50**, 2446–2457 (1969).

[53] A. Mamleev, L. Gunderova, and R. Galeev, "Microwave spectrum and hindered pseudorotation of tetrahydrofuran," *J. Struct. Chem.*, **42**, 365–370 (2001).

[54] R. Meyer, J. Lopez, J. Alonso, S. Melandri, P. Favero et al., "Pseudorotation pathway and equilibrium structure from the rotational spectrum of jet-cooled tetrahydrofuran," *J. Chem. Phys.*, **111**, 7871–7880 (1999).

[55] D. Melnik, S. Gopalakrishnan, T. Miller, and F. De Lucia, "The absorption spectroscopy of the lowest pseudorotational states of tetrahydrofuran," *J. Chem. Phys.*, **118**, 3589–3599 (2003).

[56] G. JA and H. Strauss, "SPECTROSCOPIC EVIDENCE FOR PSEUDOROTATION .2. FAR-INFRARED SPECTRA OF TETRAHYDROFURAN AND 1,3-DIOXOLANE," *J. Chem. Phys.*, **50**, 124–134 (1969).

[57] M. Theuer and J. S. Melinger, "High Resolution Waveguide Terahertz Time-Domain Spectroscopy," *J. Infrared Millim. THz W.*, **32**, 1267–1284 (2011).

[58] J. S. Mellinger, N. Laman, S. S. Harsha, S. Cheng, and D. Grischkowsky, "High-resolution waveguide terahertz Spectroscopy of partially oriented organic polycrystalline films," *J. Phys. Chem. A*, **111**, 10977–10987 (2007).

[59] N. Laman, S. S. Harsha, D. Grischkowsky, and J. S. Melinger, "7 GHz resolution waveguide THz spectroscopy of explosives related solids showing new features," *Opt. Express*, **16**, 4094–4105 (2008).

Appendix A

Python Code for THz-FCS Data Acquisition and Analysis

This appendix includes commented python code used for THz-FCS data analysis. For MATLAB code used for ASOPS-THz-TDS data analysis see the appendix of the PhD thesis of Dan Holland.

A.1 sim.py

This program is used to step the pump (master) laser repetition rate via the pump slow PID controller without locking the repetition rate of the pump laser to a frequency source.

```
import serial #import serial library, to talk to SIM mainframe
import time #import time library to define wait times
import numpy as np #import numpy library to define arrays

import mouse #import mouse library, to use mouse clicking routine

step = 100.0 #desired comb step size in Hz
time_sleep = 225 #desired rest time at each step in seconds

mouse1 = mouse.Mouse() #calls the mouse clicker routine in the mouse library

def start_acquisition():
        mouse1.invisible_click((1728,79))
        #single click on start aquisition button in AlazarTech program
        #AlazarTech program must be maximized for click coordinates to work
```

```
def save_file():
#this routine executes a series of clicks to save data files
        mouse1.invisible_click((15,31))
        time.sleep(0.5) #single click file menu
        mouse1.invisible_click((24,79))
        time.sleep(1.0) #single click save as
        mouse1.invisible_click((928,461))
        time.sleep(0.5) #single click to select channel B as the channel to save
        mouse1.invisible_click((1034,763))
        time.sleep(3.0) #single click ok to save in window
        mouse1.invisible_click((1103,571))
        #single click ok to clear save complete message
def move_comb(voltage):
#this routine sets the output voltage of the PID controller
#to a the value (voltage) specifed when calling this routine
        ser = serial.Serial('COM8', 9600, timeout=3)
        #opens serial port on computer used to talk to SIM mainframe,
        #port:COM8, baud rate: 9600, timeout: 3 ms
        ser.write('CONN 1,"xyz"\n')
        #talk to serial port 1 in SIM mainframe: slave slow PID controller,
        #defines escape string as "xyz"
        #when sending commands to the SIM mainframe all strings terminate in \n
        ser.write('AMAN 0\n') #set PID controller to manual mode
        ser.write('MOUT %s\n'%(str(voltage)))
        #set manual voltage to the desired value in Volts
        ser.write('xyz\n')
        #send escape string to close serial connection to port 1 in SIM mainframe
        ser.close() #close serial port on control computer


converted_step = step/575.0
#conversion factor to convert desired step size in Hz to the required voltage step in V
```

```
num_step = int(10.0/converted_step)
#determines the number of steps that will fit into the 10V range of the PID controller
v_list = np.linspace(-5.0,5.0,num_step+1)
#creates a 1D array of volatge steps ascending from -5V to +5V
v_list2 = np.linspace(5.0,-5.0,num_step+1)
#creates a 1D array of volatge steps descending from +5V to -5V

Loops = 1 #control variable to enable repeating voltage steps

while Loops == 1:  #run this loop while Loops equals 1
#change the condition to Loops <= N to run loop N times
        for V in v_list: #for each element V in the 1D array v_list
                move_comb(V) #move to voltage step V
                time.sleep(20) #wait 20 s to let comb equilibrate
                start_acquisition() #begin acquisition of data
                time.sleep(time_sleep) #wait while data is acquired
                save_file() #save data
                #this will run until the voltage has been incremented stepwise up to 5V
        for V in v_list2: #for each element V in the 1D array v_list2
                move_comb(V) #move to voltage step V
                time.sleep(20) #wait 20 s to let comb equilibrate
                start_acquisition() #begin acquisition of data
                time.sleep(time_sleep) #wait while data is acquired
                save_file() #save data
                #this will run until the voltage has been incremented stepwise down to -5V

        #Loops +=1
        #uncomment to increment Loops by 1 and scan voltage up and down once
        #or to scan voltage up and down N times
```

A.2 freq_counter.py

This program is used to step the pump (master) laser repetition rate via the pump slow PID controller and lock the pump laser to the Agilent E8257D frequency synthesizer.

```
import math #import math library to use math.floor()
import serial #import serial library to talk to SIM mainframe
import mouse #import mouse to use mouseclicker
import visa #import pyVisa to communicate with GPIB devices
# Agilent frequency synthesizer and frequency counter
import time #import time library to add wait times

def read_master_freq():
#when called this routine querries the frequency counter
#and returns the value of the master rep rate as an int
        rm = visa.ResourceManager()
        rm.list_resources()
        inst = rm.open_resource('GPIB0::3::INSTR')
        #these three lines of code list the avaliable GPIB devices
        #connected to the computer and then opens a connection with
        #the device on GPIB channel 3, the frequency counter
        inst.write("FU1") #sends a command to read the frequency
        #from channel A on the frequency counter
        data = inst.visalib.read(inst.session, 17)
        #stores the data from the frequency counter as a string
        #reads 17 characters in the format "FREQ 79980883"
        a =  str(data[0]) #failsafe to read only one line of FREQ data
        x = a.find("F") #finds the beginning of the string
        masterfreq = float(a[x+4:x+14])*10**7 #discard the "FREQ"
        masterfreq = int(math.floor(masterfreq)) #convert to int
        return masterfreq #returns the freq reading as an int

def setfreqsynth(targetfreq):
        #when called this routine sets the frequency of the synth
```

```
        #to the desired value given by targetfreq
        freq = targetfreq
        freq = freq*12 #calculates the 12th harmonic of the input
        #since the RF lock circuit operates at the 12th harmonic
        rm = visa.ResourceManager()
        rm.list_resources()
        synth = rm.open_resource('GPIB0::21::INSTR')
        #opens a connection on GPIB channel 21, the Agilent synth
        Command = 'FREQ '+str(freq)+" Hz\n"
        #builds a string with the appropriate syntax for the synth
        synth.write(Command)
        #sends the command string to the synth to go to the desired frequency
        print Command #prints the command in the command prompt

def lock_comb():
        #when called this routine sets the PID controller to PID control
        ser = serial.Serial('COM8', 9600, timeout=3)
        #open serial connection on port COM8, the SIM mainframe
        ser.write('CONN 1,"xyz"\n')
        #open connection to port 1 in the mainframe, the PID controller
        ser.write('AMAN 1\n') #set PID controller to PID control
        ser.write('xyz\n') #send the escape string to terminate connection
        ser.close() #close the serial connection

def move_comb(voltage):
        #when called this routine switches the PID controller to manual control and
        #sets the manual voltage on the PID controller to the desired value (voltage)
        ser = serial.Serial('COM8', 9600, timeout=3)
        #open serial connection on port COM8, the SIM mainframe
        ser.write('CONN 1,"xyz"\n')
        #open connection to port 1 in the mainframe, the PID controller
        ser.write('AMAN 0\n') #set PID controller to manual control
```

```
        ser.write('MOUT %s\n'%(str(voltage)))
        #move manual voltage to (voltage)
        ser.write('xyz\n') #send the escape string to terminate connection
        ser.close() #close the serial connection

def read_voltage():
        #when called this routine querries the PID controller
        #and returns the current control voltage
        ser = serial.Serial('COM8', 9600, timeout=6)
        #open serial connection on port COM8, the SIM mainframe
        ser.write('CONN 1,"xyz"\n')
        #open connection to port 1 in the mainframe, the PID controller
        ser.write('OMON?\n') #query PID controller output voltage
        volt = ser.read(7) #read 7 bytes of the returned serial stream
        ser.write('xyz\n') #send the escape string to terminate connection
        ser.close() #close the serial connection
        return volt #return the current voltage value

def start_acquisition():
        #this routine clicks the acquire data button to start a scan
        mouse1 = mouse.Mouse() #defines the mouseclicker routine
        mouse1.invisible_click((1728,79))
        #single clicks the start button

def save_file():
        #this routine saves the data file once the scan is complete
        mouse1 = mouse.Mouse() #defines the mouseclicker routine
        mouse1.invisible_click((15,31)) #clicks the file menu
        time.sleep(0.5) #wait for menu to open
        mouse1.invisible_click((24,79)) #clicks save as
        time.sleep(1.0) #waits for the dialog box to open
        mouse1.invisible_click((928,461)) #sets save to channel B
```

```
        time.sleep(0.5) #waits for channel to update
        mouse1.invisible_click((1034,763)) #clicks the save button
        time.sleep(3.0) #waits for file to save
        mouse1.invisible_click((1103,571)) #clicks the ok button
        #to clear the save complete dialogue box

def freq_lock():
#this routine reads the current frequency of the master laser
#from the frequency counter and rounds the frequency to the
#nearest multiple of the desired freqeuency step
#it then sets the synth to the 12th harmonic of the target freq
#and applies the appropriate voltage step to the PID controller
#to adjust the master freq to the target freq, a multiple of
#the deisred freq step, and then engages PID control to lock
#the master laser repetition rate to the desired frequency
        freq_step = 100 #desired frequency step in Hz
        freqtovolt = -0.002 #+0.100V = -50 Hz conversion factor
        masterfreq = read_master_freq()
        #reads in the master freq from the frequency counter
        current_volt = float(read_voltage())
        #reads in the current voltage of the PID controller
        round = masterfreq % freq_step
        #rounds to the nearest multiple of the freq step size
        if round <= freq_step/2: #if closer to the next lowest freq
                rounddown = round #round down by the remainder
                targetfreq = masterfreq - rounddown #to get the target freq
                targetvolt = current_volt - float(rounddown)*freqtovolt
                #then calculates the appropriate voltage adjustment
        else: #otherwise freq is closer to the next highest freq
                roundup = freq_step - round #round up by freq_step-remainder
                targetfreq = masterfreq + roundup #to get the target freq
                targetvolt = current_volt + float(roundup)*freqtovolt
```

```
                #then calculates the appropriate voltage adjustment
        print targetfreq #prints the calculated target frequency
        setfreqsynth(targetfreq) #sets the synth to the target freq
        move_comb(targetvolt) #adjusts the PID controller voltage
        time.sleep(2.0) #let masterfreq equilibrate before engaging PID
        lock_comb() #engage PID control
        return targetfreq #returns the target frequency

def freq_step_up():
#this routine steps the voltage of the PID controller
#up by the desired step amount and then locks the
#master laser repetition rate to the new frequency
        freq_step = 100 #desired frequency step in Hz
        freqtovolt = -0.002 #+0.100V = -50 Hz conversion factor
        volt_step = freqtovolt*float(freq_step)
        #calculates the size of the appropriate voltage step
        current_volt = float(read_voltage())
        #reads the current voltage of the PID controller
        move_volt = current_volt + volt_step
        #calculates the target voltage based on the current voltage
        move_comb(move_volt)
        #applies the voltage step to the PID controller
        masterfreq = freq_lock()
        #engage PID control of the master laser rep rate
        return masterfreq #returns the new master laser rep rate

def freq_step_down():
#this routine steps the voltage of the PID controller
#down by the desired step amount and then locks the
#master laser repetition rate to the new frequency
        freq_step = 100 #desired frequency step in Hz
        freqtovolt = -0.002 #+0.100V = -50 Hz conversion factor
```

```
        volt_step = freqtovolt*float(freq_step)
        #calculates the size of the appropriate voltage step
        current_volt = float(read_voltage())
        #reads the current voltage of the PID controller
        move_volt = current_volt - volt_step
        #calculates the target voltage based on the current voltage
        move_comb(move_volt)
        #applies the voltage step to the PID controller
        masterfreq = freq_lock()
        #engage PID control of the master laser rep rate
        return masterfreq #returns the new master laser rep rate

def take_data():
#this routine initiates data acquisition, waits for the scan
#to complete and then saves the data
        scan_time = 230 #scan time in seconds
        start_acquisition() #begin scan
        time.sleep(scan_time) #wait for data
        save_file() #save file

def scan_comb():
#this routine first locks the master laser repetition rate
#then scans the master laser rep rate up and back down through
#a series of defined frequency steps, saving data at each step
        masterfreq = freq_lock() #lock the master laser rep rate
        equilibrate_time = 10.0
        #time to wait for the master laser rep rate to stabilize
        time.sleep(equilibrate_time)
        upper_lim_freq = 79984300
        #upper frequency limit, highest value possible: 79984300
        lower_lim_freq = 79977200
        #lower frequency limit, lowest value possilbe: 79977200
```

```
        scan = 1 #a loop parameter used to turn infinite scanning on
        while scan == 1: #while the scan parameter is true, step freq
                while masterfreq < upper_lim_freq:
                #while the master frequency is below the upper limit
                        masterfreq = freq_step_up()
                        #step the master rep rate up by the step size
                        print masterfreq #print the new frequency
                        time.sleep(equilibrate_time)
                        #wait for master rep rate to stabilize
                        take_data() #acquire and save data
                while masterfreq > lower_lim_freq:
                        #while the master frequency is above the lower limit
                        masterfreq = freq_step_down()
                        #step the master rep rate down by the step size
                        print masterfreq #print the new frequency
                        time.sleep(equilibrate_time)
                        #wait for master rep rate to stabilize
                        take_data() #acquire and save data

scan_comb() #runs the scan comb routine when freq_counter.py is called
```

A.3 freq_comb_analysis_v3.py

This program is used to analyze frequency comb data acquired by the above routines. It generates the fft intensity spectrum for the data, which may then be further processed by boxcar_v2.py to generate an absorption spectrum.

```
import numpy as np
from numpy import array
from scipy.fftpack import fft
from math import pi,atan2,log
import os
from os import path
```

```
Main_frequency = 79980833   #Reference frequency for THz data
#should match reference frequency input specified
#within the DDS board control software

files = filter(path.isfile, os.listdir(".")) #initializes an array and populates it with
#the names and extensions of all files in the folder containing freq_comb_analysis_v3.py

comb_list = [] #initializes an empty array to hold the desired .txt files for analysis
        for file in files: #checks each entry in the array files
                if file[-4:]==".txt": #to see if the extension is .txt
                comb_list.append((file,Main_frequency)) #appends each .txt file to comb_list
#In the case that the reference frequency is different for different files,
#it must be noted manually, an example entry in comb_list is shown below
#comb_list = [('981560Hz_1000avg_1.1.B.txt',79981560)]

def fft_data(filename,Master_rep_rate):
#when called fft_data will return the processed frequency axis
#along with the corresponding fft intensity values, and raw time domain data
        oscilliscope_sample_rate = 40e6
        #Sample rate of the data acquisition in Samples per sec
        offset = 400.0 #Offset of the master rep rate relative to the slave in Hz
        sample_rate = oscilliscope_sample_rate*(1/offset)*Master_rep_rate
        #calculates the ASOPS factor based on the data acquisition parameters
        sample_rate = sample_rate/1e12 #conversion factor converts freq axis to THz

        fh = open(filename) #opens the data file specified by the filename
        data = [] #initializes an empty array to hold the data

        for line in fh: #reads data line by line from the .txt file
                data.append(float(line)) #and appends each line as a float
```

```
E_field = data #the data is a single column containing the E field values
time_values = [] #initializes an empty array to popluate with time values

for time in range(0,len(E_field)):
#generates a list of time values corresponding to E field values
        time_value = (time/sample_rate)*1e6
        #converts sampled time values to ASOPS scaled values
        time_values.append(time_value) #appends converted time values to the array

cut_E_field_new =
[float(a)*float(b) for a,b in zip(list(np.kaiser(len(E_field),8)),E_field)]
# windowing function option 8: symmetric hann
#multiplies a windowing function with the E_field values to optimize fft performance

num_fft=2**23 #zero pad fft to 2^23
df = (float(num_fft)*(1/sample_rate))
#conversion factor to adjust freq axis point spacing
#to match time axis point spacing
#fft_length = float(sample_rate)
freq_list = [] #initializes array to hold frequency values

for f in range(0,int(num_fft)):
        freq_list.append(f/df)
        #scale the range of the fft to the range of frequencies
Fourier_transform =abs(np.fft.fft(array(cut_E_field_new),num_fft))
#fft of windowed data
f_lower_bound = .15 #lower cutoff frequency
f_upper_bound = 3 #upper cutoff frequency
length_freq_list = len(freq_list)
freq_list = freq_list[0:length_freq_list/2]
#fft is symmetric around zero, select positive frequency values
Fourier_transform = Fourier_transform[0:length_freq_list/2]
```

```
        #select corresponding fft intensity values

        freq_list = freq_list[int(f_lower_bound*df):int(f_upper_bound*df)]
        #further limit to frequency values specified by the bounds
        Fourier_transform = Fourier_transform[int(f_lower_bound*df):int(f_upper_bound*df)]
        #further limit to fft intensity values specified by the bounds
        return freq_list,Fourier_transform,data #returns freq,fft int,raw time data


def peakpicker(spectrum,inten,thresh_l,thresh_h):
        #when called peakpicker takes an input of freq,fft int,
        #lower int thresh,upper int thresh and returns a list of peaks
        #in the intensity values along with the corresponding freqs
        #ignores peaks below thresh_l and above thresh_h
        freqpeaks=[] #initializes an array to hold frequency input
        intpeaks = [] #initializes an array to hold fft intensity input
        i_list = [] #initializes an array to hold index values for comb teeth
        delta_i_list = [] #initializes an array to hold index difference values
        for i in range(len(spectrum)):
                if inten[i] > thresh_l and inten[i] < thresh_h
                and inten[i] > inten[(i-1)] and inten[i] > inten[(i+1)]:
                #checks each intensity to see if it is within the threshold bounds
                #and to see if it is greater than the intesnity values on either side of it
                freqpeaks.append(spectrum[i]) #appends the corresponding frequency
                intpeaks.append(inten[i]) #and intensity values of the peak
                i_list.append(i) #also appends the index value of the peak
                if len(i_list)>1 and abs(freqpeaks[-2]-freqpeaks[-1])<8.1e-5:
                #if the spacing between adjacent comb teeth is less than 81 MHz
                        delta_i_list.append(abs(i_list[-2]-i_list[-1]))
                        #calculates and stores the difference in index between the two teeth
        if len(i_list)>1 and abs(spectrum[i_list[-1]]-spectrum[i])>10.0e-5:
        #if the spacing between adjacent comb teeth is greater than 100 MHz
                average = sum(delta_i_list)/len(delta_i_list)
```

```
                #calculates the average spacing of comb teeth
                new_value = i_list[-1]+average+1
                #calculates where the missing comb tooth should have been
                i_list.append(new_value)
                #appends the index value for the missing comb tooth
        return freqpeaks,intpeaks,i_list #returns the peakpicker values: freq,inten,index

full_spec = [] #initializes an array to hold the final data
comb_list_length = len(comb_list)
#calculates the number of files imported and stores the number
thresh_l = 0.2 #lower threshold for intensity values
thresh_h = 1000 #upper threshold for intensity values
counter = 1 #counter to keep track of number of files processed

for sample_file,Master_rep_rate in comb_list:
#for each sample file imported in the directory
        blank_file = sample_file
        freq_b,inten_b,data_b = fft_data(blank_file,Master_rep_rate)
        #run fft_data on the imported file
        freq_p,inten_p,i_list = peakpicker(freq_b,inten_b,thresh_l,thresh_h)
        #run peakpicker on the fft data
        freq_s =  freq_b
        inten_s = inten_b
        freq = [freq_s[x] for x in i_list]
        #initializes an array to hold peakpicked freq values
        #and then populates it based on the index list
        absorption = [inten_s[x] for x in i_list]
        #initializes an array to hold peakpicked inten values
        #and then populates it based on the index list
        spectrum = [(freq[x],absorption[x]) for x in range(len(absorption))]
        #compiles a 2D array containing the freq and absorption values
        full_spec+=spectrum
```

```
        #appends the spectrum for the current data file to the master spectrum
        print str(counter)+" of "+str(comb_list_length)+" combs done"
        #shows current progress in the command prompt
        counter+=1 #increments the counter

full_spec.sort() #sort the master spectrum by frequency value

file = "" #creates a blank string named file
for line in full_spec:
#reads the master spectrum line by line
        file+= str(line[0])+' '+str(line[1])+'\n'
        #appends freq and inten for each line to the blank string
        #in the format 'freq inten' with a space delimiter
fh = open("raw_peak_data.out","w")
#opens a file named raw_peak_data.out
fh.write(file) #saves the data in the string to the file
fh.close() #closes the file
```

A.4 boxcar_v2.py

This program takes data processed by freq_comb_analysis_v3.py and generates an absorbance spectrum. It generates a synthetic blank spectrum by taking a boxcar average of the fft spectrum. It takes the ratio of the fft spectrum and the synthetic blank spectrum to generate the absorbance spectrum.

```
import numpy as np
import matplotlib.pyplot as plt
from numpy import array
from scipy.fftpack import fft
from math import pi,atan2,log
import scipy.interpolate as inter
import pylab as plt
import os
```

```
from os import path

def movingaverage(interval, window_size):
        #when called this routine calculates a moving average over the
        #defined window size centered around interval
        window = np.ones(int(window_size))/float(window_size)
        #initializes an array of ones and divides by the window size
        return np.convolve(interval, window, 'same')
        #returns the value of the moving average

fh = open("raw_peak_data.out")
#opens the output from freq_comb_analysis_v3.py
full_spec = [] #initializes a blank array to hold the master spectrum
for line in fh:
#for each line in the file
        line.split() #split using space as a delimiter
        freq = float(line.split()[0])
        #the first entry is the freq
        inten = float(line.split()[1])
        #the second entry is the inten
        full_spec.append((freq,inten))
        #append each split line to the master spectrum
freq = [x[0] for x in full_spec] #split master spectrum into freq
inten = [x[1] for x in full_spec] #and inten

y = np.array(inten) #take the raw inten values
blank_boxcar = movingaverage(y, 2000)
#and perform a boxcar average with the specified window size
absorption = [100*(1-(inten[x]/blank_boxcar[x]))**2 for x in range(len(blank_boxcar))]
#calculates the absorption based on the synthetic blank spectrum
#generated by the moving average
```

```
absorption = movingaverage(np.array(absorption), 10)
#an additional boxcar may be used to provide smoothing of the absorption spectrum


a = np.dstack((freq,absorption))
#arranges the freq and absorption values as a stacked array
#in the format [[freq1,absorption1],[freq2,absorption2],etc]
print a #prints the data in the command prompt
np.savetxt("spectrum.txt",a[0])
#saves the file as the specified file name
```